PLASTIC DEFORMATION OF POLYCRYSTALLINE SODIUM NITRATE

Thesis submitted for the degree of
Doctor of Philosophy of the University of London

by

Paul Derek Tungatt

September 1982

Department of Metallurgy
and Materials Science
Royal School of Mines
Imperial College
London SW7

ABSTRACT

In this investigation into high temperature plasticity, sodium nitrate has been used as an analogue material to study microstructural changes during deformation, particularly dynamic recrystallization. The occurrance of dynamic recrystallization during creep and hot working of metals is well established, but more recently advances in geology have led to the recognition that dynamic recrystallization has played an important role in the microstructural development of many rocks. Although there have been many systematic studies of dynamic recrystallization, there is no clear evidence of how nucleation occurs.

Due to the difficulty of inferring mechanisms from resulting microstructures, a technique was developed which enabled, via the optical microscope, the continuous observation of the microstructure as it evolved during high temperature plastic deformation. In addition to these experiments, compression tests on bulk cylindrical specimens of polycrystalline sodium nitrate were also carried out. These techniques were used to survey the deformation mechanisms of sodium nitrate between $20^{o}C$ (0.5Tm) and $300^{o}C$ (0.99Tm) at strain rates of $10^{-6}s^{-1}$ to $10^{1}s^{-1}$ to strains up to 0.6.

Several deformation or microstructural mechanisms were identified. At low temperatures or high strain rates deformation twinning occurred. Between $20^{o}C$ and $200^{o}C$ inhomogeneous deformation together with dynamic recrystallization by subgrain rotation was observed. At higher temperatures rapid and extensive growth of the dynamically recrystallized grains could occur, depending on the conditions of deformation and impurity content of the sample. Grain buondary sliding was also observed at higher temperatures.

Sodium nitrate is isostructural with calcite and results from this investigation have been compared with results obtained from experimentally deformed marble. There is a great similarity of mechanical properties and microstructural development between the two materials.

CONTENTS

LIST OF FIGURES

Chapter I

INTRODUCTION

1. PLASTIC DEFORMATION AT ELEVATED TEMPERATURES

Knowledge that metals deform more easily at higher temperatures has been used by blacksmiths for many centuries. Today, plastic deformation at elevated temperatures is widely used in the fabrication of many metallic objects. Although there is a large body of literature on high temperature plasticity, there have been only a few attempts to systematically characterise microstructural changes with increasing strain. The changes in microstructure are important, as the mechanical properties of deformed materials are strongly influenced by the microstructure produced by the working process.

It is not only metals which deform more easily at elevated temperatures. The phenomenon is common to almost all crystalline materials, including rocks and minerals. Recent recognition that the same mechanisms which occur in metals have also enabled extensive plastic deformation of rocks in the earth's mantle has been an additional stimulation for this project. Microstructures of deformed rocks have received considerable attention from geologists, and much effort has been expended into estimating the deformation conditions from the microstructures. Conditions under which a rock has been deformed is an important factor in determining the history of rock formations which make up the present continents and sea beds of the earth.

This study is part of a current research programme at Imperial College into plasticity of polycrystals, with a particular interest in dynamic recrystallization.

Plastic deformation of crystalline materials by dislocation glide and climb at elevated temperatures is accompanied by concurrent softening processes, counteracting the effects of work hardening. The softening processes are thermally activated and are generally effective at temperatures above half the absolute melting point of

the material being deformed. Studies of high temperature deformation are generally classified into either creep or hot working, although the same processes can occur in both.

Creep and hot working are standard technical terms which have arisen from different methods of approach, rather than there being a fundamental distinction in the micromechanisms of deformation, hence it is not easy to draw a clear line separating the two fields of study. However, creep is used to describe small strains at strain rates below $10^{-3}\ s^{-1}$ under conditions of constant stress or load, and hot working is used to describe large strains at constant strain rates above $10^{-1}\ s^{-1}$. Recent reviews on creep include Garafalo, 1965; Weertman, 1968, 1975; Sherby and Burke, 1967, Mukherjee, 1975; Takeuchi and Argon, 1976; and hot working, Jonas Sellars and Tegart, 1969; Rossard, 1973; McQueen and Jonas, 1975; McQueen, 1979; Sellars, 1979a.

In addition to dislocation climb, deformation mechanisms other than dislocation glide can be operative at high temperatures including various diffusion mechanisms and grain boundary sliding.

Two softening mechanisms which can occur during hot working and creep are recovery and recrystallization. Recovery leads to the local rearrangement of dislocations, with the subsequent formation of subgrains; while recrystallization is the formation of new grains relatively free from dislocations. When the processes are concurrent with deformation they are referred to as dynamic recovery and dynamic recrystallization; this is to distinguish them from the static processes which occur during annealing after deformation.

In some metals and alloys, dynamic recovery alone can entirely balance the effects of work hardening, and large strains can be produced under steady state stress conditions before fracture occurs. Resultant microstructures usually have elongated grains containing equiaxed subgrains (McQueen, 1979). Formation of subgrain boundaries

involves climb and cross-slip, which are greatly hindered if the dislocations become extended (Honeycombe, 1968). Hence it is materials with high stacking fault energies which can attain a steady state flow stress during hot working by dynamic recovery alone. In other crystalline materials with lower stacking fault energies, the extended dislocations prevent rapid recovery. This can result in the accumulation of dislocations, which increases the internal energy of the crystals sufficiently for dynamic recrystallization to occur (Sellars, 1978). However, dynamic recrystallization has been observed in metals with high stacking fault energies, e.g. magnesium (Ion, Humphreys and White, 1982) and iron (Glover and Sellars, 1973).

1.1 DYNAMIC RECRYSTALLIZATION

Dynamic Recrystallization is a primary recrystallization process which can take place during hot working and creep of crystalline materials. It was first discovered and studied during creep experiments on lead (Greenwood and Worner, 1939 ; Gifkins, 1959-59). The formation of new undeformed grains during the creep tests resulted in periods of accelerated strain rate. Similar observations of accelerated creep were also noted during studies on nickel and gold (Hardwick, Sellars and Tegart, 1961-62), iron (Feltham, 1953), and copper (Feltham and Meakin, 1959). Although periods of accelerated strain rate caused by dynamic recrystallization during creep were noted, it was found that recrystallization was inhibited by impurities and alloy additions. Hence its occurrence during creep of commercial alloys was thought to be unlikely, and this aspect of creep behaviour was not investigated in great detail (Sellars, 1979,b).

Interest in dynamic recrystallization continued when it was found to occur during hot working of austenitic stainless steel, copper and nickel (Rossard and Blain, 1959; Hardwick and Tegart, 1961-62). Dynamic recrystallization has also been reported to occur during the extrusion of some aluminium alloys (Gardner and Grimes,

1979), and during high temperature compression tests of magnesium (Ion, Humphreys and White, 1982) and zinc (Humphreys, 1981).

However, interest in dynamic recrystallization is not confined to metallurgy. Recent work by geologists has led to the recognition that dynamic recrystallization has played an important role in the microstructural development of many rock forming minerals, including quartz (White, 1973), calcite (Griggs, Turner and Heard, 1960), olivine (Poirier and Nicholas, 1975) and halite (Guillopé and Poirier, 1979). It has also been noted in ice (Wilson, 1979), and in several organic crystal systems during analogue deformation experiments, camphor (Urai, Humphreys and Burrows, 1980), and paradichlorobenzene (Means, 1980).

The main interest of metallurgists in dynamic recrystallization is its effectiveness in softening materials at elevated temperatures, which facilitates the hot working of many metals. As well as reducing the flow stress, dynamic recrystallization can also increase the ductility of metals. At high temperatures grain boundary sliding becomes important, as it can lead to grain boundary fracture by the growth of cavities or triple point cracks. By eliminating the cracking grain boundaries and creating new boundaries of different orientations, dynamic recrystallization can markedly increase ductility (White and Rossard, 1966; Luton and Tegart, 1969; Gittins and Sellars, 1972).

In addition to being a general softening mechanism, the reduction in grain size by dynamic recrystallization is thought to lead to the formation of ductile shear zones in magnesium and rocks. The mechanisms within these macroscopic shear zones are very complex but extensive strains can be achieved (Etheridge and Wilkie, 1979; White, Barrows, Carreras, Shaw and Humphreys, 1979).

Geologists also have a further interest in dynamic recrystallization. One particular problem in geology is the deter-

mination of the historical development of rock formations. An important factor is the stress involved during the past plastic deformation of rocks, and estimates of this have been made using the size of the dynamically recrystallized grains, e.g. Twiss (1977). Information gained from such a technique is then used to gain an insight into the stresses within the earth's crust and mantle. However, a greater understanding of the mechanisms of dynamic recrystallization is required to improve the usefulness of this technique (Poirier and Guillopé, 1979; White 1979).

1.1.1 Effect of Dynamic Recrystallization on the Flow Stress During Constant Strain Rate Tests

The effect of dynamic recrystallization on the stress strain curve depends on the conditions of deformation. Figure 1.1 shows the effects of high and low strain rates. At high strain rates once dynamic recrystallization has begun it is continuous. Before recrystallization is complete throughout the sample, the first of the new grains formed have deformed sufficiently to start recrystallization again. Consequently, the specimen will contain a spectrum of grains which will be work hardened to various degrees, from heavily deformed grains, through to ones which have only just recrystallized.

The cyclic stress strain curve produced by low strain rates is caused by successive waves of dynamic recrystallization. The first wave of recrystallization is followed by renewed work hardening until the next wave occurs. These two types and intermediate curves are well illustrated in figure 1.2.

This figure also shows that the strain of the peak stress increases with increasing strain rate. It has been found that in general, the critical strain required for dynamic recrystallization increases with increasing strain rate, and decreases with temperature (Luton and Sellars, 1969).

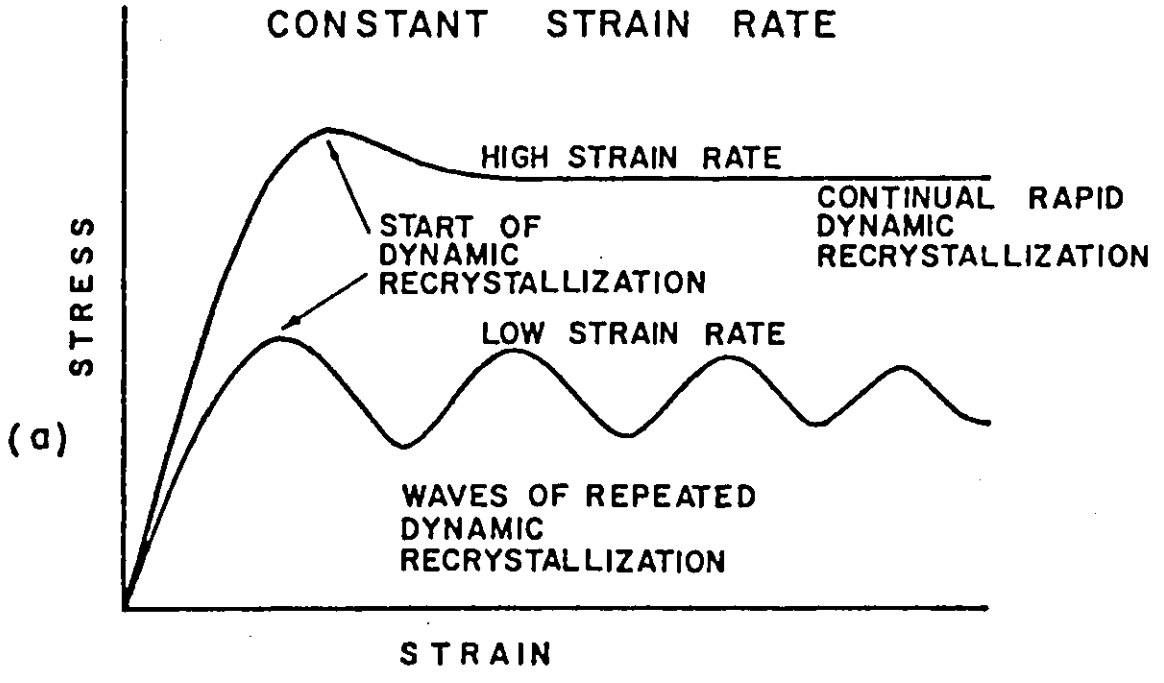

Figure I.I.

Effects of dynamic recrystallization on the flow curve during hot working; after McQueen and Jonas (I975).

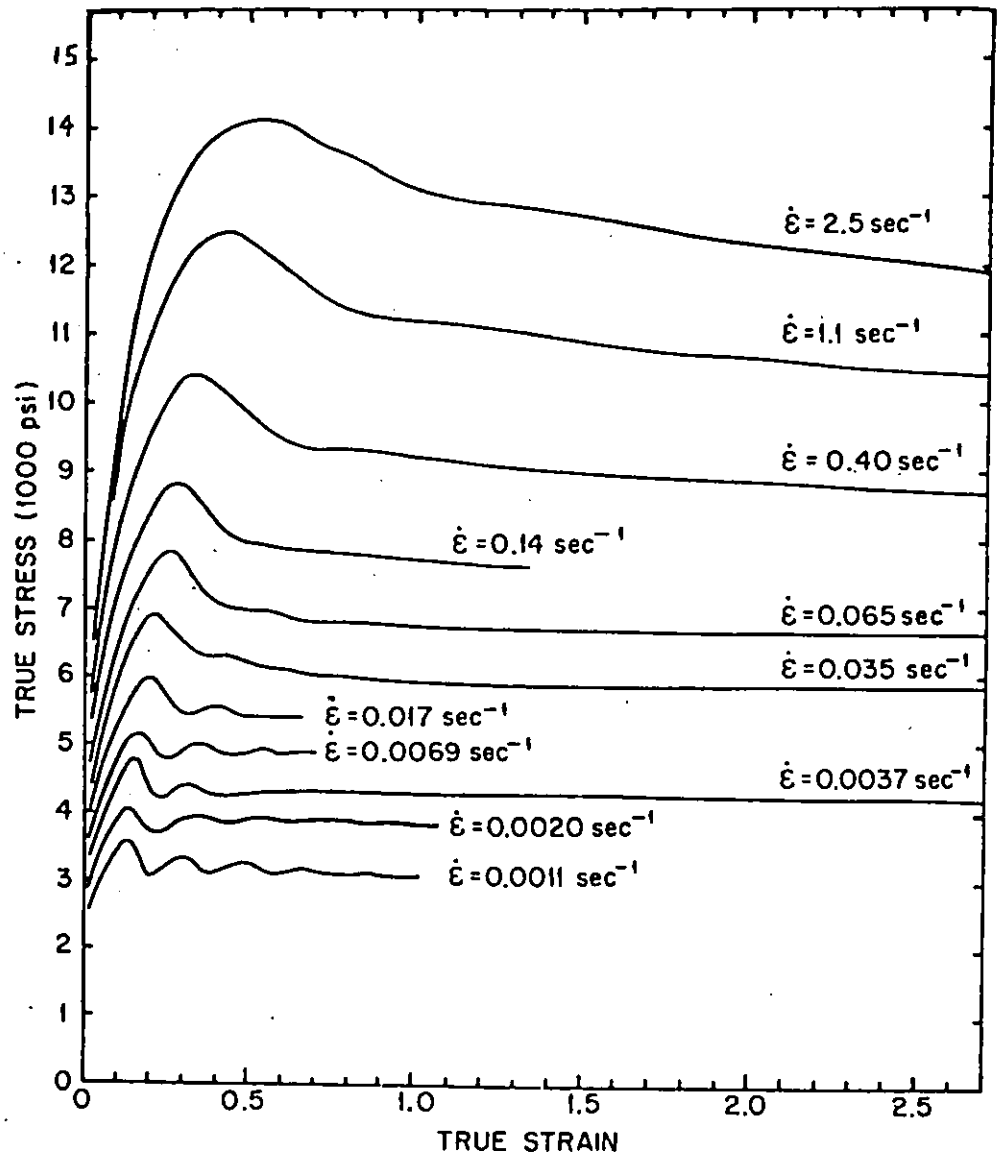

Figure I.2.

Flow curves of plain 0.25%C steel in the austenitic state at 0.75Tm illustrating the strong influence of strain rate; after Rossard (1960).

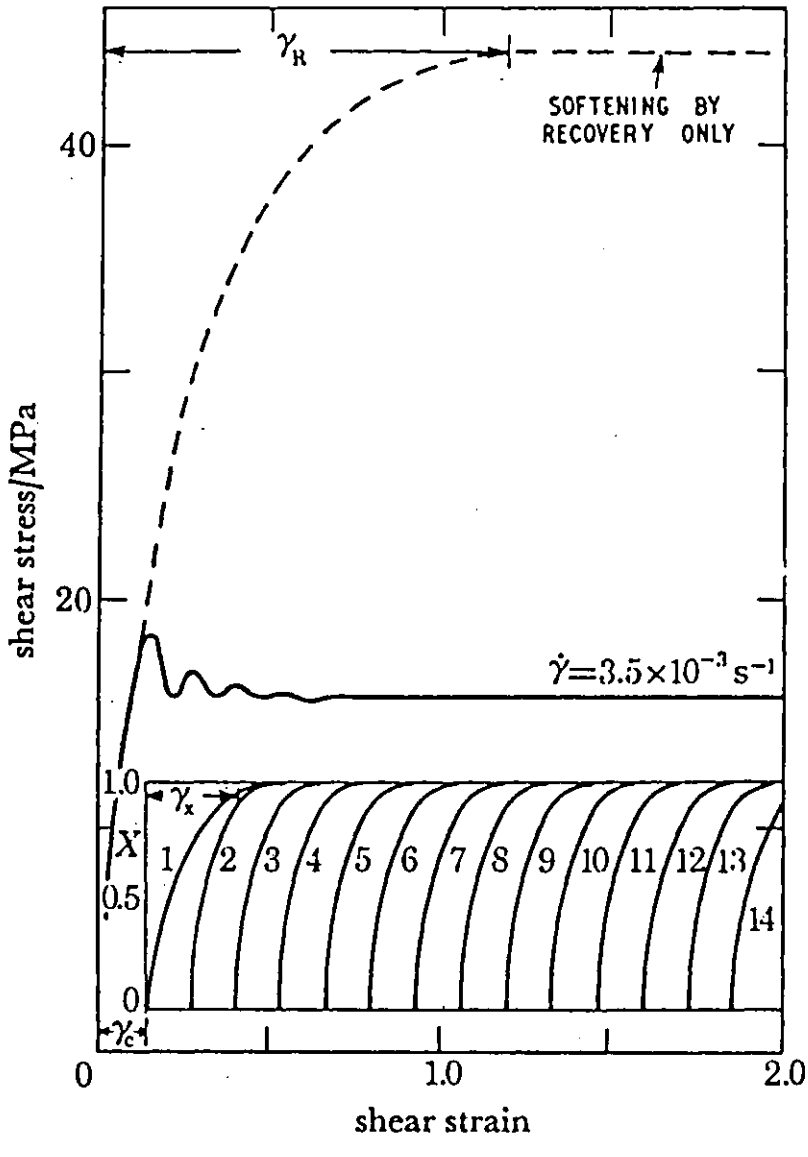

Figure I.3.

Shear stress-strain curve for 99.9% nickel deformed in torsion, at 934^{o}C. The inset shows the cycles of dynamic recrystallization during deformation; after Luton and Sellars (I969).

The effectiveness of dynamic recrystallization as a softening mechanism is clearly shown in figure 1.3. It can be seen that the critical strain for recrystallization is much less than the strain expected for the onset of steady state flow by recovery only.

1.1.2 Effect of Dynamic Recrystallization on Microstructure

In general the recrystallized grains are equiaxed and their size depends on the conditions of deformation. From studies on copper (Bromley and Sellars, 1972), iron (Glover and Sellars, 1973), and nickel (Luton and Sellars, 1969), it has been found that the recrystallized grain size is uniquely dependent on the flow stress, and is independent of the original grain size (Sah, Richardson and Sellars, 1974). This is in contrast with metals which do not dynamically recrystallize, in which the original grains become more elongated with increasing strain. The relationship between the recrystallized grain size (d) and the stress (σ) has been represented by an equation of the form

$$\sigma \propto d^{-n}$$

where n is a constant between 0.5 and 1 (Sellars, 1978).

In the early stages of recrystallization of nickel, the original grains were observed to have markedly irregular boundaries, showing evidence of localised bulging, and the formation of recrystallized grains in the boundary region (Luton and Sellars, 1969). At later stages the entire microstructure was replaced by equiaxed grains. A duplex structure is often observed during the initial stages of recrystallization, the original grains being surrounded by small equiaxed grains along their grain boundaries (Roberts, Bodén and Ahlblom, 1979; Humphreys, 1981; Gardner and Grimes, 1979). Although grain boundaries are preferential sites for recrystallization to start, dynamic recrystallization has

also been observed in single crystals of copper (Gottstein, Zabardjadi and Mecking, 1979), and halite (Guillopé and Poirier, 1979).

Dynamically recrystallized grains can be distinguished from statically recrystallized grains by the fact that they are deformed during growth by the concurrent deformation. Transmission electron microscopy has shown that the dynamically recrystallized grains contain tangled dislocation substructures (Luton and Sellars, 1969), which would not be present in statically recrystallized grains. The formation of a substructure within the growing grain also has the important effect of reducing the driving force for grain boundary migration. Dynamically recrystallized grains have been observed to rapidly obtain a constant size, determined by the conditions of deformation, before impingement with other growing grains occurs, (Sah, Richardson and Sellars, 1974).

1.1.3 Driving Force for Dynamic Recrystallization

The first mathematical model for dynamic recrystallization was proposed by Stüwe and Ortner (1974). The study did not consider how nucleation occurred, but assumed that recrystallization started by the nucleation of new grains when the dislocation density reached a critical value. Once formed the boundary of the nucleus would then move outward at a constant velocity until it met with another boundary. The theory concentrated on calculating the dislocation density and the velocity of migration of the recrystallized grain boundaries, and could account for oscillatory stress-strain curves of the type observed in materials undergoing dynamic recrystallization. However, the effects of dynamic recovery were not included.

Similar concepts were used by Sandström and Lagneborg (1975) in their theoretical model, but the effects of dynamic recovery were taken into account. The driving force for recrystallization

was taken to be the difference in dislocation density on either side of a grain boundary, which would have to exceed a critical value before any significant migration of the boundary occurred. Their theory reproduced the oscillatory behaviour of the stress-strain curve at low strain rates, and at high strain rates, a peak followed by an approximate steady state flow stress. Again the process of nucleation was not considered in detail.

However, Roberts and Alblom (1978) did consider the nucleation mechanism of dynamic recrystallization in their theoretical paper on the criterion for the initiation of dynamic recrystallization during hot deformation. It was assumed that dynamic recrystallization was initiated by bulging of pre-existing grain boundaries, in the manner originally proposed by Bailey and Hirsch (1962). A principal conclusion from the analysis was that the initiation of dynamic recrystallization requires a critical dislocation density, irrespective of whether dynamic recovery is occurring simultaneously or not. The recrystallized grain size was calculated using Cahn's treatment for grain boundary nucleated reactions (Cahn, 1956).

1.1.4 Nucleation Mechanisms for Dynamic Recrystallization

Although the driving force for dynamic recrystallization has been considered in some detail, the nucleation mechanism by which it is initiated is still not clear. The main difficulty of observation is due to the process taking place during plastic deformation at elevated temperatures, which has greatly hindered direct observation of the process as it occurs. Consequently, the theories for the mechanisms of dynamic recrystallization have been derived from stress-strain curves and from microstructures after deformation.

1.1.4.1 Metals

It was the observation of localised bulging of the original grain boundaries, with the formation of recrystallized grains in

the boundary regions during the creep of nickel, which led to the proposal of nucleation by grain boundary bulging (Richardson, Sellars and Tegart, 1966). The bowing of a grain boundary was explained by the boundary being pinned by the highly tangled dislocations of the subgrain walls, and the boundary bulging by the difference in strain energy across it. Once a grain boundary had bowed to a hemisphere, it would then be able to grow spontaneously, if the radius was greater than the critical size for growth, as in the Bailey and Hirsch model for static recrystallization.

Although the growth of a grain boundary bulge into a deformed grain will lead to the recrystallization of the material contained within the bulge, and create a volume of undeformed material, the mechanism does not lead to the creation of grains with different orientations. Nor does it fully explain the observations of new grains along grain boundaries, or the occurrence of dynamic recrystallization in single crystals.

These drawbacks are overcome by a second nucleation mechanism proposed in the metallurgical literature. In a review paper, McQueen and Jonas (1975), support the grain boundary bulging mechanism at low strain rates, but suggest that dynamic recrystallization at high strain rates occurs by subgrain misorientation. They proposed that at high strain rates, the fine tangled substructure does not leave grain boundary segments sufficiently long enough between pinned points to bulge, but claimed that there is evidence that, with increasing strain, some tangles build up to high misorientations, giving rise to nuclei throughout each grain. The preferential nucleation of dynamically recrystallized grains along grain boundaries was attributed to there being a higher density of nuclei near grain boundaries. McQueen and Jonas explained that the cause of the higher density of nuclei at the boundaries was due to the larger strains at grain boundaries, which were a result of the accommodation of plastic anisotropy.

This theory overcomes the problem of creating new grains with different orientations by the creation of high angle boundaries, which means that part of an original grain will have a different orientation from the rest of the grain. Another advantage of this model is that it can be applied to single crystals. However, there is little evidence in the metallurgical literature for the build up of high misorientations between subgrains. The reference quoted for supporting evidence, McQueen and Bergerson, 1972, states that after hot deformation of copper, the grains were subdivided by cell walls, and exhibited internal misorientations as high as $6^{o} - 8^{o}$. Unfortunately, it is not clear whether the misorientations of $6^{o} - 8^{o}$ occurred across a single boundary, or whether it was the cumulative misorientation from one side of a grain to another across several subgrains. There is little supporting evidence from other work; results from studies on the creep of nickel show that the misorientations between subgrains did not exceed 0.4^{o} (Richardson, Sellars and Tegart, 1966). Also, in a recent review (McQueen 1981), it is noted that substructure misorientations do not increase with strain, which is supported by work on the extrusion of aluminium, where subgrain misorientations were found not to exceed 4^{o} (Wong, McQueen and Jonas, 1967).

A third mechanism has been proposed for single crystals of copper deformed at slow strain rates (Gottstein, Zabardjadi and Mecking 1979). After deformation, the crystal contained many small equiaxed subgrains, plus one huge subgrain. This was attributed to an instability of the dislocation substructure, which lead to the catastrophic growth of the subgrain into macroscopic dimensions.

1.1.4.2 Minerals

Although there is little evidence for the build up of large misorientations between subgrains in cubic metals, dynamic recrystallization by subgrain rotation has been proposed for rocks and minerals

by geologists. Evidence for this mechanism has been implicitly referred to many times in the geological literature before its significance was fully recognised (Poirier and Guillopé, 1979).

One of the first papers to explicitly state this mechanism for dynamic recrystallization was by Hobbs, (1968). Subgrain misorientations were measured after experimental deformation of single crystals of quartz. It was found that subgrains formed in deformation bands at low strains increased their relative misorientations as the strain increased, until an array of diversely oriented grains with sharp grain boundaries developed. Over large regions of the specimen, the misorientation between adjacent subgrains was approximately 5°, but on approaching a deformation band boundary, misorientations increased rapidly to 10° - 30°. As the strain increased the misorientations between subgrains in the deformation bands increased from 1° - 5° to 20° - 30°, and local misorientations as high as 90° may have developed. The subgrains outside the deformation bands maintained 1° - 5° misorientations independent of the amount of strain, but as the strain increased the deformation bands increased in width, so that more and more subgrain boundaries were made into high angle boundaries. Some areas of the samples contained larger than average grains with highly serrated boundaries and were thought to have occured by strain induced boundary migration.

The theory of progressive subgrain rotation is further supported by evidence from naturally deformed quartz (White 1973). As a result of both optical and electron microscopy studies, White proposed a sequence of continual dynamic recovery with dynamic recrystallization as an integral part of it, with no sharp demarcation between each stage. He suggested that during deformation dynamic recovery led to the formation of subgrains, which continued to misorientate by the addition of dislocations to the higher angle

subgrain boundaries. Once high enough misorientations were achieved the subgrains then appeared as small recrystallized grains. Due to the new grains being individual and distinguishable entities, this stage was termed dynamic recrystallization. Further deformation resulted in continued rotation and growth by stress induced grain boundary migration. Growth of the grains ceased when the migrating grain boundaries 'interlocked'. The process recommenced by the increase of dislocation density produced by internal stresses caused by the interlocked grain boundaries.

An interesting observation from this study was that the large subgrains observed optically contained smaller subgrains, which had only slight misorientations of 1^{o} or less when observed using an electron microscope. So the recrystallized grains observed optically were clusters of subgrains sufficiently misorientated from their neighbours to be visible as an individual entity. The clustering was first observed as optical subgrains, which then apparently became more misorientated to form the recrystallized grains. However, few measurements of subgrain misorientations are given to support the arguments presented in the paper.

Deformation induced recrystallization due to progressive misorientation of subgrains has also been proposed after studies of naturally deformed Olivine, (Poirier and Nicolas, 1975). Misorientations between adjacent subgrains were found to increase with strain up to a maximum of 12^{o}.

1.1.5 Growth of Dynamically Recrystallized Grains

During a study of creep on single crystals of halite under experimental conditions (Guillopé and Poirier, 1979), extensive growth of some dynamically recrystallized grains was noted, this being in addition to the mechanism of subgrain rotation without grain boundary migration. At lower temperatures, recrystallization by subgrain rotation produced small, equiaxed, subgrain size grains, with misorientations up to 44^{o}. This mechanism was also observed to occur at higher temperatures, but in addition, very large grains

with bulging or scalloped and corrugated boundaries were observed. These were interpreted as the result of extensive migration of a rotationally recrystallized grain boundary. A low angle polygonized substructure behind the migrated boundaries proved that they formed during deformation, and not under static conditions. It was proposed that any high angle boundary formed during deformation may be able to bow out locally and grow by strain induced boundary migration. A critical curve was found which separated the high and low temperature behaviour, figure 1.4. The critical curve was found to be strongly dependent on the impurity content of the material. As the impurity concentration increased, a higher temperature was required for the onset of extensive growth of the recrystallized grains. For very impure crystals the migration phenomenon was completely suppressed.

These results were explained within the framework of a theory for impurity controlled grain boundary migration by Lücke and Stüwe (1971). It has been proposed that the solute atoms segregate to grain boundaries, and when the boundary moves it can do so in two ways, depending on the strength of the driving force. The boundary can either move slowly, dragging its cloud of impurities along with it, or it can break free, leaving the impurities behind and migrate rapidly. Hence it was thought that below the critical curve of figure 1.4 the grain boundaries move very slowly, due to the dragging force exerted by the impurities, but above the curve the boundaries can break free from the impurities and move rapidly. The transition from the loaded to the free boundary condition leads to a discontinuous change in velocity, which is assumed by Guillopé and Poirier to be responsible for the two recrystallized grain sizes, although no direct information was available about the actual rates of boundary velocities. Application of the Lücke and Stüwe theory to dynamic recrystallization is reviewed by Poirier and Guillopé (1979).

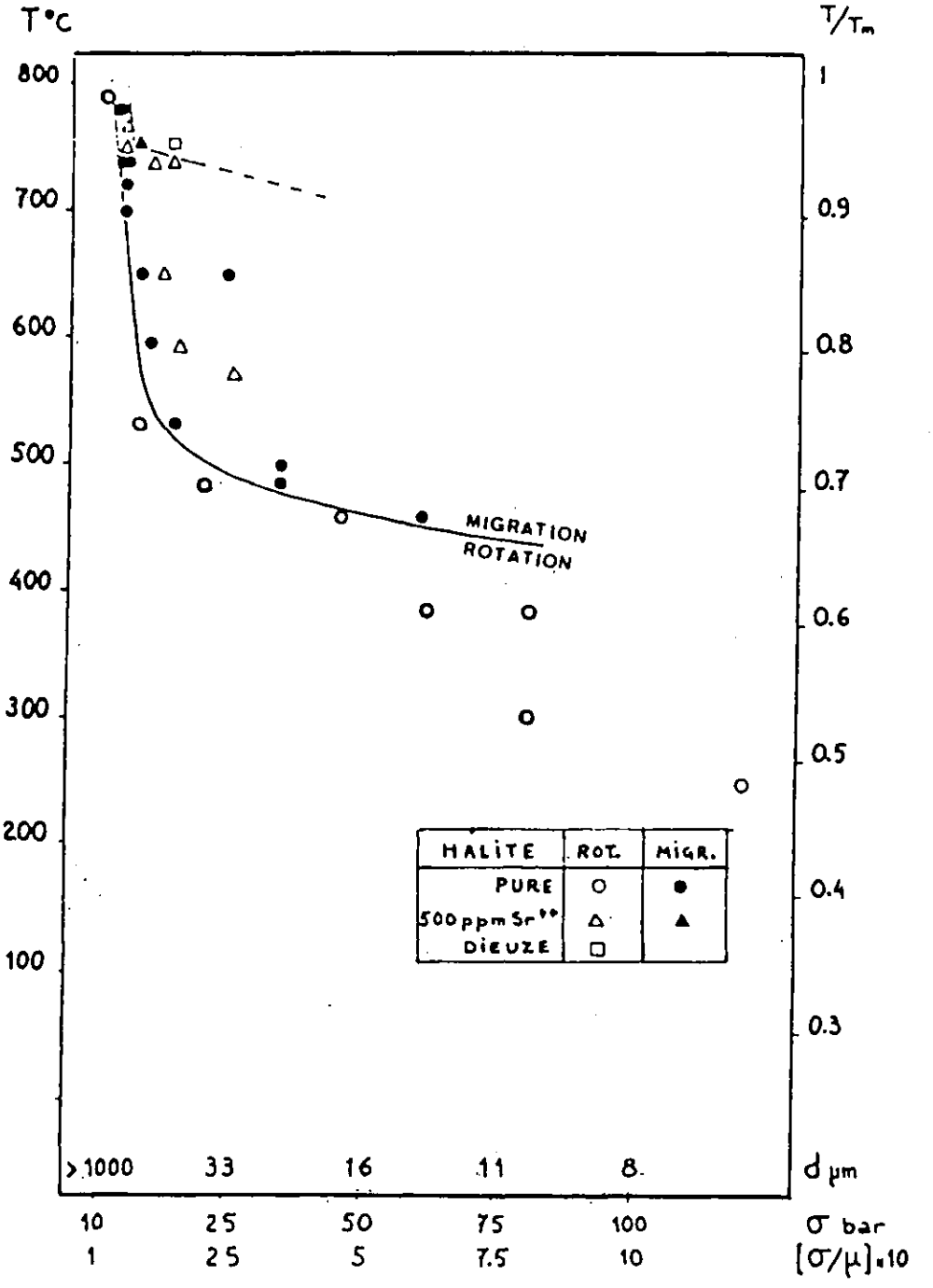

Figure I.4.

Critical curve between the domains of rotation recrystallization and migration recrystallization; after Guillopé and Poirier (1979).

1.2 Analogue Materials

Analogue materials have been used on several occasions to overcome the difficulties of direct observation, for example, during studies on solidification (Hunt and Jackson, 1966), and grain growth (Simpson, Aust and Winegard, 1969). More recently organic polycrystals have been used to study microstructural changes in situ during plastic deformation (Means, 1980; Urai, Humphreys and Burrows, 1980). Although these deformation studies have provided a useful insight into the geometry of deformation, the use of organic analogue materials may be limited. The different type of bonding in the organic crystals may prevent detailed comparisons of microstructural changes with either ionic or metallic crystalline materials.

Direct observations of static recrystallization and phase transformations have been made on metals using transmission electron microscopy, but there are many problems associated with the plastic deformation of thin foils at elevated temperatures. However, it was thought that if a suitable analogue material could be found, then the process of dynamic recrystallization could be observed directly, albeit at low resolution, using a deformation stage and an optical microscope. A suitable analogue material would be crystalline, transparent, have a fairly low melting point and preferably be ionically bonded.

1.2.1 Sodium Nitrate

From a survey of low melting point ionic crystals, sodium nitrate was selected for study. In addition to several basic pre-requisite properties of transparency and a low melting point of 306.8°C, sodium nitrate also possesses several other properties useful to this investigation. It is colourless, non-hydroscopic, chemically stable up to its melting point, and has the same crystal structure as calcite, $Ca(NO_3)_2$. The fact that sodium nitrate is isostructural with calcite has two important consequences

for this investigation. Firstly, it is birefringent, which gives it useful optical properties, and secondly, it has enabled the direct comparison of results with those obtained from marble deformed under experimental conditions.

Very little information has been reported in the literature about the mechanical properties of sodium nitrate. However, the cleavage and twinning behaviour have been reported by Palache, Berman and Frondel (1951). There is perfect cleavage parallel to the rhomb planes, and with reference to the hexagonal morphological unit cell, the most common twins are the 'e' type $[1012]$, with twinning less commonly on $[10\bar{1}1]$ and $[02\bar{2}1]$ planes. Both cleavage and twinning behaviour are similar to calcite. The calcite crystals structure can be represented in various forms as shown in figure 1.5.

Although the crystal structure of sodium nitrate remains essentially constant up to its melting point, a gradual transition occurs as it is heated (Kracek, 1931). Completion of the transition is at 275.5^{oc} and was accounted for by the initiation of rotation of the nitrate ion about the trigonal axis of the crystal (Kracek, Posnjak and Hendrics, 1931). The transition was detected by studying differential thermal capacity and thermal expansion. However, no change was detected in the optical properties of the crystals as they were heated through the transition region (Kracek, 1931). More recent detailed X-ray analysis suggests that in the high temperature phase above 276^{oc}, the nitrate groups seem to be statistically distributed between two twofold disordered, non-equivalent sets of positions in the trigonal unit cell (Strømme, 1969).

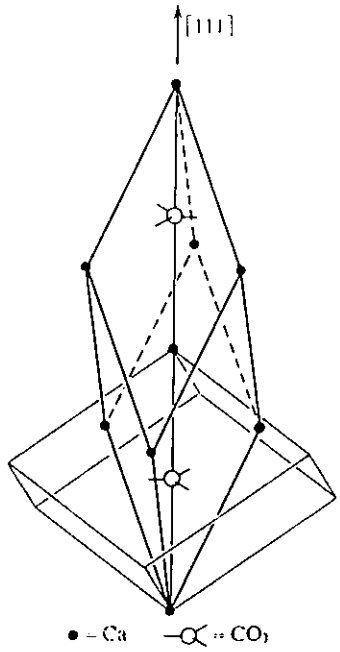

The structure of calcite ($CaCO_3$). The primitive rhombohedral unit cell is shown which contains two formula units of $CaCO_3$. The cell outlined with weak lines is the smallest 'cleavage rhombohedron' and contains four units of $CaCO_3$.

After Kelley and Groves (1970)

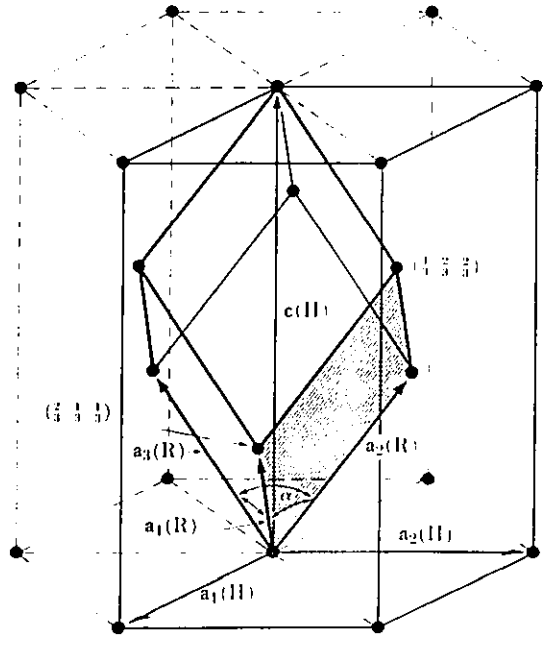

Rhombohedral and hexagonal unit cells in a rhombohedral lattice.

After Cullity (1956)

Figure 1.5

Crystal Structure of Calcite

Chapter 2

EXPERIMENTAL TECHNIQUES

2. EXPERIMENTAL TECHNIQUES

2.1 IN SITU EXPERIMENTS

2.1.1. Apparatus

The in situ experiments consisted of confining a thin sample of polycrystalline sodium nitrate between two pyrex discs, mounted in a hot stage. A thin steel strip, inserted between the pyrex discs, was used to deform the specimen. Figures 2.1a and b show the hot deformation stage in section, and as an exploded diagram. When mounted on the stage of a transmission polarizing light microscope, the microstructure of the sample could be observed continuously during deformation, albeit at low resolution. Both 35mm roll film and 16mm time lapse cine photography were used to record the microstructural changes. A control box was constructed to control and monitor the temperature, and to vary the speed of the motor driven ram. Figure 2.2 shows the circuit diagram.

2.1.2 Specimen Preparation

Preparation before the commencement of an in situ experiment involved hot pressing a small sample of sodium nitrate to the correct thickness inside the deformation cell. The clamping plate and top pyrex disc were removed, leaving the lower pyrex disc in the heating block, with the steel spacers in position. A small quantity of sodium nitrate was then placed in the centre of the lower disc, and heated until molten. On cooling, it formed a small solid hemisphere, which could be slid along the pyrex disc until it was just in contact with the back spacer. This precaution ensured that after hot pressing, the back of the sample would be in contact with the spacer, which would prevent the specimen sliding backwards when an attempt was made to deform it. While maintaining the temperature between 280^{oc} and 290^{oc}, the top pyrex disc was carefully lowered into position, followed by the clamping plate. The three nuts were

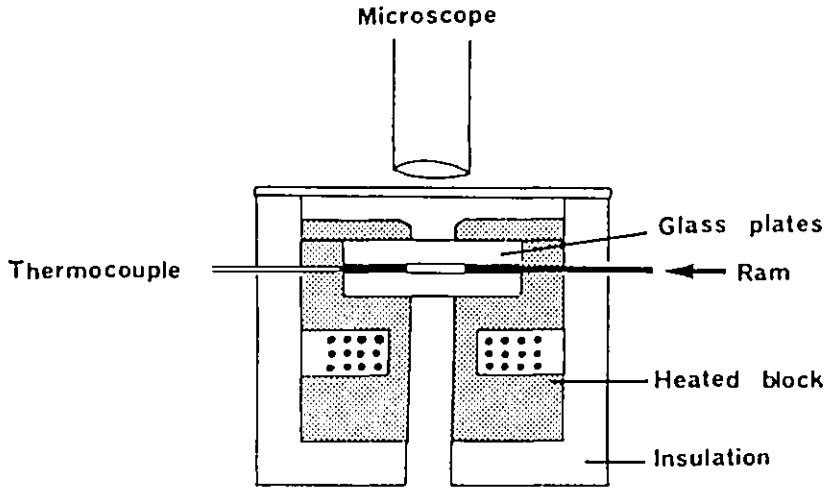

2.I.a Section

2.I.b Exploded diagram

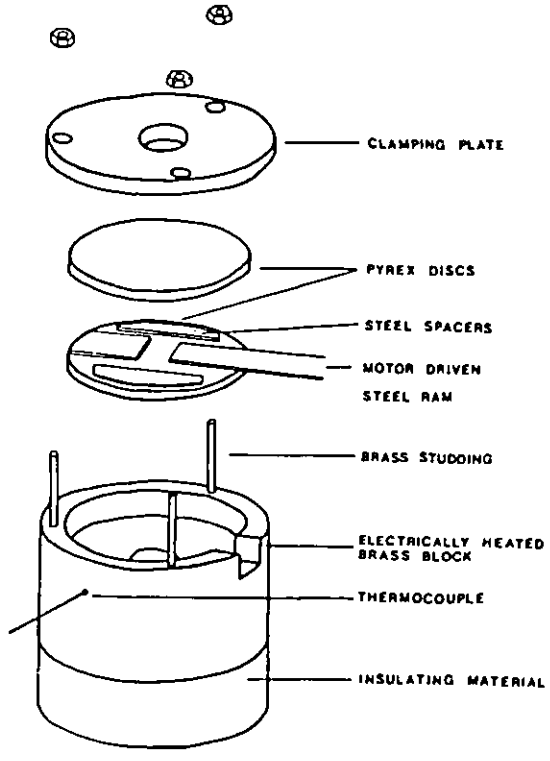

Figure 2.I.

Deformation stage

then used to carefully tighten down the top pyrex disc onto the metal spacers. This action hot pressed the sample to a uniform thickness of 170μm, and ensured good contact between the sample and the pyrex discs over an area of approximately 3 x 3mm. Good contact between the sample and the pyrex discs minimised the amount of light scattering at the interfaces.

At 290^{oc} the sample would readily recrystallise after deformation. This was exploited to obtain a suitable grain size before the start of an experiment. The temperature was then changed to the one required and the plunger was driven in at a constant rate, using a small electric motor and a series of gears. The speed of the motor was adjusted by changing the supply voltage to the motor.

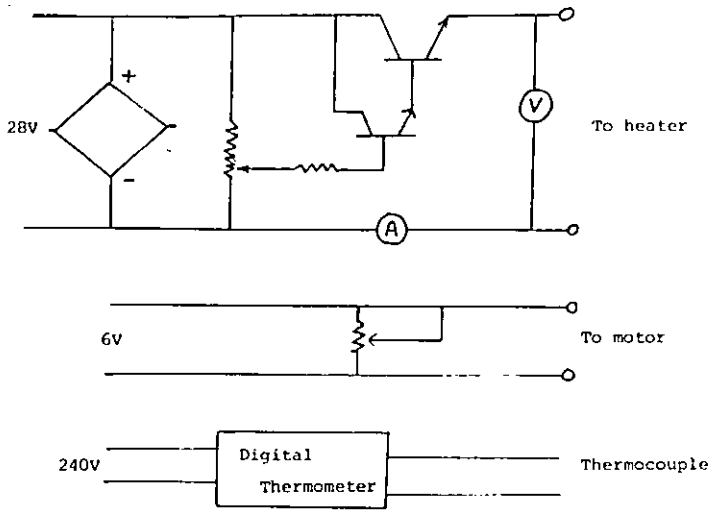

Figure 2.2.

Circuit diagram of the in situ control box

2.2 BULK TESTS

2.2.1 Preparation of Compression Specimens

Castings of sodium nitrate were very porous and had an undesirable columnar grain structure. In order to overcome this problem a technique which extruded cast ingots of sodium nitrate was developed. A diagram of the simple extrusion rig designed and built for this purpose is shown in figure 2.3.

After placing the extrusion chamber on a steel cooling block, molten sodium nitrate was cast into it within 2cm of the top. On cooling the chamber was placed over the supporting steel tube, and the plunger was positioned in the top. Thus assembled, the rig was placed inside a compression cage mounted on an Instron machine. A 'eurotherm' controller was used to maintain the temperature of the chamber at 300^{oc}, and the compression cage was used to extrude cylindrical rods, by forcing the plunger into the extrusion chamber.

After cooling to room temperature a jeweller's saw was used to cut the rods into approximately 2cm lengths. The ends of the cut sections were then ground parallel and polished. Standard 600 grade silicon carbide grinding paper with absolute alcohol was used to grind the samples, before being polished. A polishing technique using a 'selvyt' cloth from Metaserv, and a gamma alumina/absolute alcohol slurry was developed. The cylindrical compression samples were between 15 and 17mm in length and 10mm in diameter.

2.2.2 Compression Testing

2.2.2a Instron Tests at Atmospheric Pressure

Specimens were deformed in a high temperature compression rig mounted on an Instron. A sketch of the apparatus is shown in figure 2.4. After deformation the crosshead of the Instron was quickly reversed, and the sample was lowered out of the furnace and air cooled.

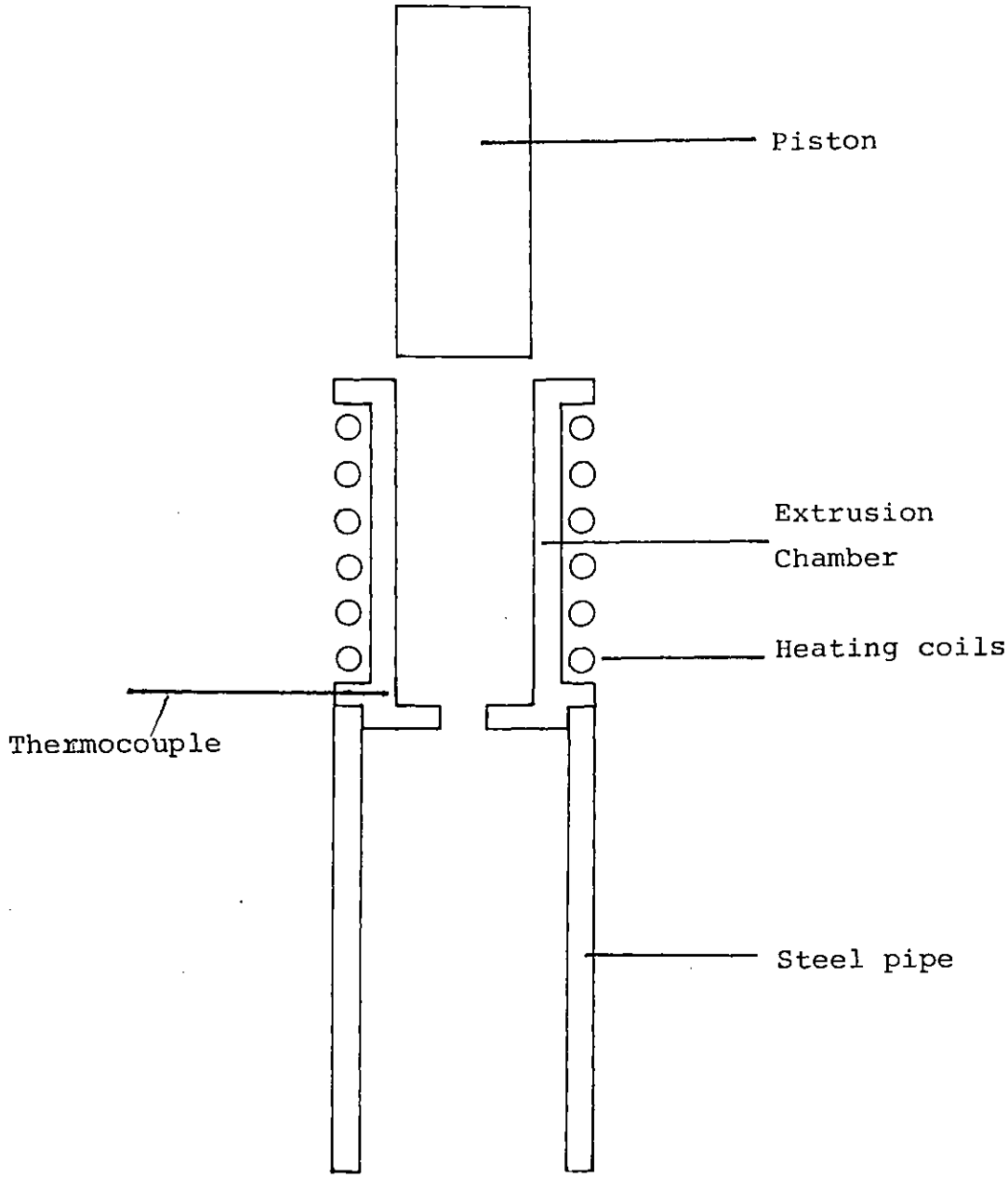

Figure 2.3.

Section of extrusion rig.

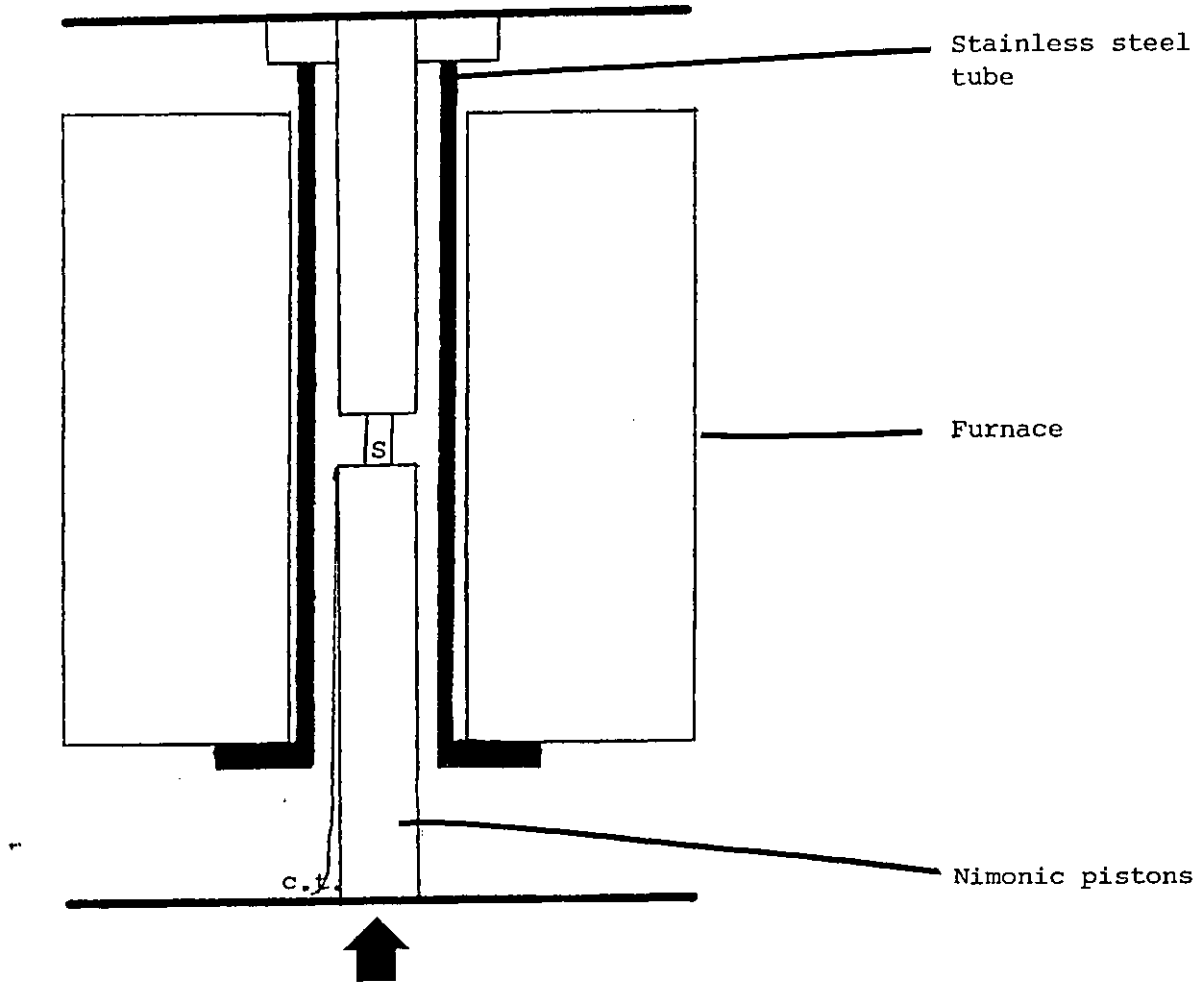

S - Sample

c.t. - control thermocouple

Figure 2.4.

High temperature compression rig

2.2.2.b Tests Under a Confining Pressure

Room temperature compression tests were performed in a geological deformation apparatus, which enabled specimens to be compressed while under a confining pressure. Figure 2.5 shows a diagram of the apparatus. Specimens of sodium nitrate were protected from the confining medium by a rubber jacket. I am greatly indebted to Dr. B.K. Atkinson for performing all the room temperature tests using this rig.

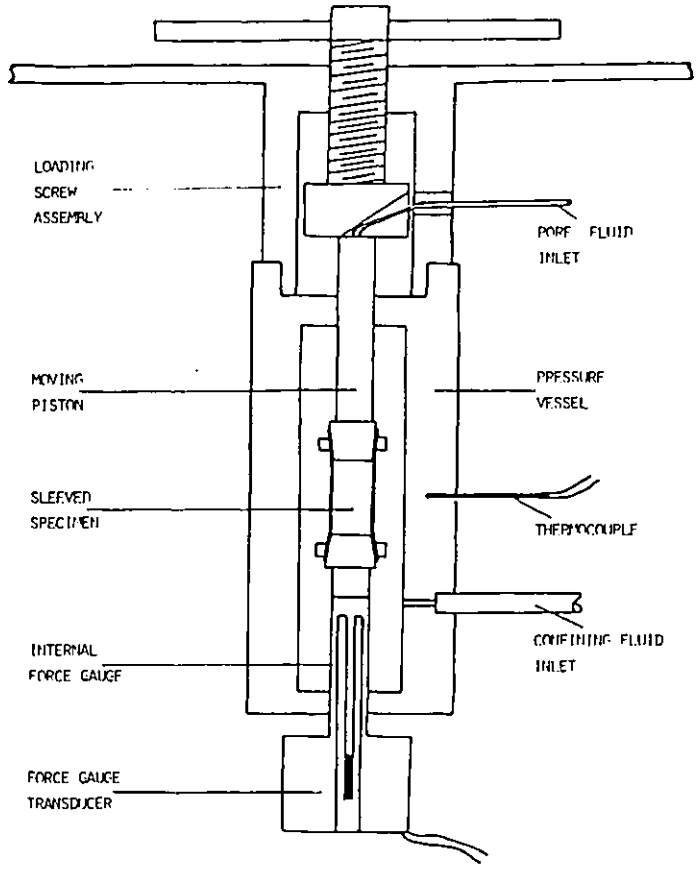

Figure 2.5.
Sketch of Heard type deformation apparatus; courtesy of B.K. Atkinson.

2.2.3 Preparation of Thin Sections

A jeweller's saw was used to carefully section samples parallel to the compression axis. The cut face was then ground flat to remove all saw marks. After polishing the face was dried before being stuck on to a one inch glass disc with "UHU Supalok glue". A small weight was placed on top of the sample, and the glue was left for twenty four hours to dry. Again a jeweller's saw was used to remove the back of the sample, leaving an approximate 2mm thick slice stuck onto the glass disc. The slice was then ground to 0.5mm using silicon carbide paper before the glass disc was put into a holder of an automatic polishing rig. The rig was set up using the polishing materials described above, and was used to thin the sections to approximately 30μm. Finally, the sample was polished down to a thickness between 5 and 10μm by hand, after which a glass cover slip was glued in position over the thin section.

2.2.4 Optical Microscopy

Optical examinations of the thin sections were performed using a transmission polarizing light microscope. Microstructures were recorded on 35mm photographic film for subsequent grain and subgrain size measurements. Subgrain misorientations were also determined using a universal stage.

Universal stage work is a standard technique used by geologists to determine the orientation of particular crystallographic directions within grains in a thin section of a rock. Essentially the universal stage enables thin sections to be rotated to any orientation, the four rotation axes are shown in figure 2.6. The thin sections are mounted between two glass hemispheres, which prevent refraction of light rays between the air and the spherical glass surfaces.

Determination of crystallographic directions depends on the anisotropic properties of the material being studied. Sodium nitrate

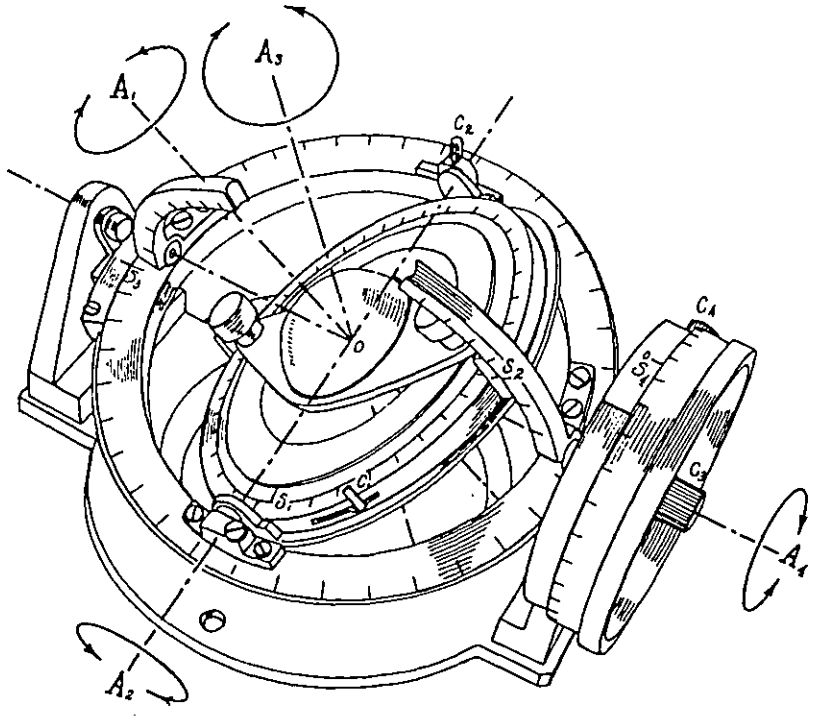

Rotation axes for a four-axis universal stage (E. Leitz Inc.). All rotation axes intersect at the center (O) of the flat side of the glass hemisphere. A_1 is the rotation axis normal to the plane of the thin section, which is placed between the glass hemispheres. Rotation about A_1 is read as S_1 on the periphery of the inner rotating ring. Clamp is at C_1. A_2 is the horizontal N–S axis when A_3 and A_4 are at zero. Rotation about A_2 is read at S_2 on the hinged Wright arcs. Clamp is at C_2. A_3 is normal to the A_2-A_4 plane, and rotation about A_3 is read at S_3 on the periphery of the outer rotating ring. Clamp is at C_3. A_4 is horizontal and E–W when the microscope axis A_5 is at zero. Rotation about A_4 is read at S_4 on the large vertical drum on the right. Clamp is at C_4. A_5 (not shown) is the axis of the microscope stage.

Figure 2.6.

A universal stage; after Phillips(I97I)

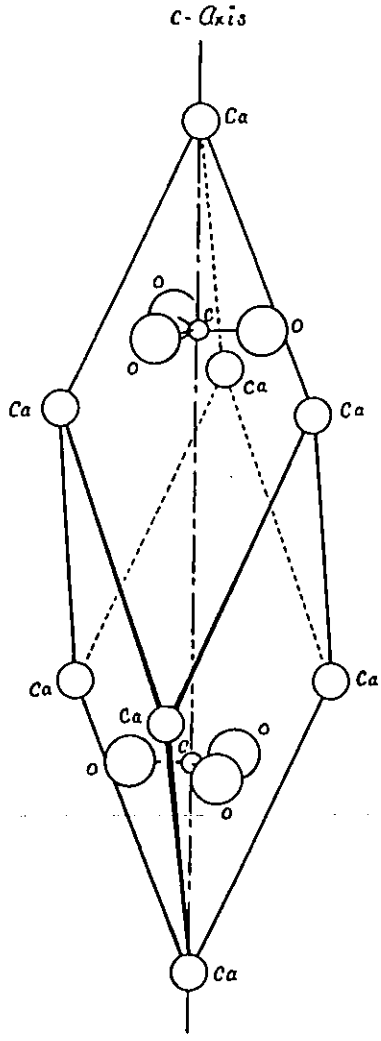

Figure 2.7.

The C-axis of calcite;
after Phillips (I97I).

has the calcite structure so it is a birefringent uniaxial crystal. The fact that it is birefringent means that a ray of light entering the crystal will split into two rays, an ordinary ray and an extra-ordinary ray. It is this property which gives rise to the double image of objects when observed through a calcite crystal. Also the crystals are uniaxial, that is, the vibration directions of the two refracted rays of light bear a simple relationship to one optical axis. The ordinary ray vibrates perpendicular to it, and the extraordinary ray in a plane containing it. The optical axis of the calcite structure is coincident with the crystallographic 'c' axis (figure 2.7).

When a crystal of sodium nitrate is placed between crossed nicols, it will go into extinction when its optical axis is parallel to either one of the nicols. By following a set procedure (Phillips 1971), the crystal can be rotated using a universal stage to bring the optical axis to one of two known positions. From measurements taken off the stage, a pole figure may be constructed showing the orientation of the optical axis with respect to the plane of section.

Chapter 3

EXPERIMENTAL RESULTS

3. RESULTS

This chapter contains experimental results from both the in situ experiments and bulk compression tests performed on sodium nitrate. Results from the in situ work will be described first, as these give an overall qualitative description of the microstructural changes which occur when sodium nitrate is deformed over a wide range of temperatures (0.5Tm - 0.98Tm) and strain rates (10^{-6}-10^{1}). Also included in this section are quantitative measurements made on grain boundary velocities, and results from experiments using sodium nitrate of high purity and samples containing known trace additions.

After the in situ section, results from the experiments using bulk samples of sodium nitrate will be described. In addition to the stress-strain data gained from these tests, thin sections prepared from bulk samples enabled detailed quantitative analysis of the microstructures after deformation. All experiments involving the deformation of bulk samples used laboratory grade sodium nitrate.

3.1 IN SITU EXPERIMENTS

The in situ experiments enabled the continuous observation of the microstructure as it evolved during deformation. Using this technique a survey was made of the deformation mechanisms as a function of temperature and strain rate. Four deformation or microstructural mechanisms were identified for laboratory grade sodium nitrate: twinning,inhomogeneous lattice rotations, rapid growth of dynamically recrystallized grains and grain boundary sliding.

3.1.1. Twinning

Deformation twinning could be induced at all temperatures between 20°C and 300°C, although faster strain rates were necessary at higher temperatures, as shown in figure 3.1. Although twins were formed at 300°C under shock loading conditions, the rate of deformation was too rapid to be measured, even when using the cine camera at its maximum speed of 24 frames per second, indicating a strain rate greater than $10s^{-1}$. After shock loading, the samples rapidly recrystallized within seconds, replacing the twins with new underformed grains. No annealing twins were ever observed.

Two types of twins were observed, as shown in figure 3.2a and b. Initially all twins were thin as in figure 3.2a, but with subsequent straining, some broadened into thicker lenticular or lensoid twins, figure 3.2.b. Twinning occurred at low strains, and at 20°C, further straining resulted in deformation of the twins, particularly near grain boundaries (figure 3.2a).

At higher temperatures dynamic recrystallization (see section 3.12) initiated along the twin boundaries, eventually destroying the twins, figures 3.3a-d.

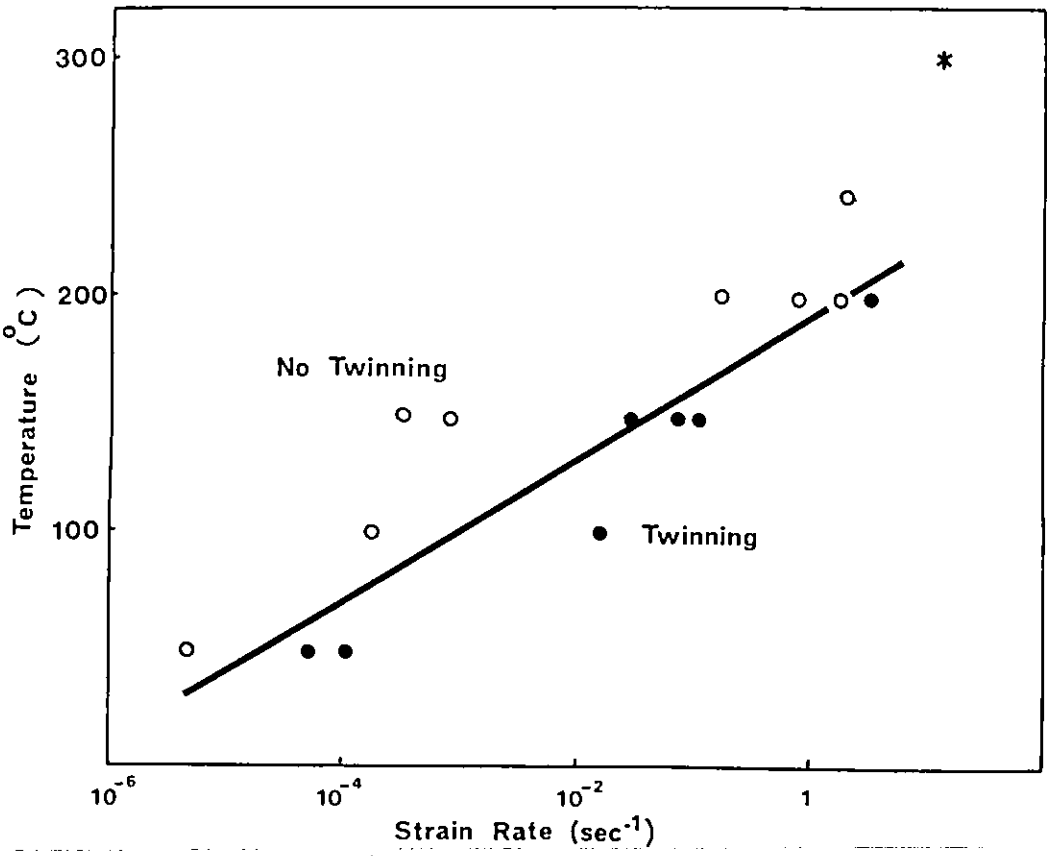

Figure 3.I.

Conditions under which deformation twinning occurred.

* Twinning at 300°C occurred at strain rates above the limit of measurement.

Figure 3.2 Twins formed at 20°C

(a) Thin twins. Subsequent deformation has distorted the originally straight twins near the grain boundary.

(b) Further deformation also led to the broadening of some twins to form lenticular shaped twins.


a
20 µm


b
20 µm

Figure 3.3 Formation of a twin and its subsequent destruction by dynamic recrystallization (150°C)

(a) undeformed sample

(b) formation of a twin (strain 0.15)

(c) twin broadens and dynamic recrystallization initiates along its boundaries

(d) Final destruction of the twin by dynamic recrystallization (strain 0.5).

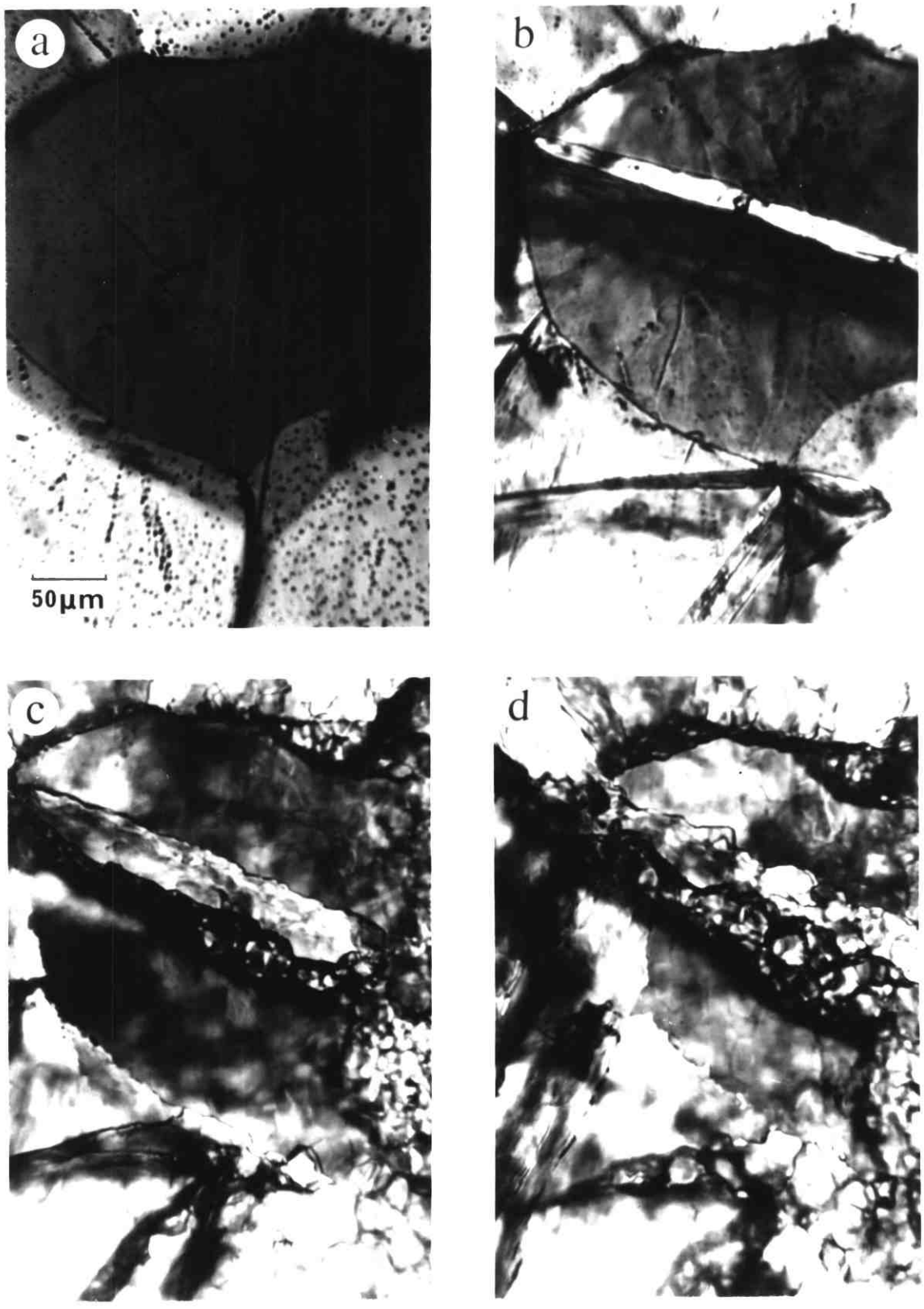
a
50µm
b
c
d

3.1.2 Lattice Rotations

At all temperatures deformation resulted in the formation of subgrains within the original grains. With increasing strain the changes in contrast of the substructure became more pronounced at the grain boundaries, as shown in figure 3.4. Although no direct measurements of the crystal orientations were possible, it was inferred that the substructure became progressively more misorientated with strain, and that high angle boundaries, and hence new grains, were being formed. Further evidence for the formation of high angle boundaries are the 120^{o} angles at the intersection of the subgrain boundaries with the old grain boundaries (figure 3.4). However, recent work on aluminium has demonstrated that similar distortions of grain boundaries can occur without the formation of high angle boundaries (Humphreys, 1982).

Once formed, the recrystallized grains did not change size greatly during subsequent deformation, although some slow growth did occur. At higher temperatures grains were observed to grow to approximately double their original size before the microstructure was completely overprinted by the rapid migration of high angle boundaries throughout the sample. The rapid growth of the dynamically recrystallized grains is discussed in the next section.

Figure 3.4 Substructure formed at $285^{o}C$ (strain approx. 0.5)

Note the progressive change in contrast across the grain from the centre of the grain at A, towards the grain boundary at B, and the formation of approx. 120^{o} angles at the intersection of the subgrain walls with the grain boundary, e.g. at C.


C
B
A
50µm

3.1.3 Rapid Growth of Dynamically Recrystallized Grains

Although dynamic recrystallization by subgrain rotation was seen to occur at all temperatures, there was a temperature above which dynamically recrystallized grains were observed to grow rapidly to a very large size, consuming both the old grains, and the small, slow growing, recrystallized grains. This process is clearly seen in the sequence of micrographs shown in figure 3.5.

In figures 3.5 a-c the deformation results in the formation of subgrains, which appear to misorientate and form new grains, e.g. along boundary A B. Micrograph 3.5c was taken 20 minutes after the start of deformation, the next sequence d to f were all taken in the following minute, and show the rapid and extensive growth of the dynamically recrystallized grain formed at C, consuming much of the surrounding deformed structure.

Figure 3.5 In situ sequence at 300°C (strain rate approx. $10^{-4}s^{-1}$)

(a) Undeformed sample

(b)-(c) Formation of substructure within grains and dynamically recrystallized grains at triple points, and along grain boundaries, e.g. A-B

(d)-(f) Rapid and extensive growth of dynamically recrystallized grain formed at C.

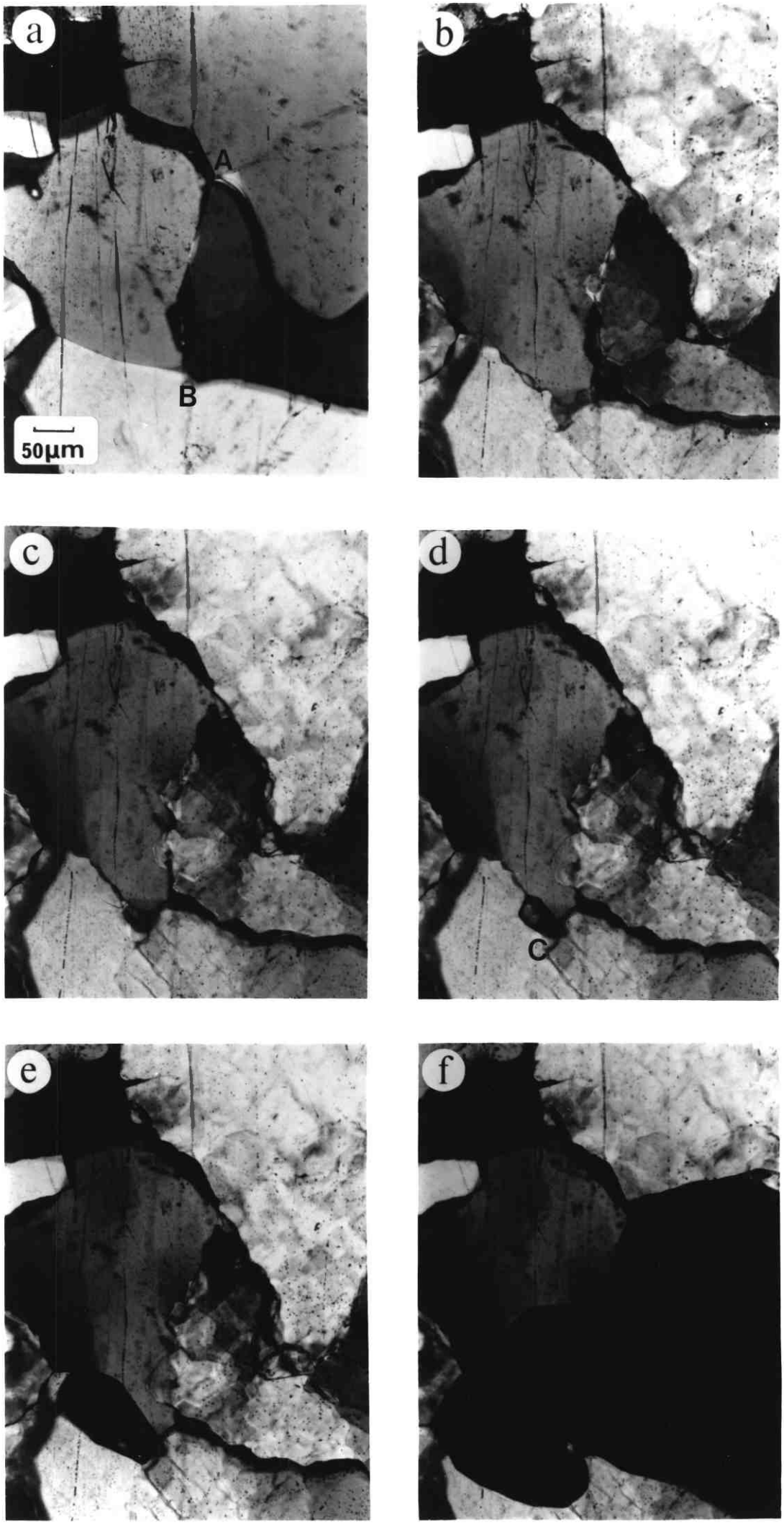
a
A
B
50µm
b
c
d
C
e
f

Conditions of temperature and strain rate under which rapid migration of dynamically recrystallized grain boundaries occur are shown in figure 3.6. It can be seen that the critical temperature for rapid migration is only weakly dependent on strain rate.

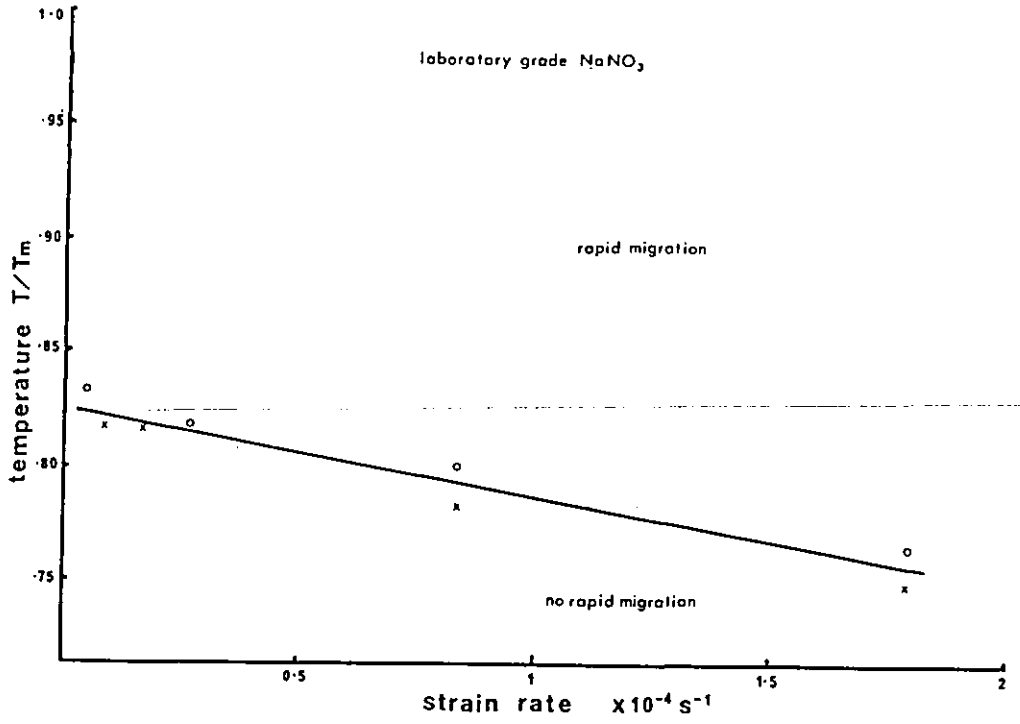

Figure 3.6.

Critical curve between domains of rapid migration and no rapid migration for laboratory grade $NaNO_3$

The microstructure resulting from the rapid growth of dynamically recrystallized grains is one of very large grains. However the process, particularly at higher temperatures, is cyclic. As the large recrystallized grains deform they develop a substructure, which increases in misorientation to form new grains, and ultimately rapid growth occurs again.

3.1.4 Grain Boundary Sliding

Evidence of grain boundary sliding during deformation was observed at the higher temperatures, although in the large grained samples used, it did not contribute greatly to the total strain. Grain boundary sliding could be detected by observing offsets in the rows of small bubbles which were occasionally present between the sample and the pyrex discs. An offset in a row of bubbles indicating grain boundary sliding is shown in figure 3.7.

Figure 3.7 Grain Boundary Sliding at 300°C

(a) before deformation rows of bubbles are continuous across the grain boundary

(b) offsets in rows of bubbles indicating grain boundary sliding

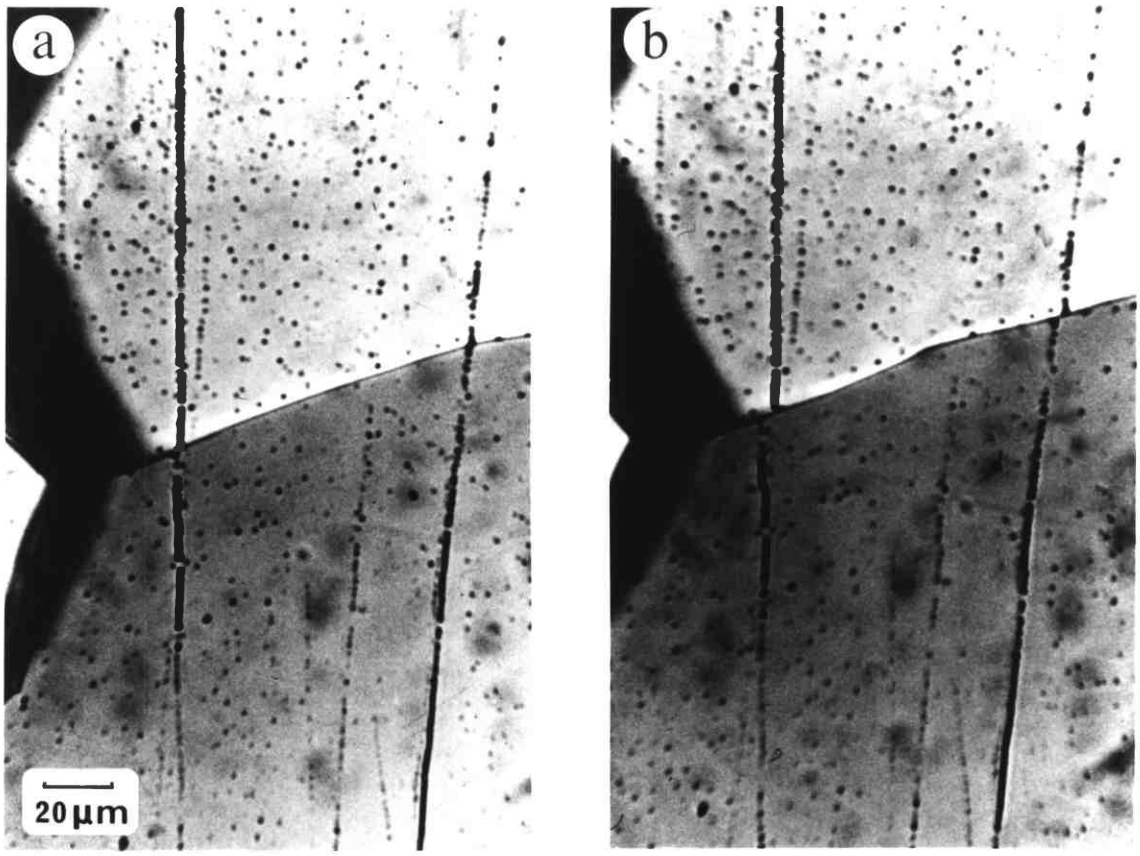
a
20 µm
b

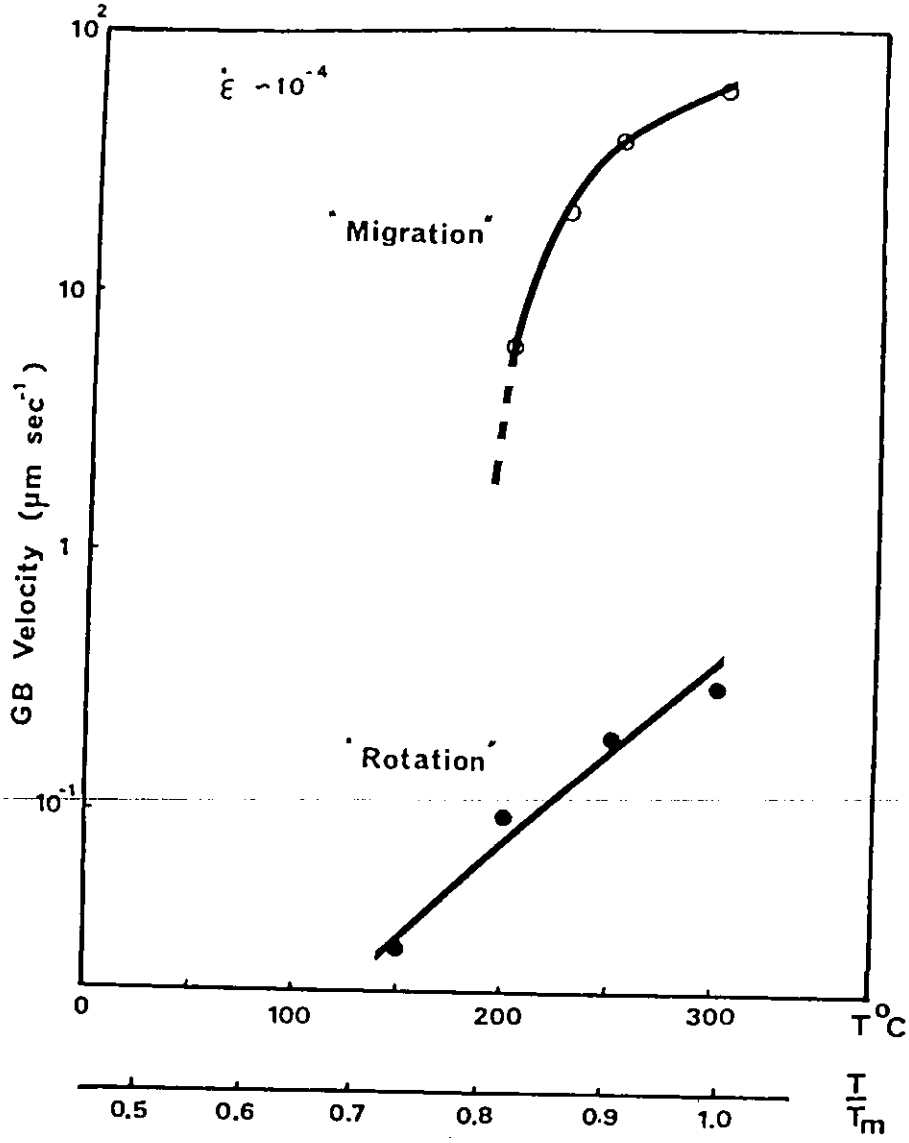

Figure 3.8.

Grain boundary velocity as a function of temperature

3.1.5 GROWTH OF DYNAMICALLY RECRYSTALLIZED GRAINS

As described in sections 3.1.2 and 3.1.3 the dynamically recrystallized grains can grow slowly at all temperatures, but above a critical temperature some grains could grow rapidly, resulting in a large final grain size. However, not all grains formed above the critical temperature grew rapidly. Some did not grow at all, while others grew slowly until they were consumed by rapidly migrating boundaries. At high temperatures both types of growth were observed in the same sample, which enabled direct comparisons of the two rates of growth. For example, a specimen was deformed at 275°C and the development of the microstructure was recorded on cine film. Subsequent analysis of the film revealed that some grains grew at a rate up to $1\mu ms^{-1}$, increasing their size several fold, while other grains had growth rates up to $30\mu ms^{-1}$, increasing their size by an order of magnitude. Figure 3.8 shows the grain boundary velocities as a function of temperature, and clearly demonstrates the two growth rates.

The two growth rates gave rise to two dynamically recrystallized grain sizes, figure 3.9.

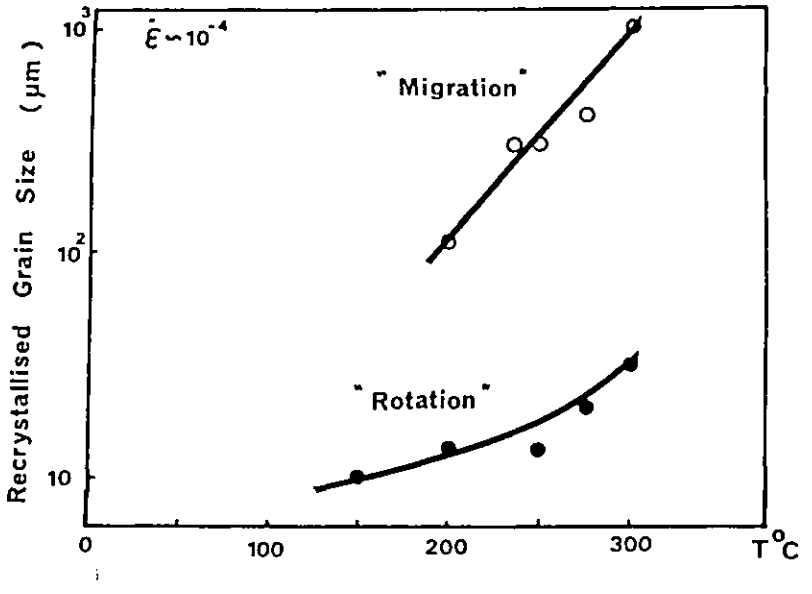

Figure 3.9.

Two dynamically recrystallized grain sizes resulting from the two growth rates

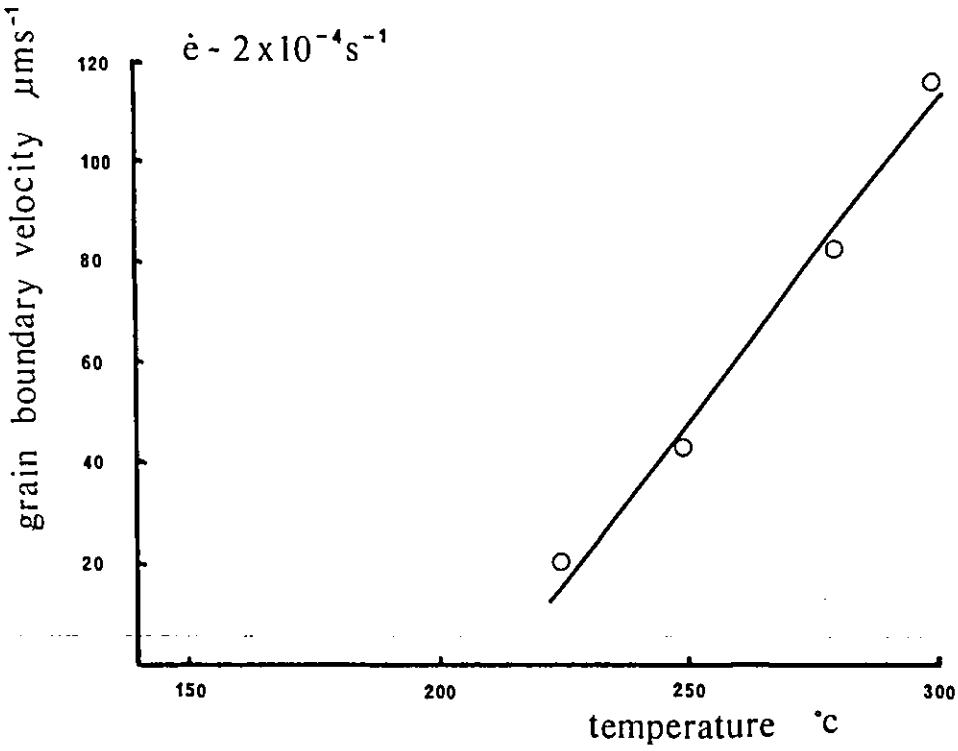

Figure 3.10.

Rapid grain boundary velocity as a function of temperature for laboratory grade sodium nitrate

The rate of rapid growth is strongly dependent on temperature, as shown in figure 3.10.

A small change in temperature caused a marked difference in the maximum velocity of the migrating boundary. Maximum recorded velocities are used in figure 3.10 as there is a considerable range of velocities over which different boundaries migrate, and a migrating boundary rarely moved with a constant velocity. The velocity of a boundary would change greatly as it moved consuming the microstructure around it. If the boundary encountered a change in microstructure, then its velocity would change.

However, one feature was common to a great many migrating boundaries, and that was a slow tail off in velocity just before the grain stopped growing. An example of this is shown in figure 3.11. This is an unusually good example, as the migrating grain boundary was moving into a very large grain and stopped before it reached a grain boundary. Also the grain being consumed had developed a fairly uniform substructure. Initially the velocity of the boundary was great (upper curve figure 3.8), but as the new grain was strained, the velocity decreased. Below a critical value it can be seen that the velocity decreased sharply to a very low value, corresponding to the lower curve in figure 3.8. Hence it is possible for the same migrating boundary to exhibit the two rates of migration.

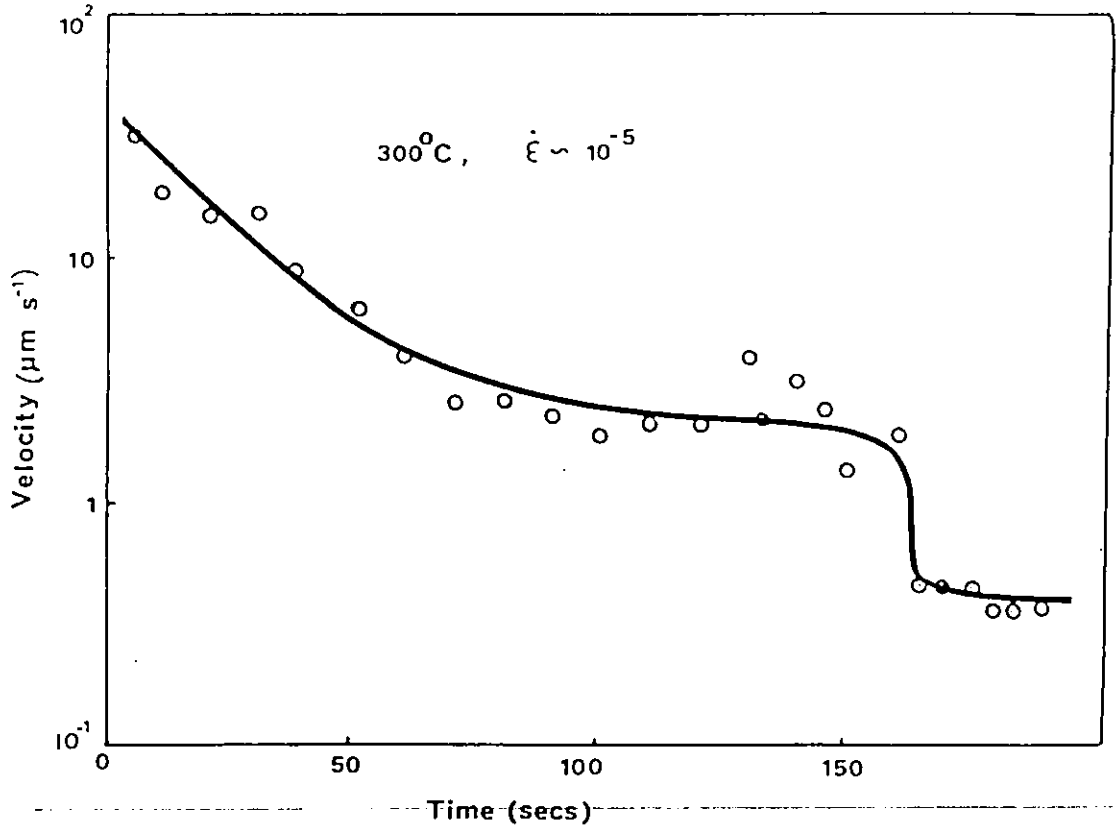

Figure 3.11.

The change in velocity of a migrating grain boundary during deformation at 300°C

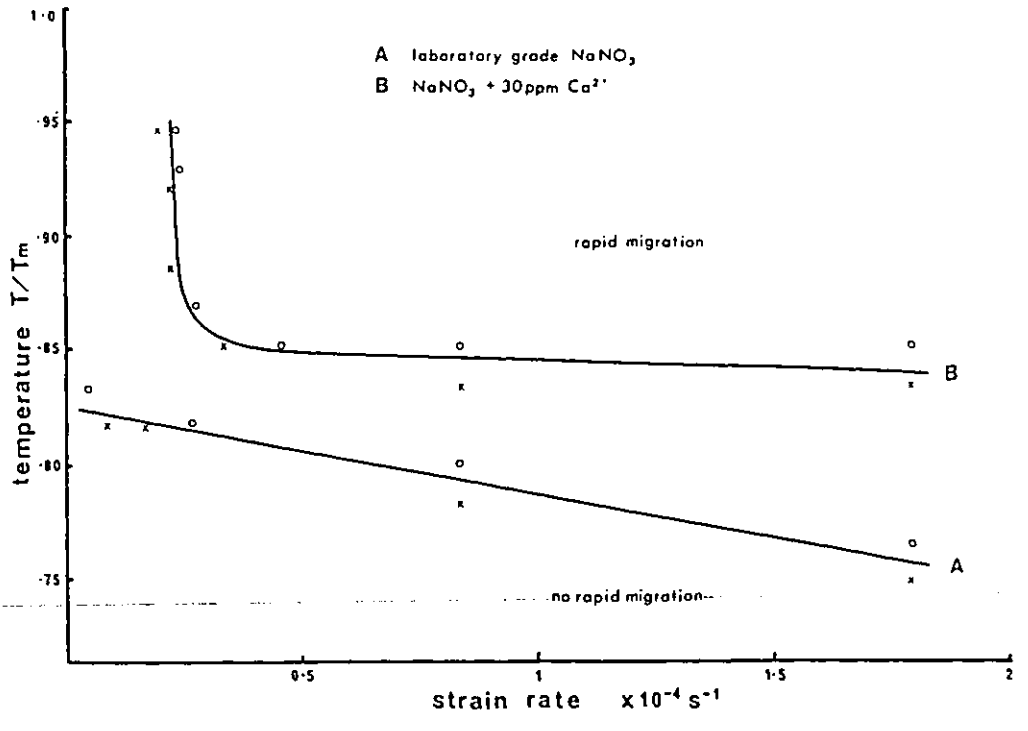

Figure 3.12.

Critical curve between the domains of rapid migration and no rapid migration for both laboratory grade $NaNO_3$ and a sodium nitrate alloy containing 30ppm Ca^{2+}

3.1.6 EFFECTS OF IMPURITY ADDITIONS

The rapid migration phenomenon was found to be very sensitive to the impurity content of the material, particularly divalent impurity ions. An alloy containing 1 wt % $Ca(NO_3)_2$ was produced and the rapid migration was completely suppressed. An alloy containing .01wt%$Ca(NO_3)_2$ did exhibit rapid migration, but the transition temperature was raised, as shown in figure 3.12.

Although the onset of rapid migration did not occur until a higher temperature, the rate of rapid migration was not diminished by the presence of the impurity. In fact the migration rate tended to be slightly greater at the lower temperatures, as shown in figure 3.13.

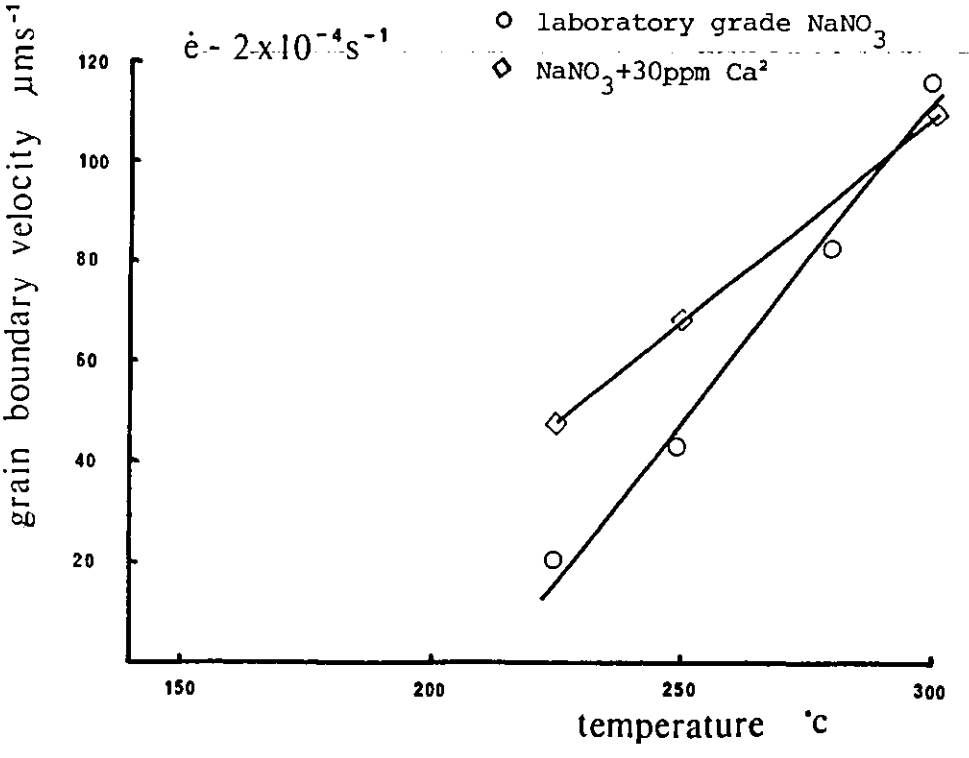

Figure 3.13.

Rapid grain boundary velocity as a function of temperature for laboratory grade $NaNO_3$ and $NaNO_3$ containing 30ppm Ca^{2+}

The suppression of the rapid migration which dominated the microstructure at higher temperatures, enabled the observation of the slow growth of the small dynamically recrystallized grains to be observed more easily.

Figure 3.14 shows the development of microstructure with strain at 275°C for the 0.01wt% $Ca(NO_3)_2$ alloy. Features of note are: the slow (0.1 μms^{-1}) but extensive growth of the dynamically recrystallized grain, A, the progressive change in contrast exhibited by the dark grain, B, in figure 3.16c; and the development of subgrains along grain boundaries (figure 3.14d) into dynamically recrystallized grains (figure 3.14f).

Although the rate of slow growth of 0.1μms^{-1} recorded from figure 3.14 is less than the 1μms^{-1} recorded for laboratory grade sodium nitrate deformed under the same conditions, cine film analysis of the calcium alloy at 300°C and 275°C indicate that there is no marked difference between the slow growth rates for the two materials.

Figure 3.14

In situ sequence of 0.01 wt% $Ca(NO_3)_2$
alloy at 275°C
strain rate = 2.3 x $10^{-5}s^{-1}$
approximate strain

(a) 0
(b) 0.06
(c) 0.11
(d) 0.14
(e) 0.18
(f) 0.26

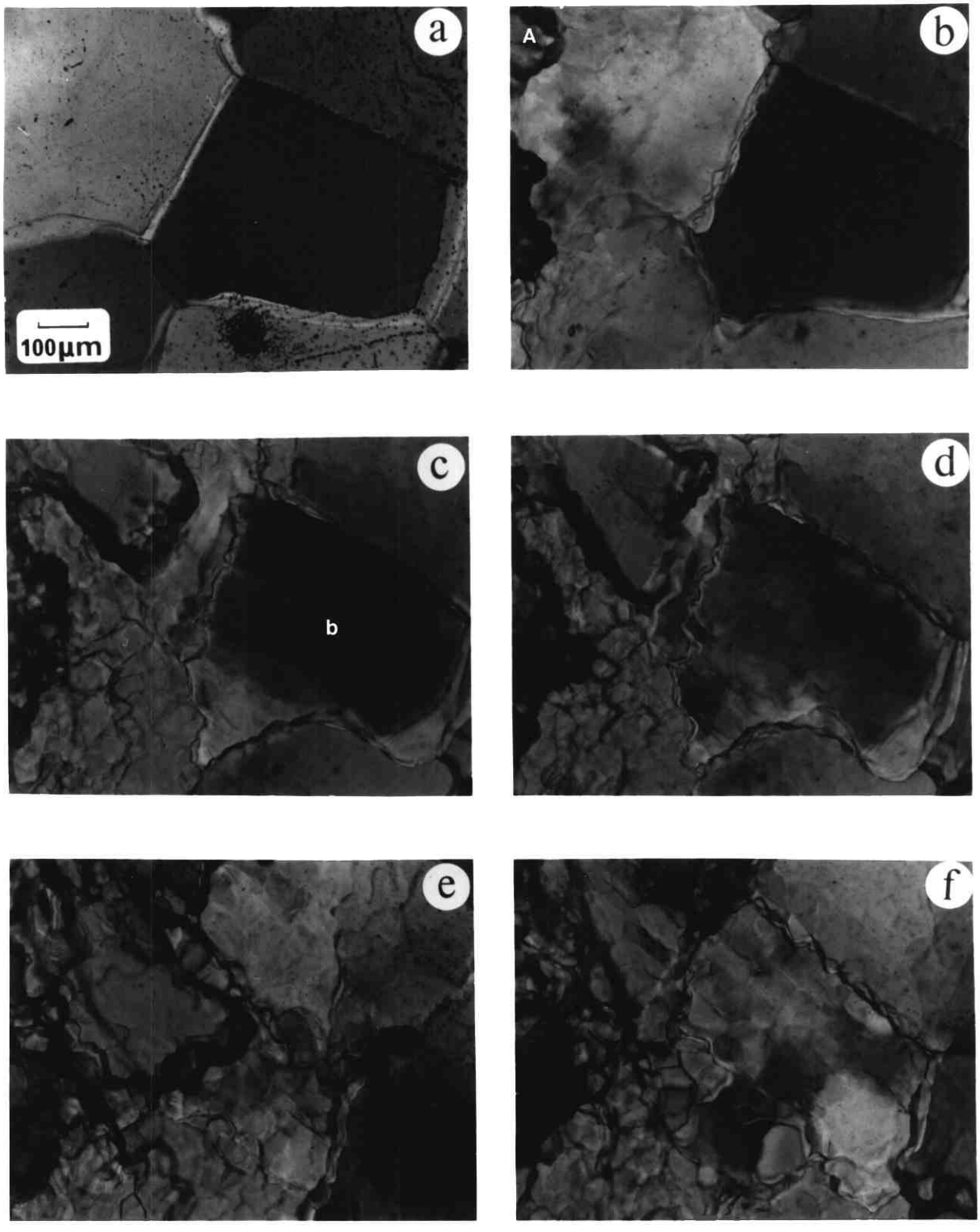
a
100µm
A
b
c
b
d
e
f

3.1.7 EFFECTS OF INCREASING PURITY

In addition to in situ experiments on B.D.H. 'Laboratory grade' sodium nitrate, further tests were performed on B.D.H. 'Analar' and Johnson Matthey Chemicals 'Specpure' sodium nitrate; the minimum assay for each is given in table 3.1.

TABLE 3.1

Material	Minimum assay
Laboratory grade	98%
Analar	99.5%
Specpure	99.999%

Overall there was little difference in behaviour between Analar and Laboratory grade sodium nitrate. The transition temperature for the onset of rapid migration was slightly raised for the Analar material, as shown in figure 3.15.

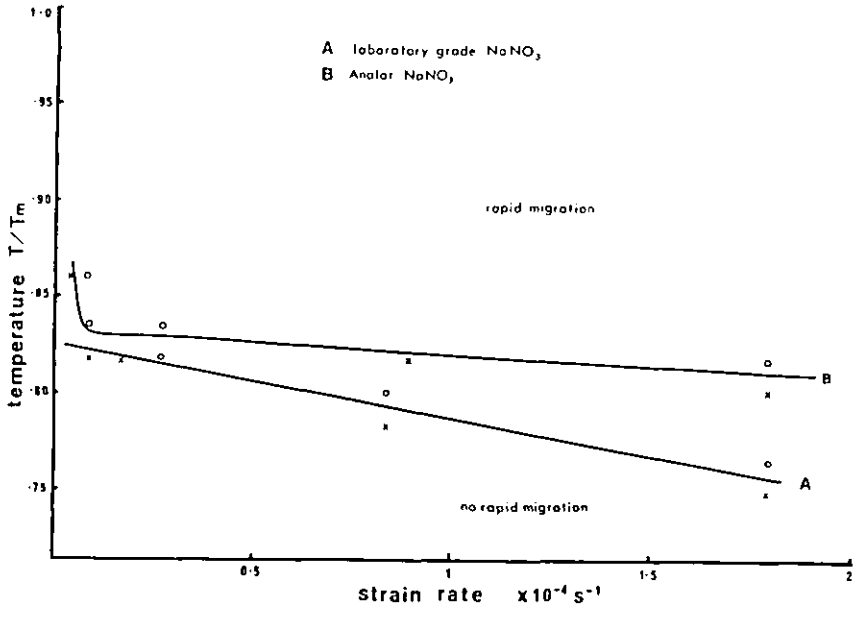

Figure 3.15.

Critical curves between the domains of rapid migration and no rapid migration for both laboratory grade and Analar $NaNO_3$

However, there were a few differences in behaviour at the very high temperatures investigated (300°C, 0.99 Tm). The original grain boundaries of the 'Analar' material exhibited a greater tendency for small rearrangements at the onset of deformation, and tended to align at 45° to the applied stress. A greater amount of grain boundary sliding was observed, and the grain boundaries of the dynamically recrystallized grains also aligned themselves at 45° to the stress axis. All of these features can be seen in the sequence of migrographs of figure 3.16.

Figure 3.16

In situ sequence of Analar sodium nitrate, 300°C.

(Strain rate = $1.8 \times 10^{-4} s^{-1}$)

(a) unstressed sample

(b) onset of deformation. Note the result of grain boundary sliding at A

(c) original grain boundaries aligned at 45° to stress axis which is parallel to the micron marker. (Strain = 0.162)

(d) A rapidly migrating grain boundary consumes deformed material. (Strain = 0.164)

(e) Second migrating boundary. (Strain = 0.183)

(f) Note the alignment of the boundaries to 45° to the stress axis. (Strain = 0.194)

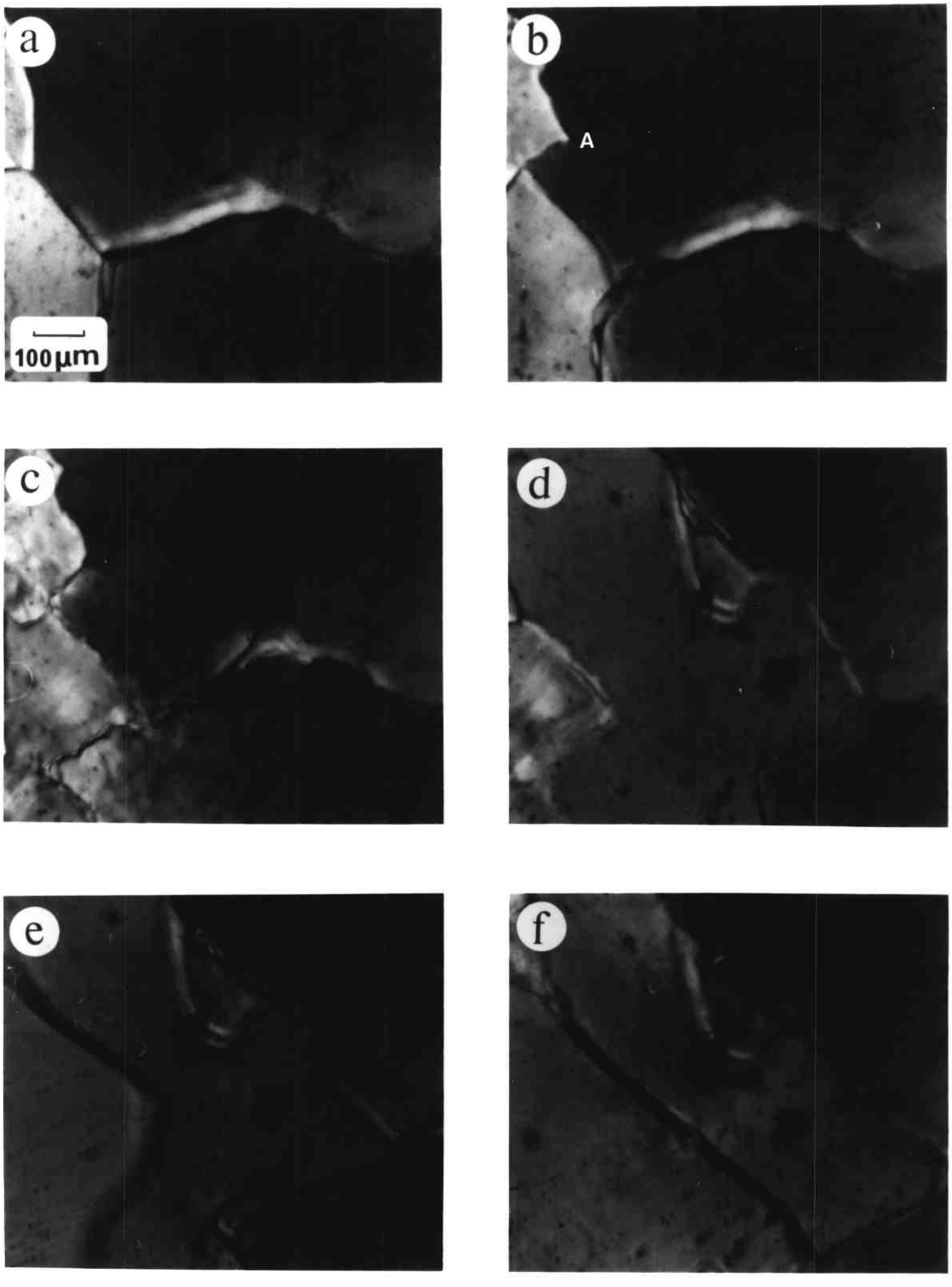
a
100µm
b
A
c
d
e
f

Preliminary experiments using 'Specpure' sodium nitrate from Johnson Matthey Chemicals Limited demonstrated a further increase in the mobility of the original grain boundaries, which greatly affected the mechanisms of dynamic recrystallization. When subgrains started to misorientate at grain boundaries, the boundary would migrate in such a way as to remove the misorientated region. This did not generally result in a highly convoluted boundary, instead, parts of the boundary would bow out slightly in one direction removing subgrains, and then bow back in the opposite direction, maintaining the general position of the boundary. This led to a slow oscillatory movement of the boundary, which could be most clearly seen in the cine film recordings. However, figure 3.17 does show the movement of a grain boundary as the sample is deformed.

Figure 3.17

In situ sequence of 'Specpure' sodium nitrate, 300^{o}C
(Strain rate = 1.4 x 10^{-5}s^{-1})
Sequence shows the oscillatory movement of a grain boundary during deformation.

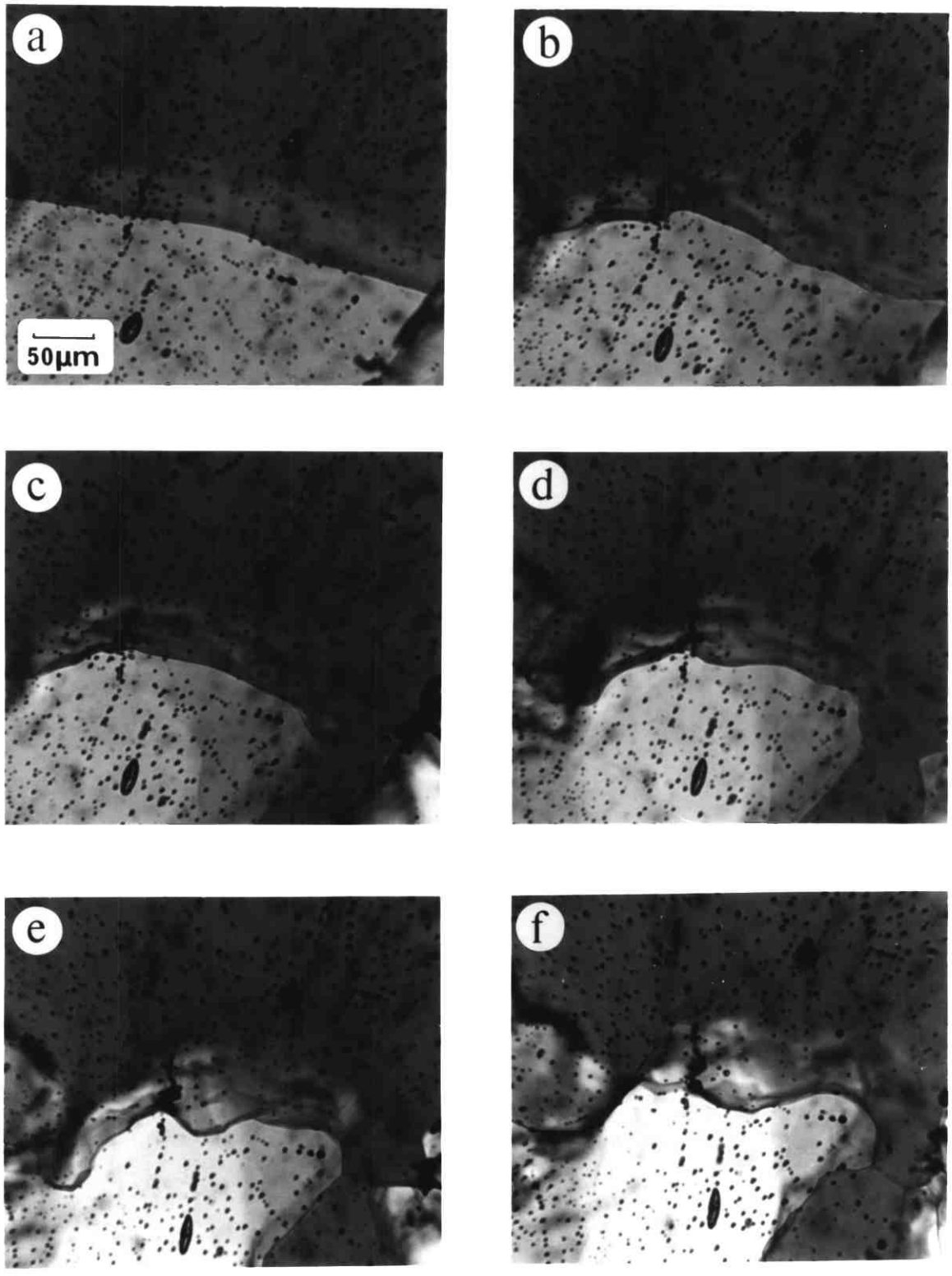
a
50µm
b
c
d
e
f

Although this movement of grain boundaries removed misorientated subgrains, dynamic recrystallization was observed in 'Specpure' sodium nitrate samples. At strain rate around $10^{-4}s^{-1}$, recrystallized grains originated at the edge of the sample next to the moving ram, and rapid boundary migration of the recrystallized grains into the sample was observed. Figure 3.18 shows a marked difference in the rate of rapid migration between the 'Specpure' and 'laboratory grade' sodium nitrate.

Figure 3.18.

Rapid grain boundary velocity as a function of temperature for laboratory grade ○ and 'specpure' $NaNO_3$ ◇

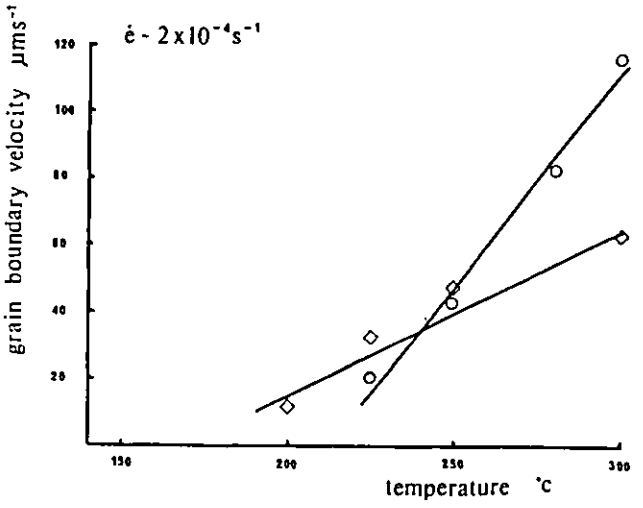

At lower strain rates around $10^{-5}s^{-1}$ and at high temperatures ($300^{\circ}C$), dynamically recrystallized grains formed within pronounced bulges of the grain boundaries, as seen in figure 3.19.

Figure 3.19 In situ sequence of 'Specpure' sodium nitrate, $300^{\circ}C$ (Strain rate = $10^{-5}s^{-1}$)

(a) unstressed sample

(b) small bulges of original grain boundary

(c) one bulge becomes more pronounced

(d) the very tip of the bulge misorientated and a high angle boundary is now sweeping back, consuming the material within the bulge

(e) slow growth of new grain

(f) final recrystallized grain at the grain boundary

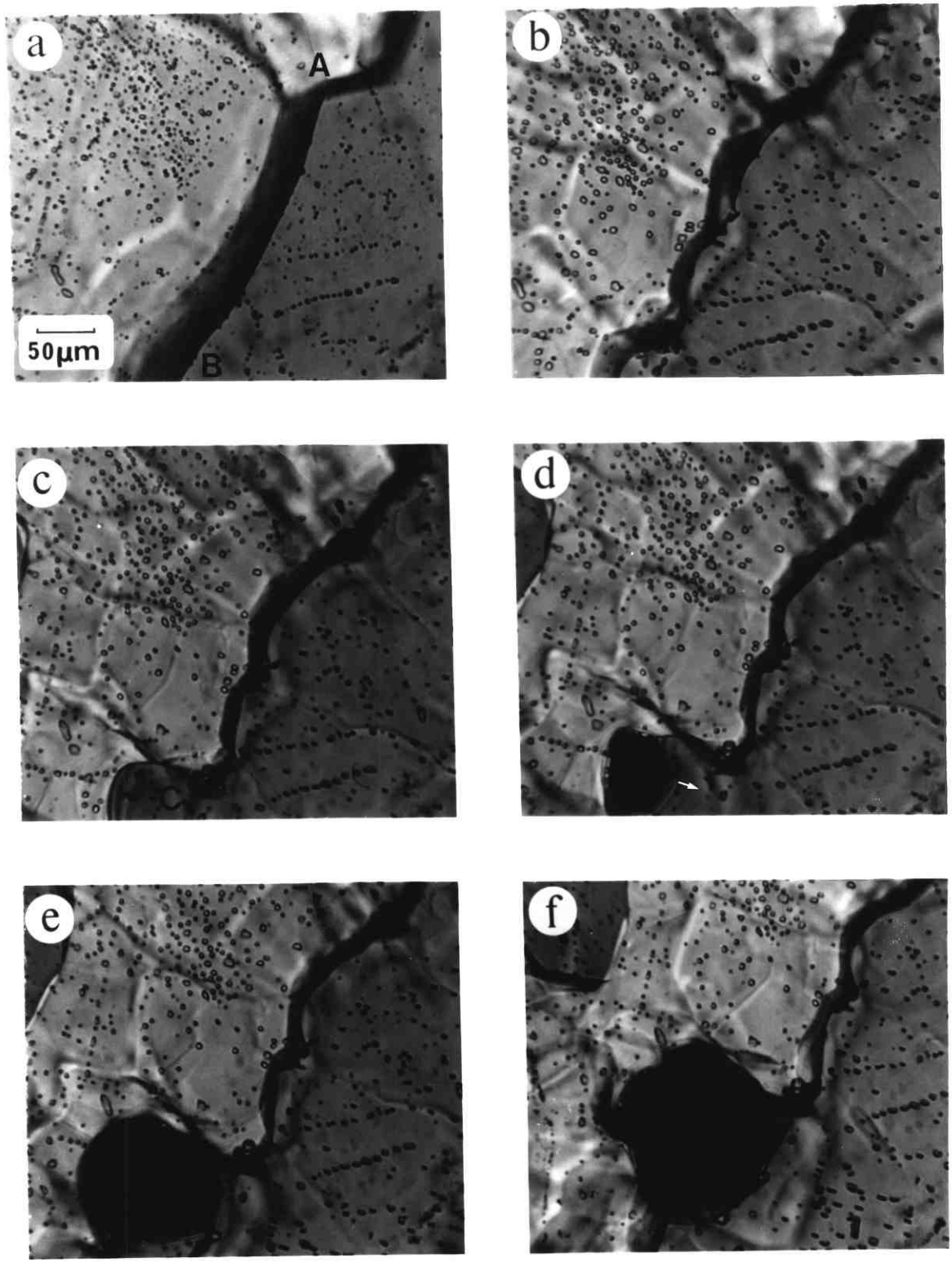
a
A
B
50µm
b
c
d
e
f

3.2 COMPRESSION TESTING OF BULK SAMPLES

The mechanical behaviour of laboratory grade sodium nitrate was determined from compression tests on bulk samples. In addition to stress-strain data at various temperatures and strain rates, other mechanical parameters were also determined, including the strain rate sensitive stress exponent n, and the activation energy for plastic flow. Detailed optical analysis of the microstructures was possible from thin sections prepared from the bulk samples, and relationships between the applied stress and microstructural features were assessed. Use of a geological universal stage enabled grain and subgrain orientation information to be determined from the thin sections.

All bulk samples were cylindrical compression specimens 10mm in diameter and 17mm long, with a grain size of 500μm.

3.2.1 MECHANICAL BEHAVIOUR

3.2.1a Instron Tests at Atmospheric Pressure

A high temperature compression cage mounted on an Instron machine was used to deform samples to true strains up to 0.7, at temperatures between 100°C and 300°C. Attempts to deform samples below 100°C failed due to fracturing of the samples. Three strain rates were used, and the results of the tests for each strain rate are shown in figures 3.20 - 3.22. Figure 3.20 shows the stress-strain curves obtained at a strain rate of $7 \times 10^{-3} s^{-1}$. After a strain of 0.1, the flow stress remains essentially constant, although at the higher temperatures there is a distinct peak in the curve. Specimens tested at lower strain rates showed similar behaviour, although the initial peak in the curves was more pronounced, figures 3.21 and 3.22 Due to fracturing of samples at 100°C during testing at the two higher strain rates, the only available data at 100°C is that obtained at the lowest strain rate of $7 \times 10^{-6} s^{-1}$.

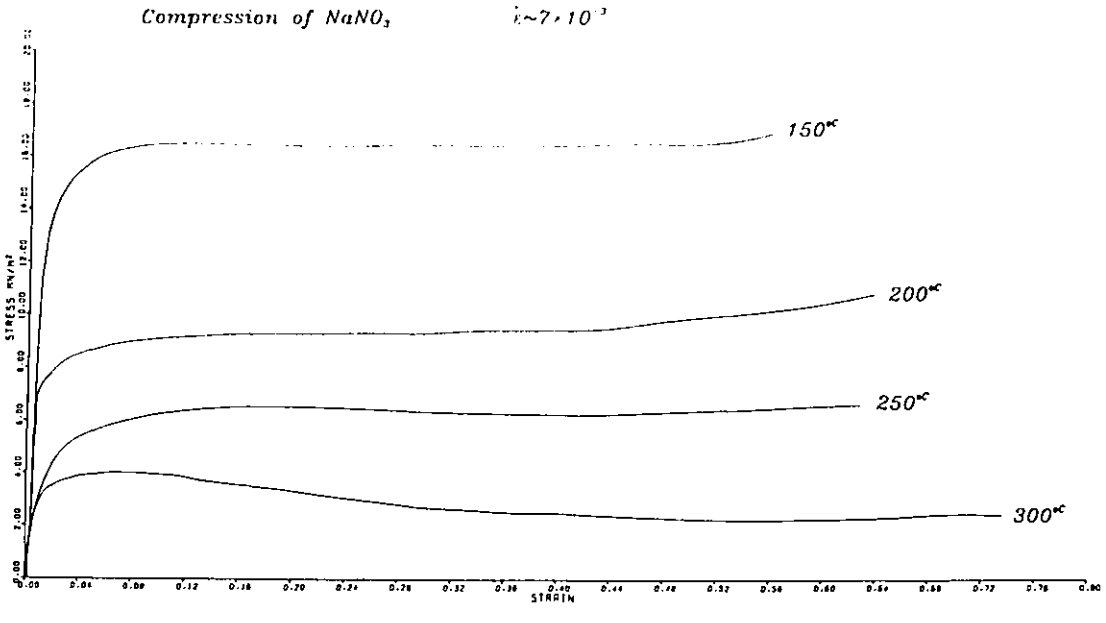

Figure 3.20.

Atmospheric pressure stress strain curves, strain rate = 7×10^{-3} s^{-1}.

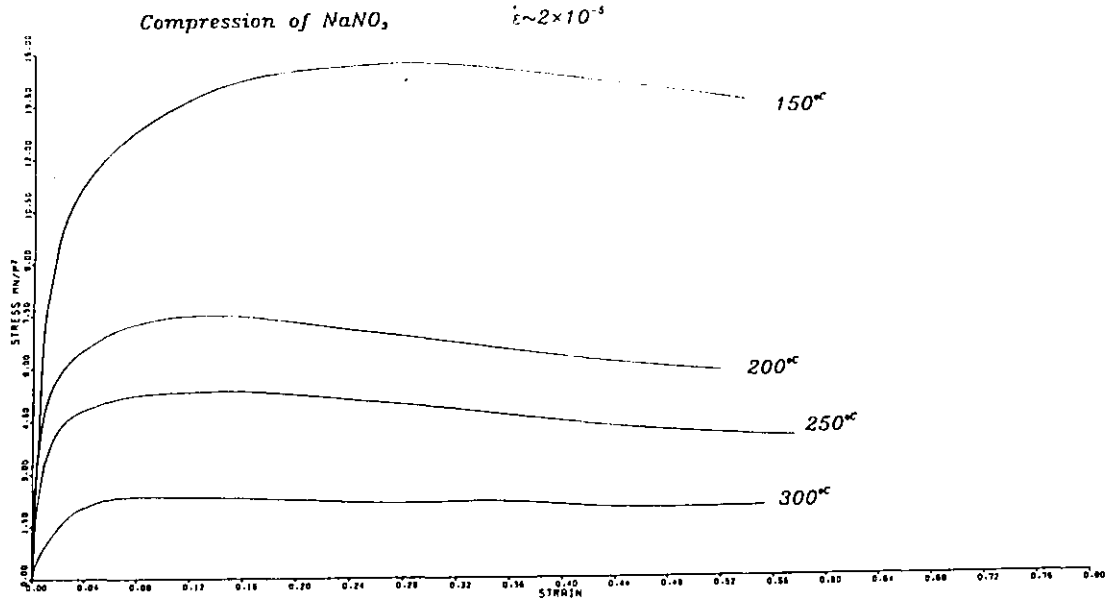

Figure 3.21.

Atmospheric pressure stress strain curves, strain rate = 2×10^{-5} s^{-1}.

Compression of $NaNO_3$

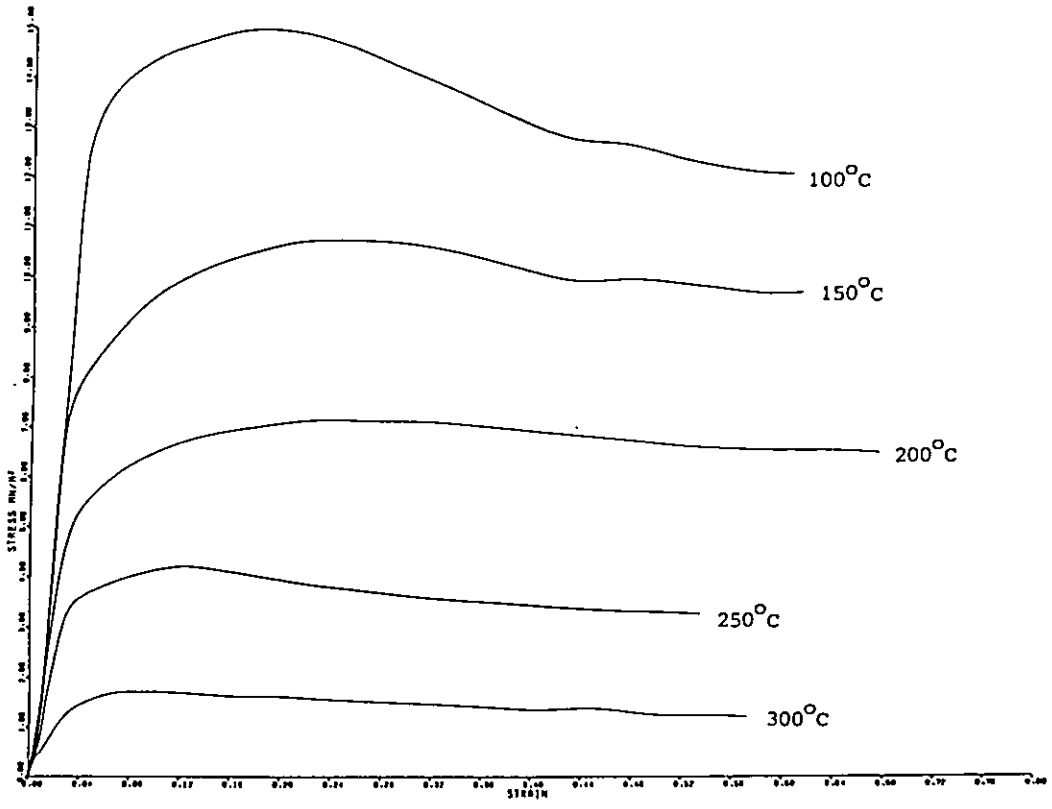

Figure 3.22.

Atmospheric pressure stress strain curves, strain rate = $7 \times 10^{-6} s^{-1}$.

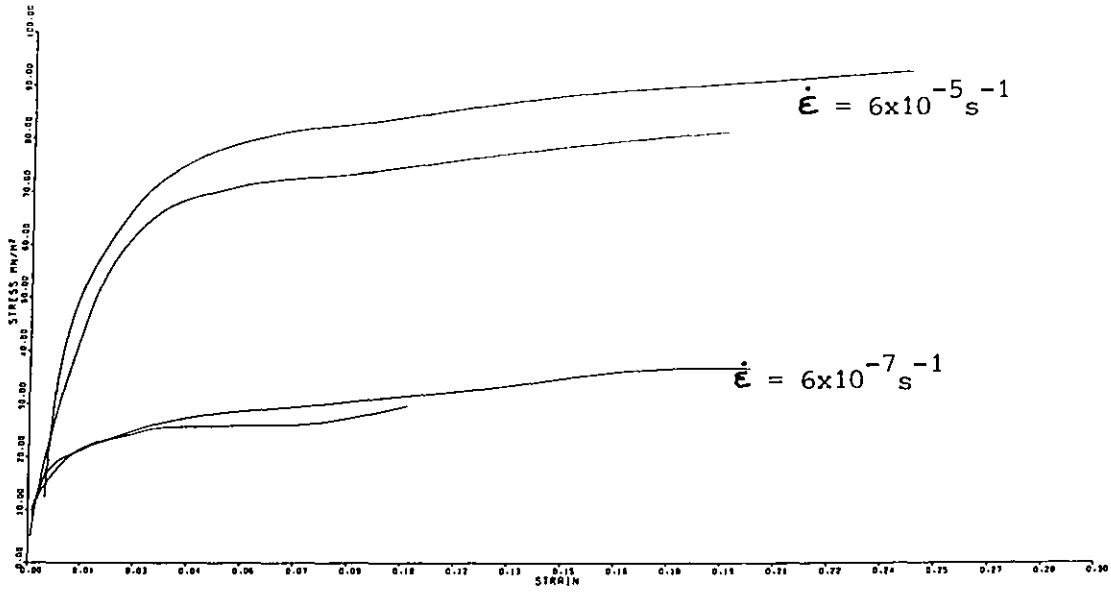

Figure 3.23.

Stress strain curves obtained at 25°C, under a confining pressure of 70MNm^{-2}.

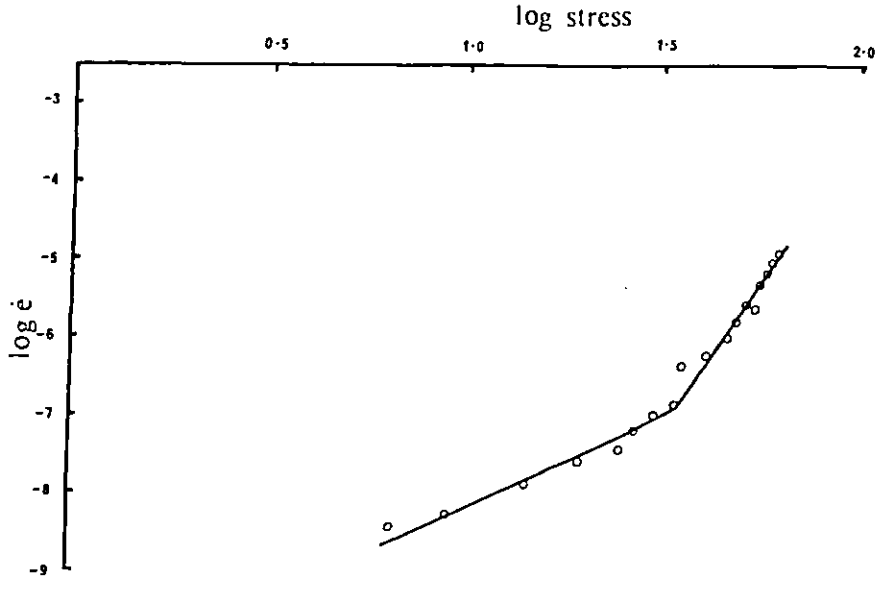

Figure 3.24.

Stress relaxation test at 25°C, under a confining pressure of 70 MNm^{-2}.

TABLE 3.2.

Data for calculating stress exponent n

		$\dot{\epsilon}$	σ/MNm^{-2}	n
Temperature	300°C	4.4×10^{-6}	0.96	
		4.8×10^{-5}	1.96	4.2
		5.2×10^{-4}	3.11	
	250°C	4.98×10^{-6}	3.20	
		6.0×10^{-5}	5.62	4.8
		4.7×10^{-4}	8.22	
	200°C	4.1×10^{-6}	4.40	
		4.9×10^{-5}	7.84	4.3
		3.7×10^{-4}	12.56	
	150°C	5.7×10^{-6}	7.08	
		6.2×10^{-5}	11.20	6.0
		7.4×10^{-4}	16.00	

3.2.1b Tests Under a Confining Pressure

Further tests were carried out at 25°C using a confining pressure of $70MNm^{-2}$ in a hydrostatic test rig by Dr. B.K. Atkinson, who kindly performed the tests and supplied the data for the stress strain graphs shown in figure 3.23 and the stress relaxation test, figure 3.24 The constant strain rate tests at 25°C showed a slight increase in stress with strain, but the stress-strain graphs were essentially very similar to the ones obtained from tests at atmospheric pressure.

3.2.1c Stress Exponent n and Activation Energy Q

In addition to the standard compression tests performed on the Instron, strain rate stepping tests were carried out in order to determine the stress exponent, n. For these tests a sample was deformed at the lowest strain rate until a steady state flow stress was reached, then the strain rate was increased and a new steady state flow stress was achieved before the strain rate was increased again. Each test was performed at a constant temperature, and the results are tabulated in table 3.2.

The stress exponent n was calculated assuming an empirical relationship of the form

$$\dot{\varepsilon} = \sigma^n \exp(-Q/RT)$$

At constant temperature the (-Q/RT) term is assumed to be constant, and the equation can be written

$$\dot{\varepsilon} = B\sigma^n \qquad \text{at constant } T$$

$$\ln \dot{\varepsilon} = n \ln \sigma + \ln B$$

Hence the values of n were determined from the gradients of ln(strain rate) vs ln(stress) graphs, and are tabulated in table 3.2.

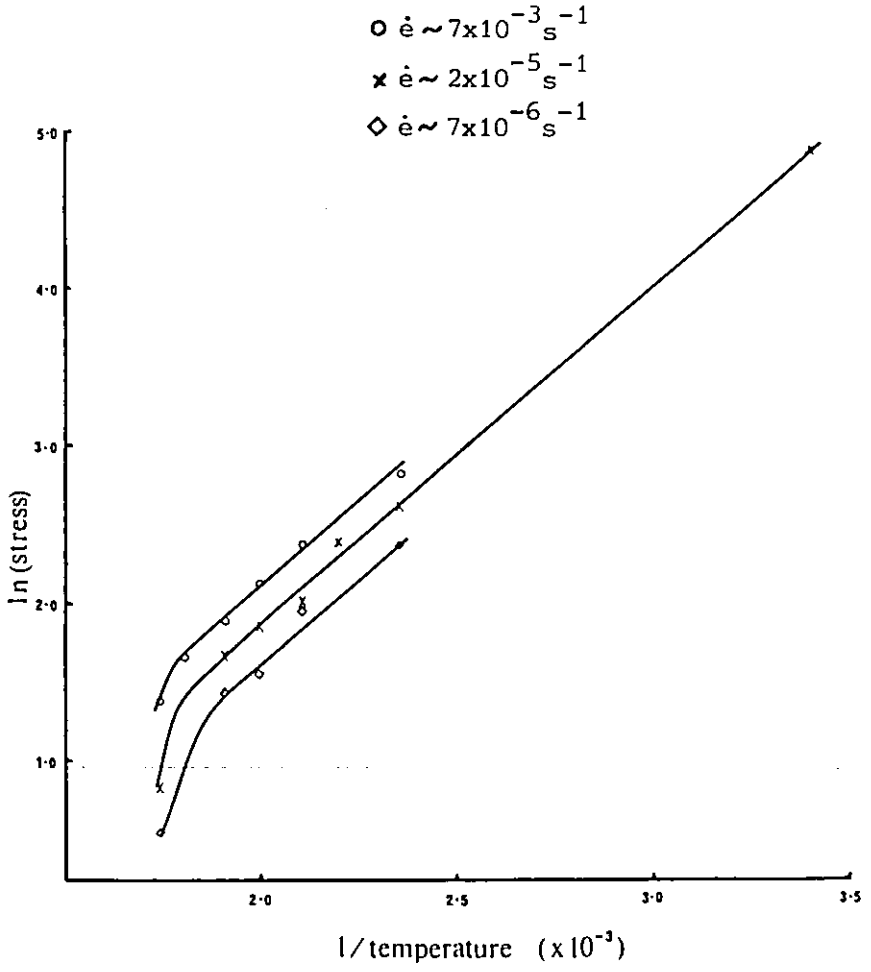

Figure 3.25.

Graph of ln(stress) against 1/temperature

The stress exponent n is approximately constant over the temperature range of 200-300°C, and averages to be 4.4 $\pm$ 0.4, but increases to 6.0 $\pm$ 0.5 at 150°C. Two values of n were obtained from the stress relaxation tests at room temperature, figure 3.24. At strain rates between 10^{-4} and 10^{-7} n = 7.5, and below 10^{-7}, n = 2.3.

The value of the activation energy, Q, for plastic deformation, was determined from the data used in figures 3.20 to 3.22 and the values of n. If the strain rate is constant then the equation can be written

$$C = A\,\sigma^{n}\exp(-Q/RT)$$

$$\ln C = n \ln \sigma + \ln A - Q/RT$$

$$Q/RT = n \ln \sigma + \ln A - \ln C$$

$$1/T = \frac{R\,n \ln \sigma}{Q} + \frac{R}{Q}(\ln A - \ln C)$$

Thus the gradient of the graph of $\ln\sigma$ vs $1/T$ is equal to Q/Rn, from which Q can be found, as R is the universal gas constant and n has already been determined. Graphs of $\ln\sigma$ vs $\frac{1}{T}$ for each of the three strain rates are shown in figure 3.25 (the values of stress used for these graphs were the maximum stress values of the stress strain graphs).

From the gradient of the graphs the value of Q was determined to be $85\pm5\,KJmol^{-1}$ between 20°C and 280°C, with evidence of a significant increase at higher temperatures.

3.2.2. MICROSTRUCTURES

3.2.2.1 Dynamically recrystallized Grain Size and Subgrain Size

Thin sections (5 - 15 μm), prepared from bulk specimens, cut parallel to the compression axis, enabled details of the microstructure to be observed under the polarizing optical microscope.

The microstructures were very similar to those seen during the in situ experiments and confirmed many of the observations presented in section 3.1. Additionally, the subgrains and the small recrystallized grains observed in the thin sections could be resolved in greater detail due to the sections being thinner than the in situ samples.

Observations made on the thin sections from the bulk samples confirmed the two dynamically recrystallized grain sizes observed during the in situ experiments, and are clearly demonstrated in figure 3.26.

In addition to the variation of the dynamically recrystallized grain size with temperature, the grain size relationship with the applied stress was also determined, figure 3.27. Assuming the empirical relationship, $\sigma \propto d^{-n}$, figure 3.28 was plotted to find the values of n for the subgrains and the two dynamically recrystallized grain sizes. Results from the three sets of strain rate tests are combined in figure 3.29 (subgrains) and figure 3.30, (small dynamically recrystallized grains). A similar plot for the large recrystallized grains was not possible due to rapid migration only occurring at the very high temperatures when tests were performed with the lower strain rates. Lowering the strain rate suppressed to onset of extensive growth to high temperatures. For example, at a strain rate of $7 \times 10^{-3} s^{-1}$ extensive growth occurred at $200^{o}C$, but at a strain rate of $7 \times 10^{-6} s^{-1}$, large grains were only observed at temperatures in excess of $250^{o}C$.

From figures 3.29 and 3.30 the values of n for the subgrains and the recrystallized grains were found to be:-

Subgrain size (d)	$\sigma \propto d^{-n}$	$n = 0.85$
Dynamically recrystallized grain size (D)	$\sigma \propto D^{-n}$	$n = 0.65$

It is interesting to note that figure 3.28 indicates that the value of n is the same for both types of dynamically recrystallized grains.

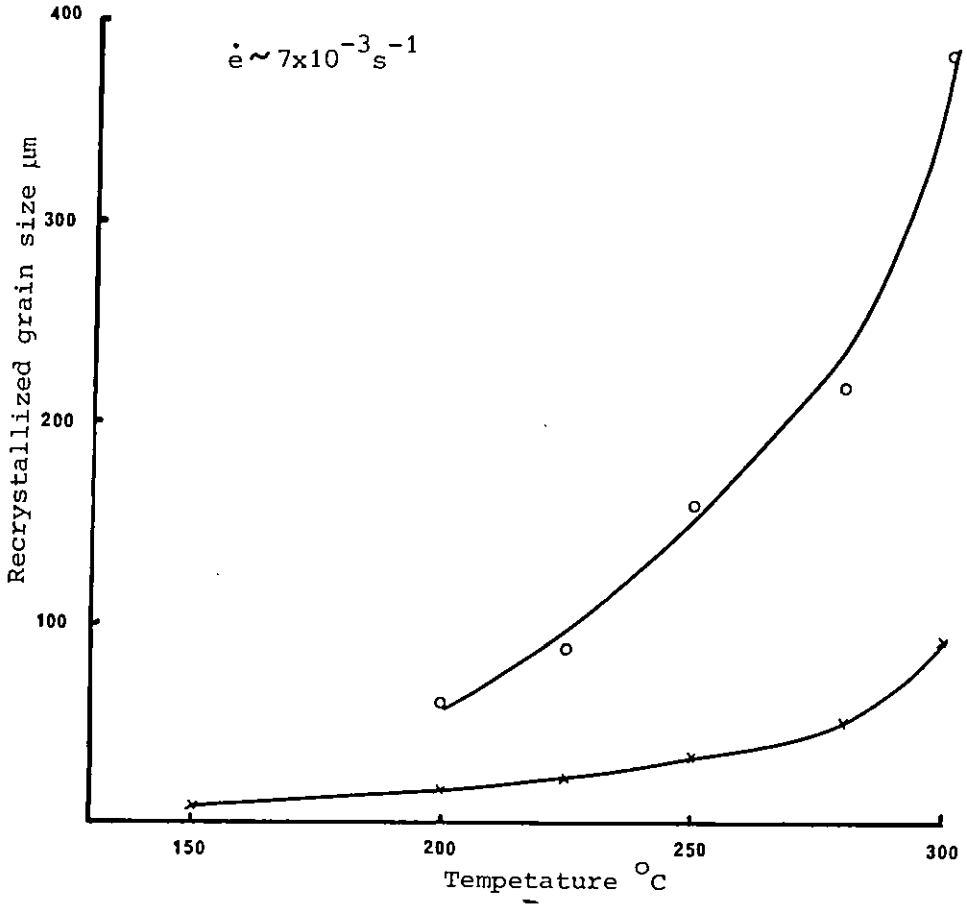

Figure 3.26.

Graph of dynamically recrystallized grain size against temperature

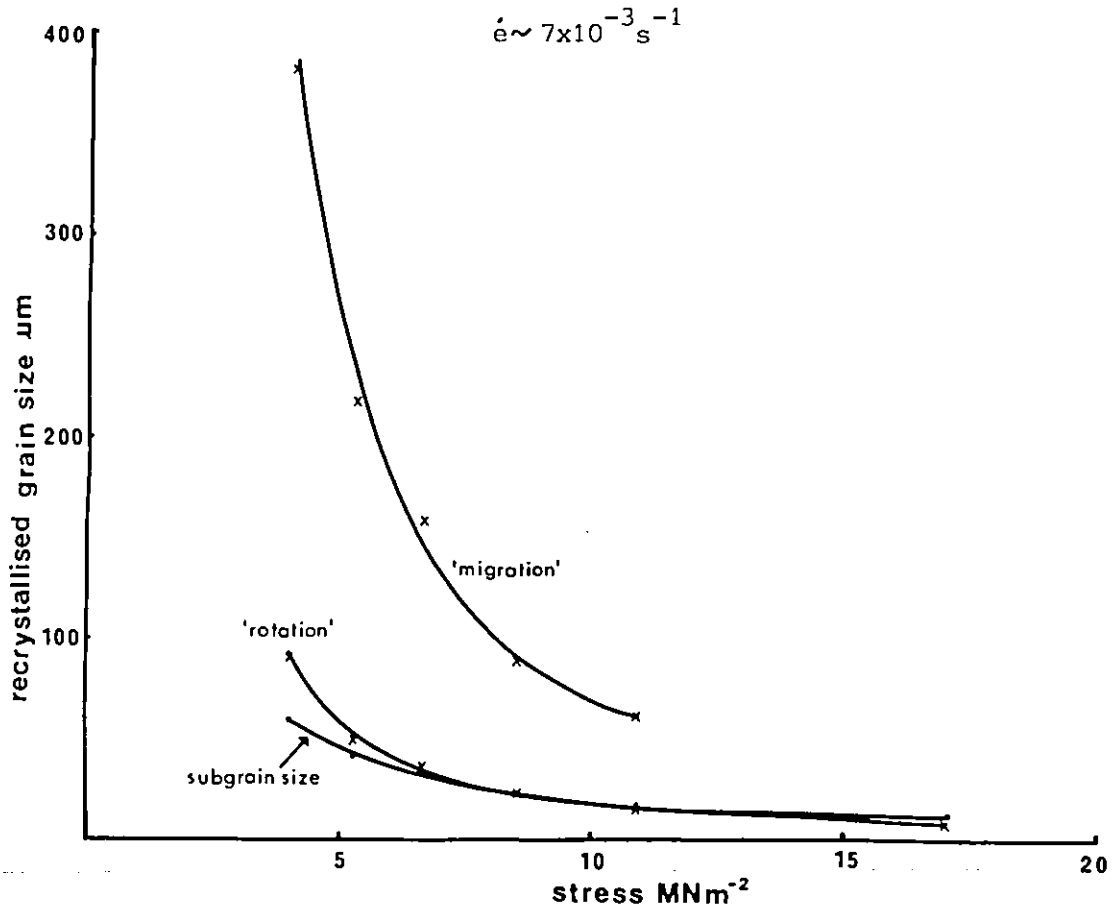

Figure 3.27.

Graph of Dynamically Recrystallized Grain Size against stress

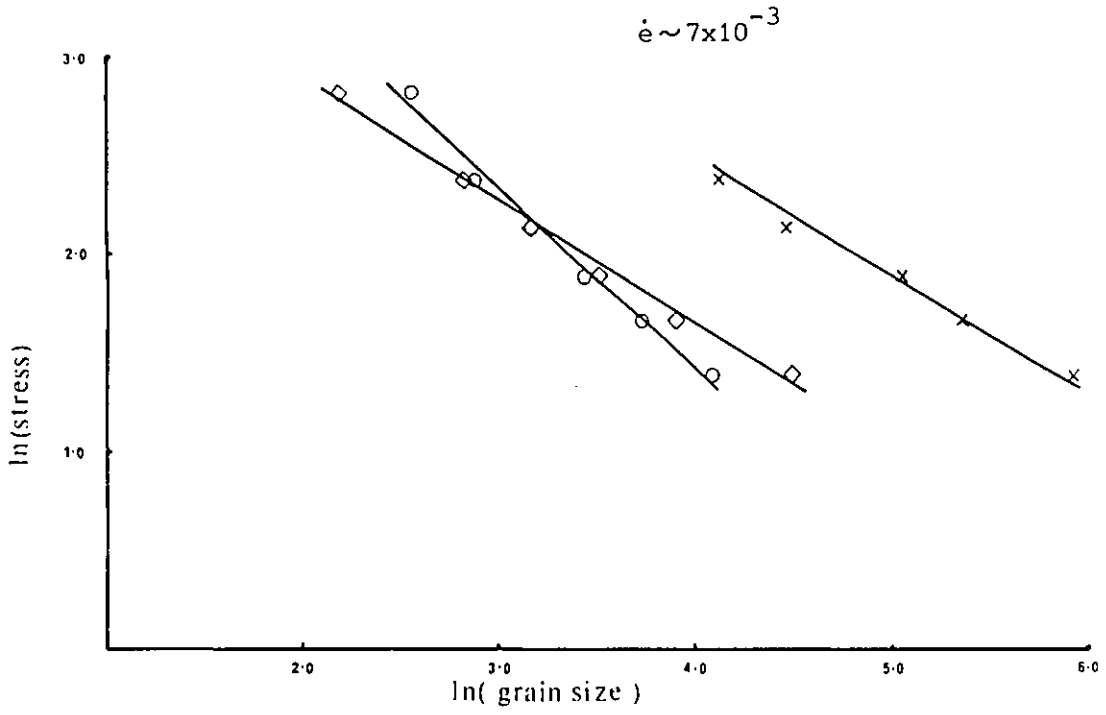

Figure 3.28.

Graph of ln(stress) against:

□ ln(subgrain size)

○ ln(small dynamically recrystallized grain size)

× ln(large dynamically recrystallized grain size)

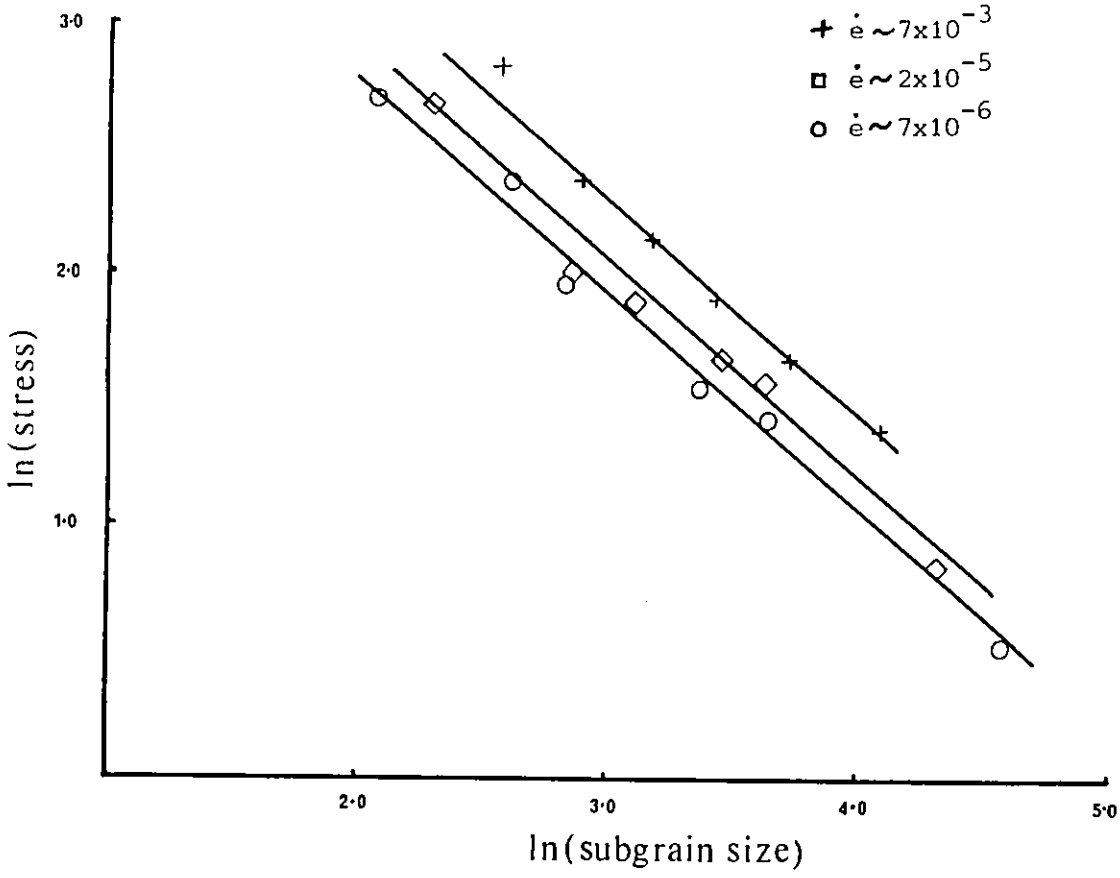

Figure 3.29.

Graph of ln(stress) vs ln(subgrain size)

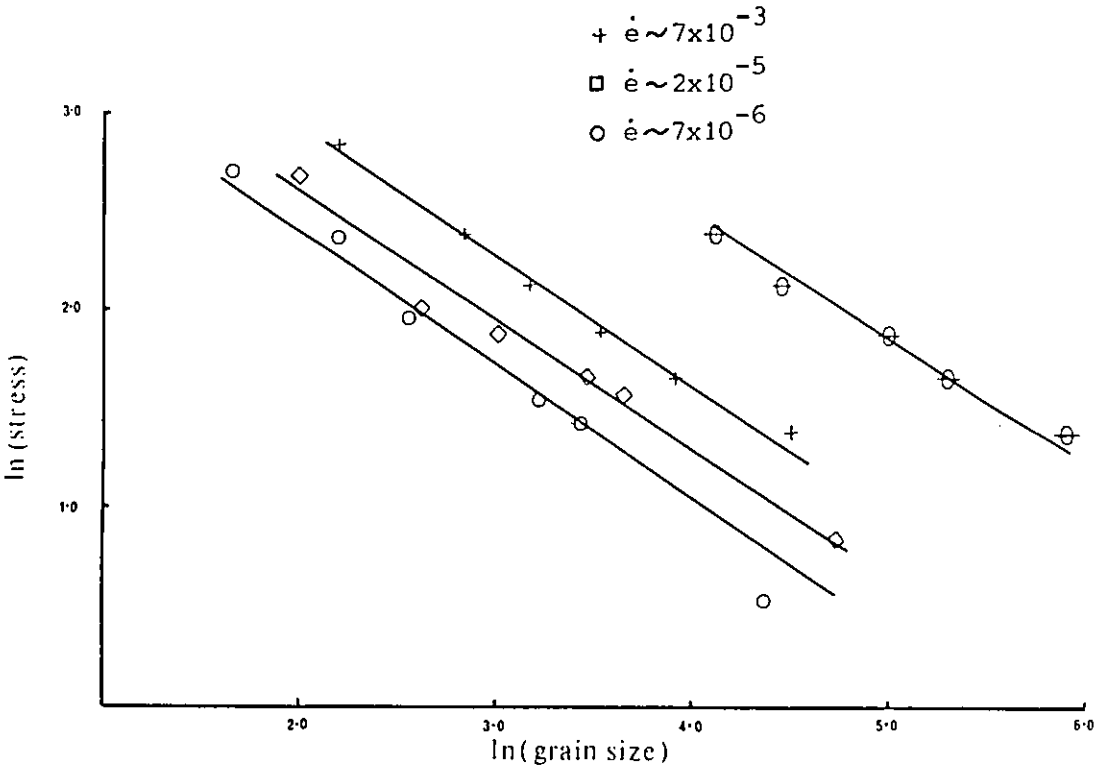

⊖ large dynamically recrystalliized grains ($\dot{e} \sim 7x10^{-3}$)

Figure 3.30.

Graph of ln(stress) vs ln(dynamically recrystallized grain size)

3.2.2.2 Effect of Temperature on Microstructures

The following micrographs of thin sections of bulk samples were prepared after room temperature tests under a confining pressure, and atmospheric tests at higher temperatures. Results from the atmospheric tests are from samples deformed at the lowest strain rate ($7 \times 10^{-6} s^{-1}$), as the larger subgrains could be more easily studied when using an optical microscope.

A summary of the development of microstructure with temperature between 100°C and 300°C is shown in figure 3.31.

Figure 3.31 Development of microstructure with temperature

Each sample was taken to the same strain of 0.6 at a strain rate of $7 \times 10^{-6} s^{-1}$ and photographed at the same magnification.

(a)	100°C	Very inhomogeneously deformation microstructure containing elongated grains with deformation banding
(b)	150°C	Again elongated grains containing bands of alternating light and dark subgrains
(c)	200°C	Fewer, broader deformation bands
(d)	225°C	More homogeneous deformation structure with poligonised grains
(e)	250°C	Large changes in contrast between subgrains, particularly at grain boundaries
(f)	300°C	Internal substructure of very large dynamically recrystallized grain

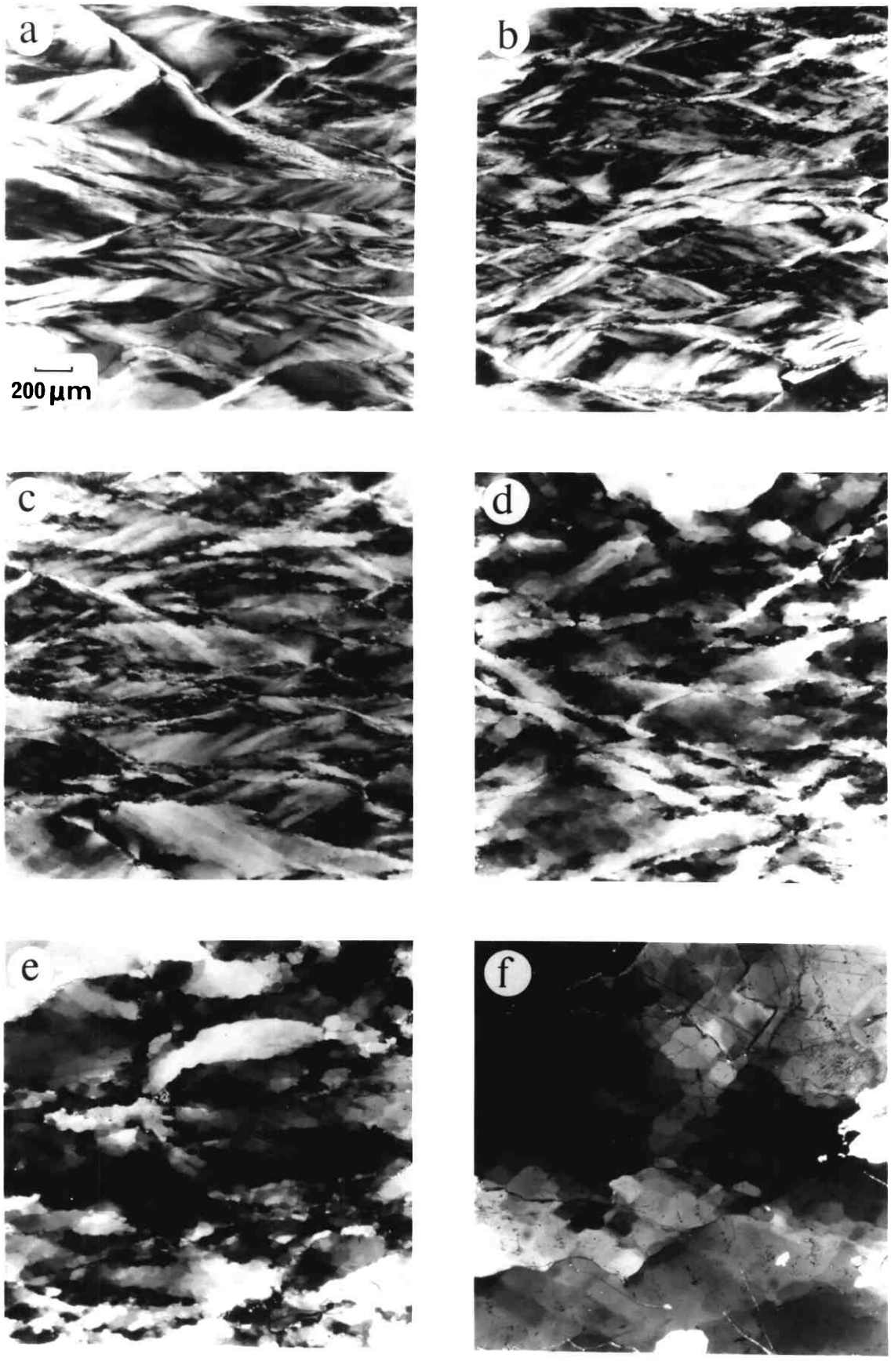
a
200 µm
b
c
d
e
f

Room Temperature Tests Under a Confining Pressure

After deformation at room temperature, lenticular deformation twins were observed, particularly at the edges of the specimens, figure 3.32b. The crystallography of the twins, as determined from the orientation of the C-axis, are consistent with those found for calcite. Two types of twins reported to occur in calcite were found in Sodium Nitrate, with changes in the c axis orientation of 35^{o} and 60^{o} .

Details of the fine deformation structure within the other grains could not be resolved using an optical microscope. A noticeable feature of the microstructure was the presence of large, straight sided grains, which contained no observable deformation features, figure 3.32a. The size of these grains increased in specimens deformed to higher strains. Such grains were never observed in specimens deformed at atmospheric pressure at higher temperatures. It was concluded that these grains had formed by static recrystallization following the tests under a confining pressure.

Figure 3.32 Micrographs of sodium nitrate deformed at $20^{o}C$

Strain = 0.25

Strain rate = $6.4 \times 10^{-3} s^{-1}$

(a) large, straight sided statically recrystallized grains

(b) lenticular twins

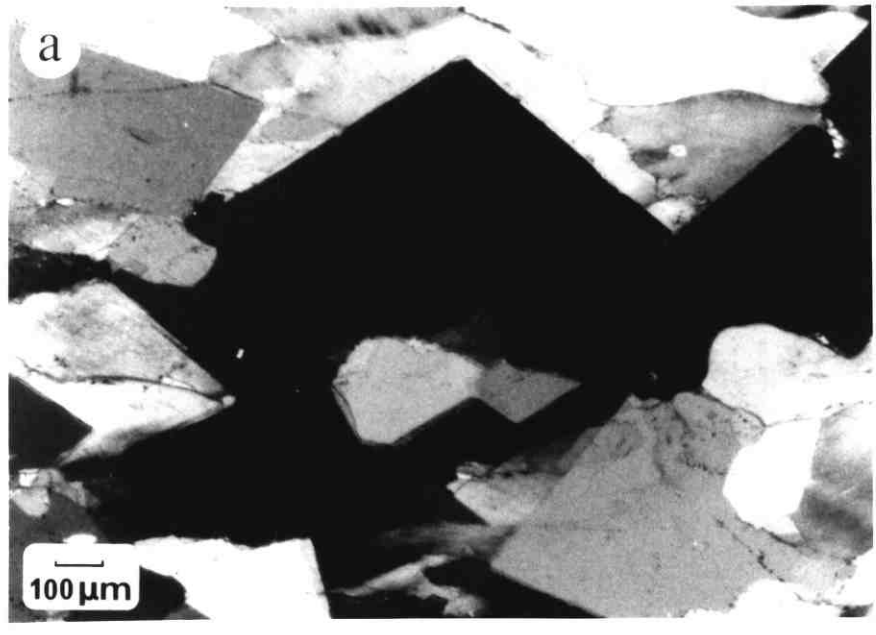
a
100 µm

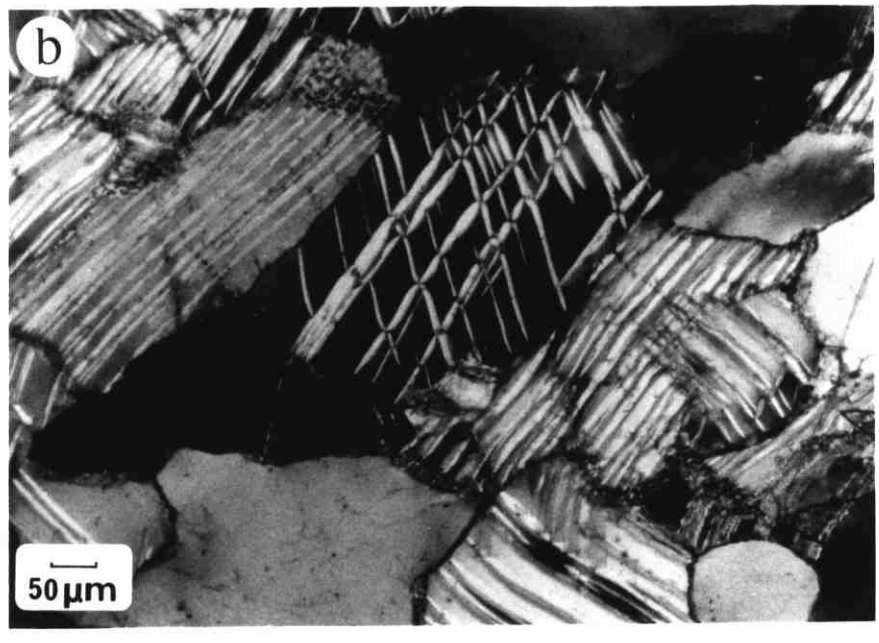
b
50 µm

Atmospheric Pressure Test 100°C

As seen in figure 3.33a the deformation structure within the extensively flattened grains consisted of small subgrains arranged in bands of alternating black and white contrast. Universal stage measurements of the variation of C axis orientation across a banded grain, are shown in the pole figure 3.33e, where the dark subgrains are shown as 'x' and the white as 'o'. From this figure it can be seen that the grains have kinked into a zig-zag configuration, as shown schematically in figure 3.33f. The average misorientation being approximately 30°.

Some of the resulting grain shapes indicate that localised shearing occurred during deformation e.g. note the shape of grain A in figure 3.33b. Other grains contained shear bands, figure 3.33c. Also some very small dynamically recrystallized grains were observed along some of the grain boundaries, figure 3.33d.

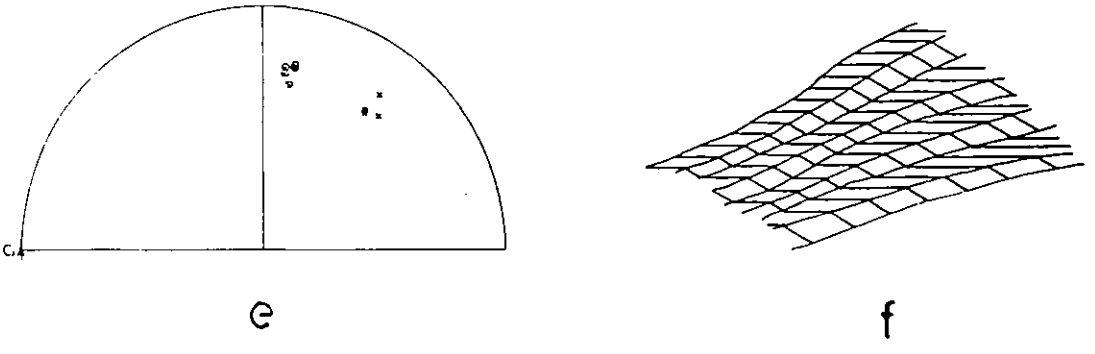

Figure 3.33 Structure of sample deformed at 100°C

(Strain = 0.6)

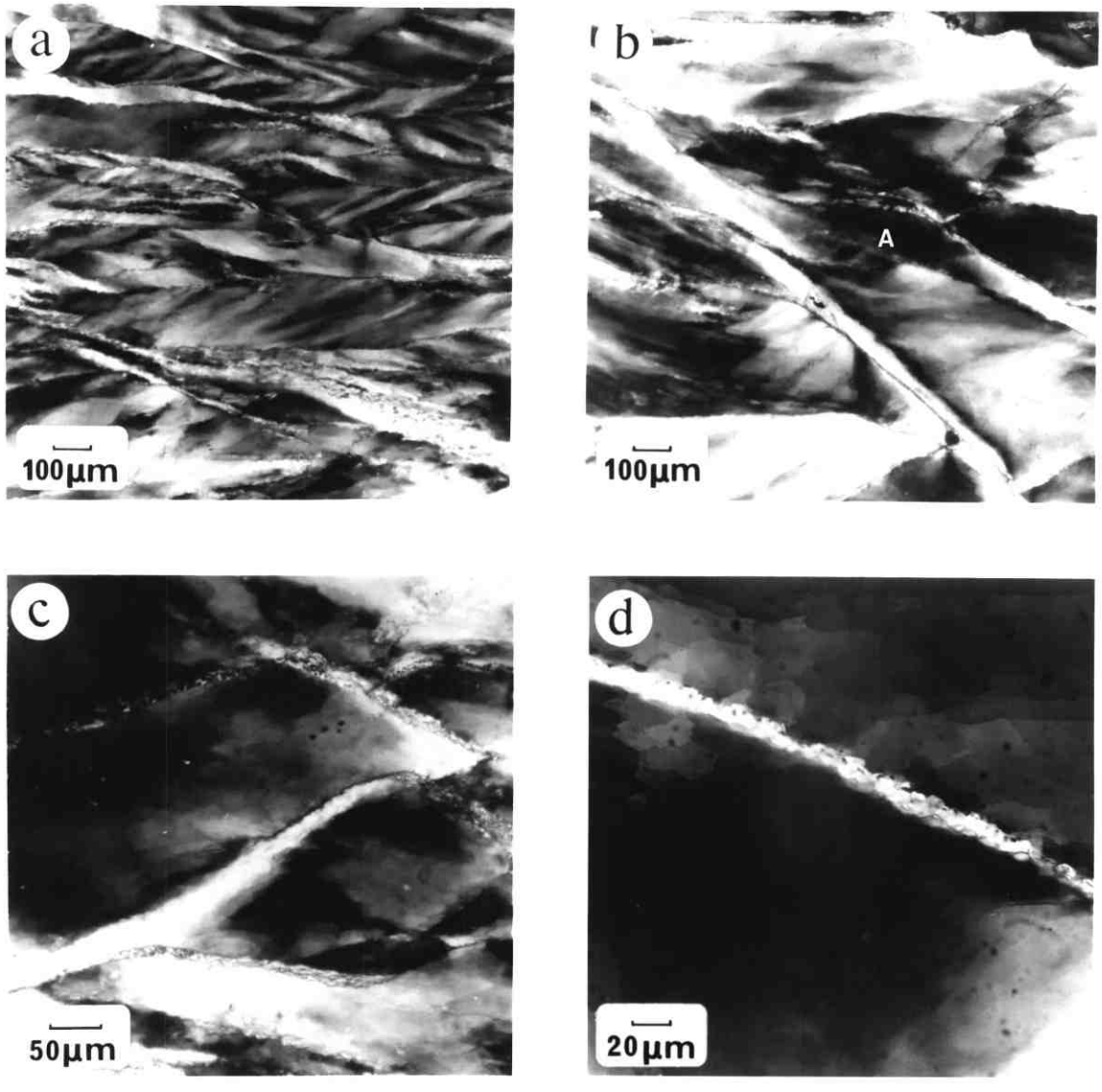
a
100μm
b
A
100μm
c
50μm
d
20μm

Atmospheric Pressure Test 150°C

The sample deformed at 150°C exhibited many of the features observed at 100°C. The increase in subgrain size shows some of the details more clearly. Again the zig-zag configuration of bands of subgrains was present, figure 3.34a, as well as small dynamically recrystallized grains along the grain boundaries, figure 3.34b. Shear bands were also observed, figure 3.34c.

Figure 3.34 Micrographs of sample deformed at 150°C

(Strain = 0.6)

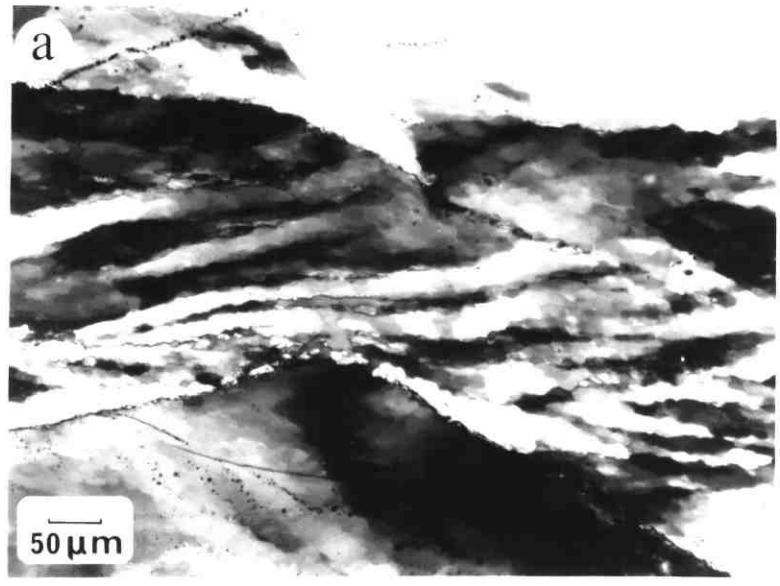
a
50 µm

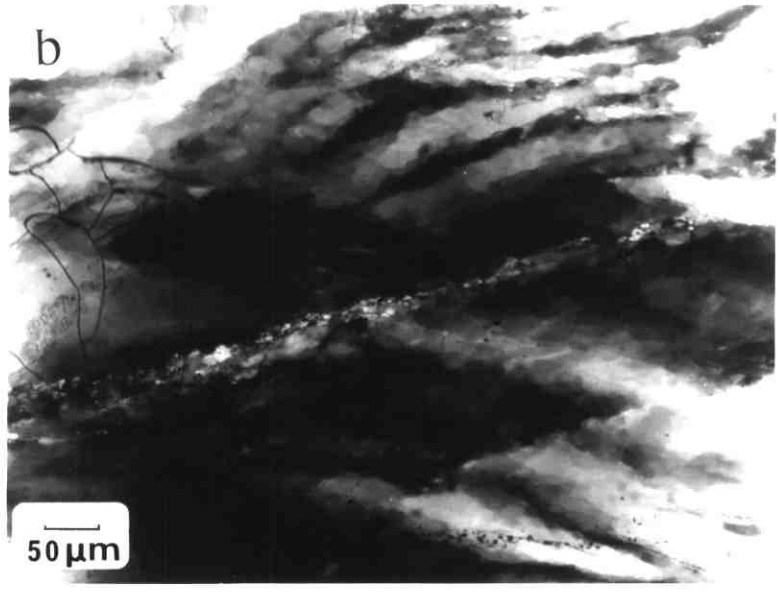
b
50 µm

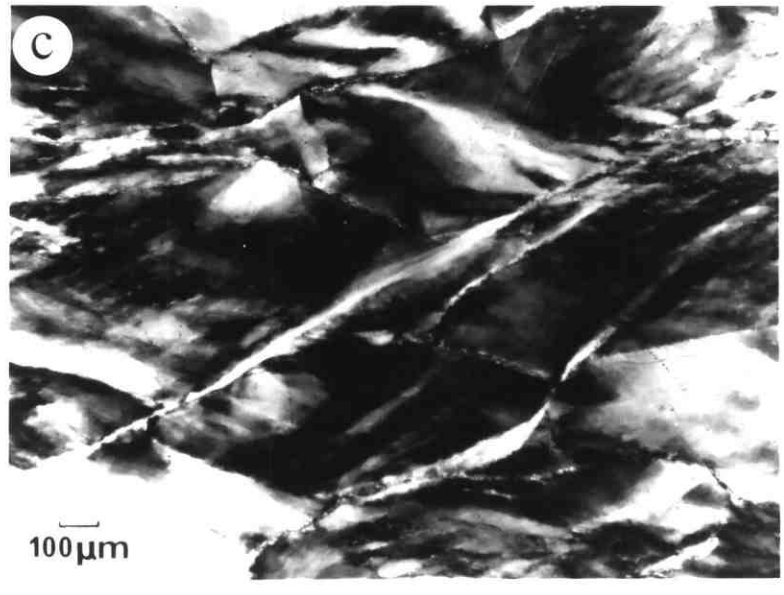
c
100 µm

Atmospheric Pressure Test 200°C

At 200°C the deformation bands were less frequent and broader, and had started to lose the zig-zag configuration observed at lower temperatures, figure 3.35a. The banded structure was replaced by a more poliganised (mosaic) substructure, figure 3.35b, with dynamically recrystallized grains along the grain boundaries, figure 3.39c.

Figure 3.35 Micrographs of sample deformed at 200°C

(Strain = 0.67)

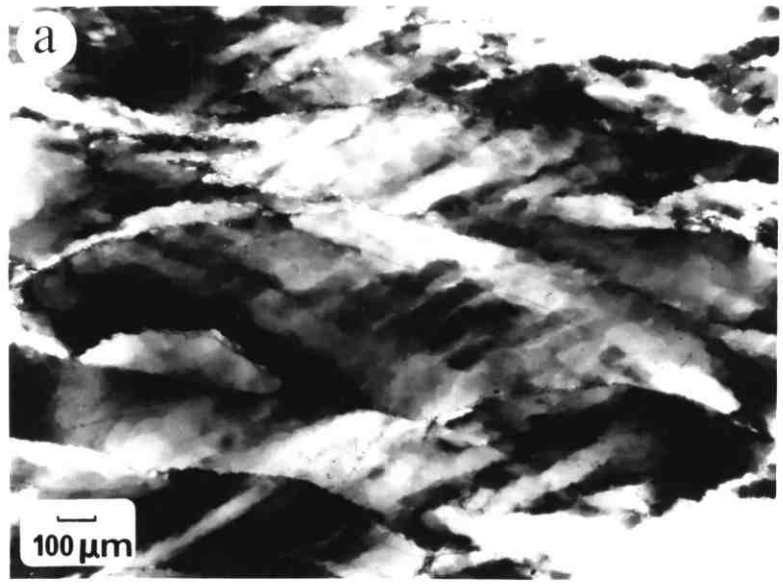
a
100 µm

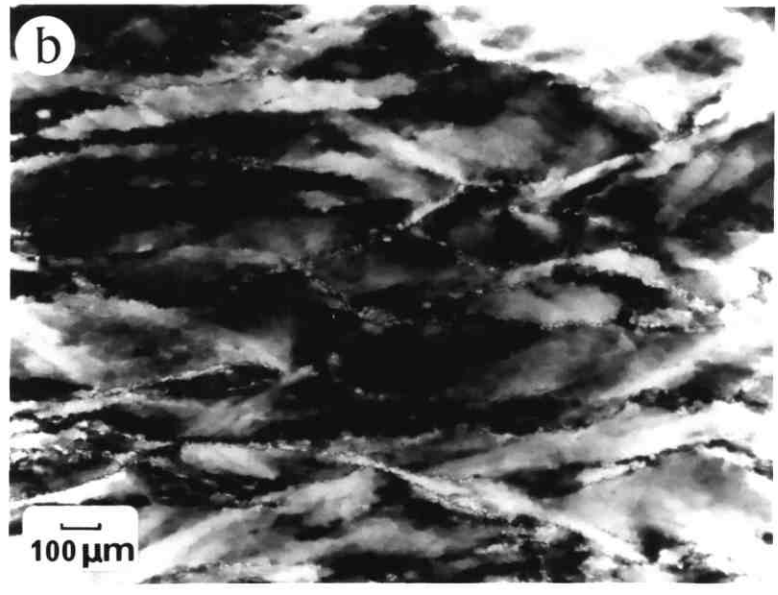
b
100 µm

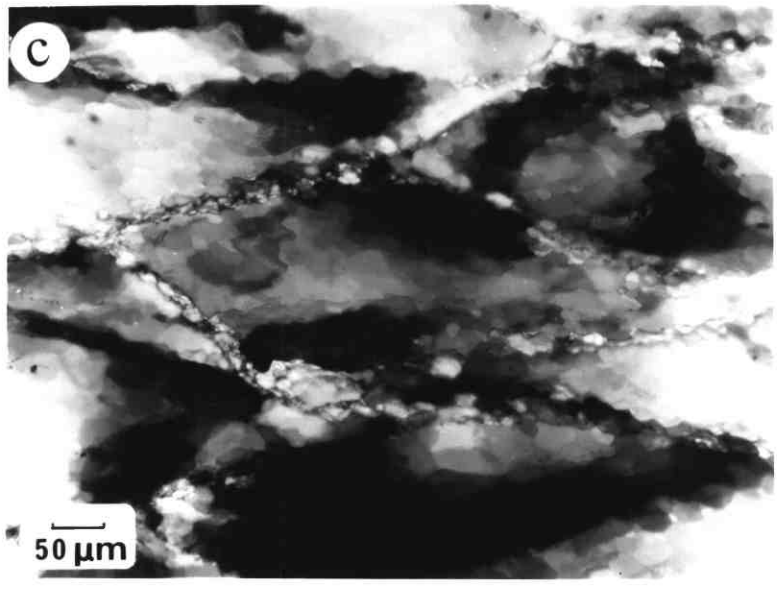
c
50 µm

Atmospheric Pressure Test 225°C

Figure 3.36 clearly shows a progressive change in contrast from the centre of a grain towards the grain boundaries. The change in C axis orientation across such a grain is shown in figure 3.37a, the number on the pole figure identifying successive subgrains in a traverse across a grain. Figure 3.37b shows, schematically, the orientation change shown in the pole figure. Substantial misorientations up to 18° have been measured between adjacent subgrains.

Figure 3.36 Micrograph of sample tested at 225°C

(Strain = 0.6)

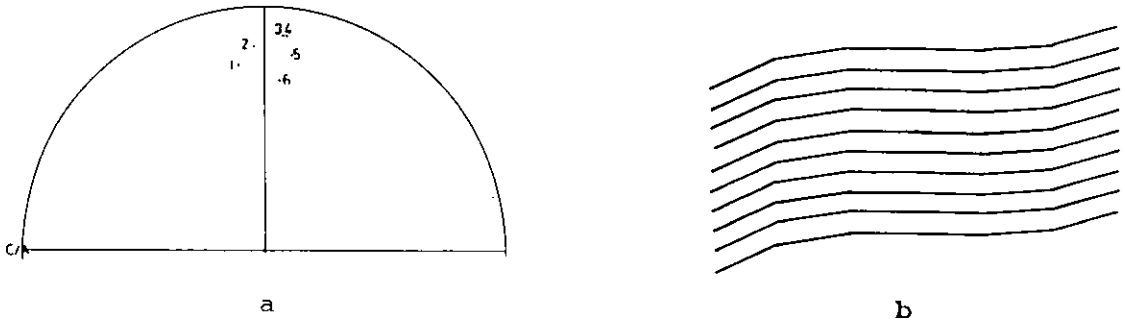

Figure 3.37.

Results of U-stage analysis of the thin section shown in figure 3.36.


20µm

Atmospheric Pressure Tests at 250°C and 300°C

At 250°C there was more evidence for the build up of high misorientations between subgrains, leading to the formation of dynamically recrystallized grains, with misorientations over 30° from the parent grain, figure 3.38a.

Figure 3.38b shows the very large dynamically recrystallized grains formed at this temperature. Although not seen in this micrograph, the large grains do contain subgrains, proving that they formed during deformation (figure 3.31f shows the subgrains within the large grains).

Figure 3.38 Micrographs of samples tested at 250°C and 300°C

(a) 250°C (Strain = 0.53)

(b) 300°C (Strain = 0.6)

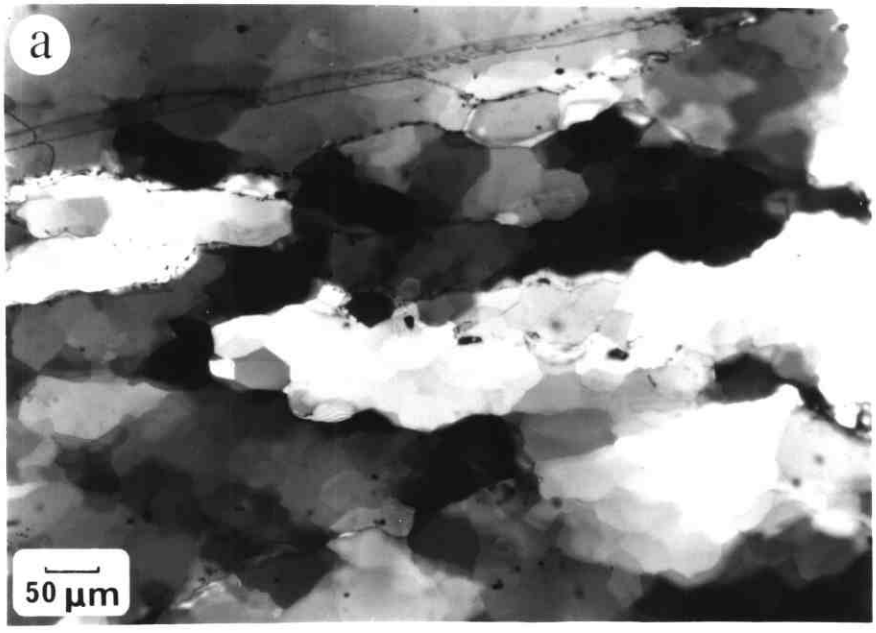
a
50 µm

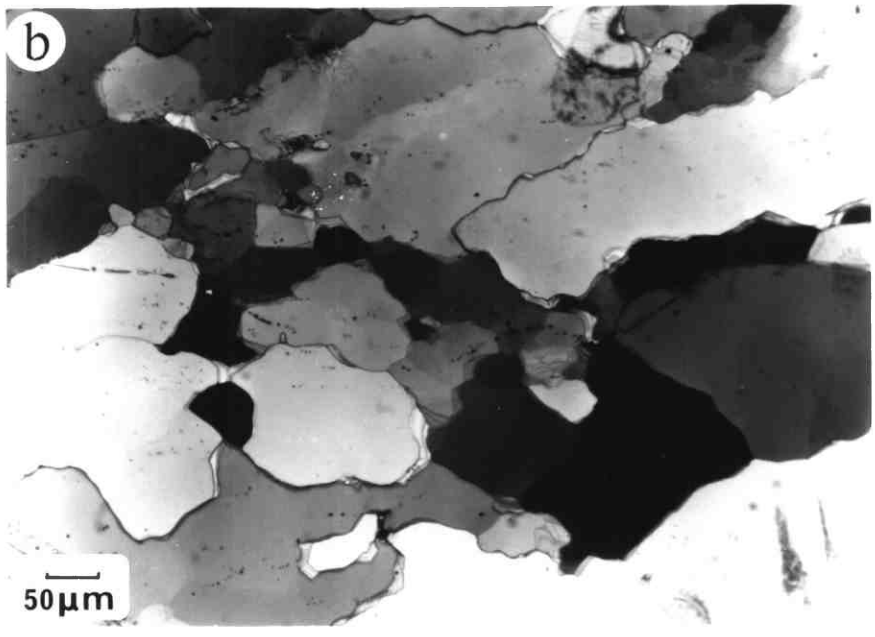
b
50µm

3.2.2.3 Effect of Strain on Development of Microstructures

Figure 3.39 shows the microstructures of five samples compressed to different strains at 250°C.

Figure 3.39 Development of substructure with strain at 250°C

(a) Strain = 0.11 Early development of substructure and serrations of grain boundaries. Average misorientation between subgrains = 3°.

(b) Strain = 0.23 Boundaries aligning to 45° to the stress axis (vertical axis of micrographs). Average misorientations between subgrains = 8°.

(c) Strain = 0.37 Increasing contrast between subgrains. Average misorientation between subgrains = 10°.

(d) Strain = 0.53 Well developed subgrains within elongated grains. Average misorientation between subgrains = 15°.

(e) Strain = 0.70 Very elongated grains with highly misorientated subgrains/dynamically recrystallized grains, with average misorientations of 20°, but with some as high as 40°.

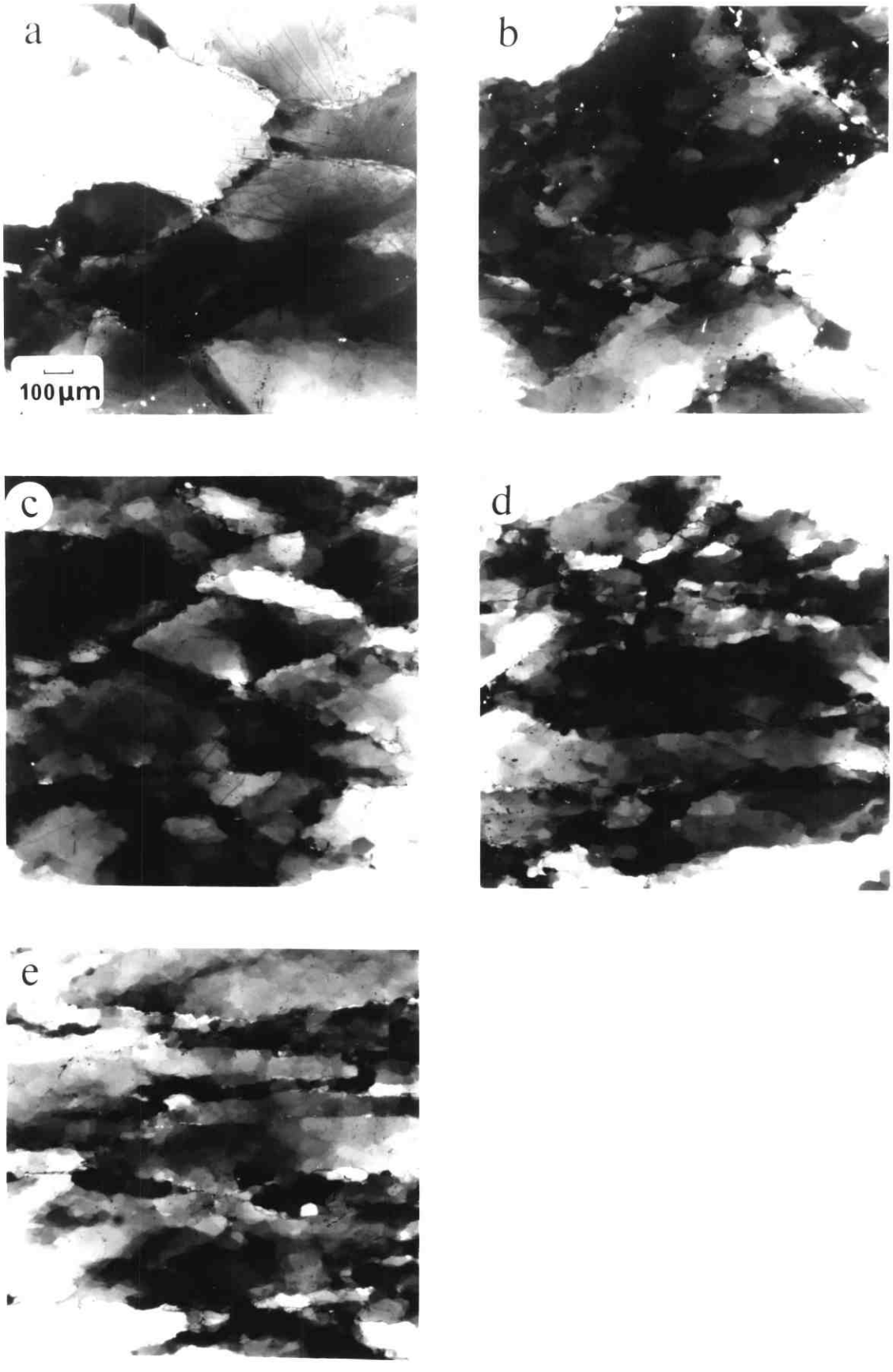
a
100µm
b
c
d
e

Chapter 4

DISCUSSION

4. DISCUSSION

4.1 COMPARISON BETWEEN THE DEFORMATION BEHAVIOUR OF SODIUM NITRATE AND CALCITE

Two common rocks formed from the mineral calcite ($CaCO_3$) are marble and limestone. Limestone is a sedimentary rock, which after metamorphism becomes marble. Compared with other minerals, calcite has been found to be more ductile than most, and for this reason, it has often been used by geologists for experimental studies. Although calcite is considered to be ductile for a mineral it is necessary to use a confining pressure to prevent fracture during deformation of polycrystalline samples. Despite this problem, a large amount of work has been done on the experimental deformation of marble (Turner, Griggs and Heard, 1954; Heard 1963; Heard and Raleigh, 1972; Spiers, 1978; Schmid, Paterson and Boland 1980) and limestone (Barber and Wenk, 1973; Schmid, Boland and Paterson, 1977).

4.1.1 Microstructures

During their study, Schmid, Paterson and Boland (1980) identified three deformation regimes, each with its own microstructural imprint:-

Regime 1 (over 100 MN/m^2)

At high flow stresses above 100 MN/m^2 twinning was predominant, but it was not sufficient to account for the total strain, so dislocation glide was also operative. The twins were lensoid in shape with constricted ends at grain boundaries, or at intersections with other twins. As the boundary of the next regime was approached, the ease of dislocation slip increased, and the amount of twinning decreased.

Regime 2 (between 20 and 100 MN/m^2)

This regime was characterised by the almost total absence of twinning and by a strong subgrain development within the grains,

with a distinctly different structural development near the grain boundaries. The grain boundary, or mantle, regions exhibited a substructure consisting of an equiaxed mosaic of boundaries. Across some of these boundaries the difference in orientation was small, so that the enclosed domains were classified as equiaxed subgrains. Across other boundaries the difference in orientation was found to be sufficiently large that some domains were classed as recrystallized grains of the same size as the subgrains.

The original grain boundaries also developed a highly convoluted or scalloped shape. Although this was attributed to a high grain boundary mobility, there was no tendency for particular grains to enlarge at the expense of others. Further evidence for the movement of grain boundaries was the observation that grain boundaries tended to align along two directions bisected by the compression axis.

Regime 3 (below 20 MN/m^2)

On entering this region, the equiaxed substructure that mantled the grains in regime 2, began to fill entire grains, suppressing the core and mantle structure. The original grains were observed to be wholly subdivided by a recrystallization that overprinted the original microstructure at high strains.

At 1000°C and 1050°C, this microstructure was further overprinted by an exaggerated grain growth. Some of these large grains were practically free of strain features, but others had been deformed, indicating that they had grown during deformation.

Additional split cylinder work indicated that grain boundary sliding became increasingly important at higher temperatures, and could account for up to 50% of the total strain. Accommodation of the sliding was thought to occur, at least in part, by inhomogeneous deformation within the grains.

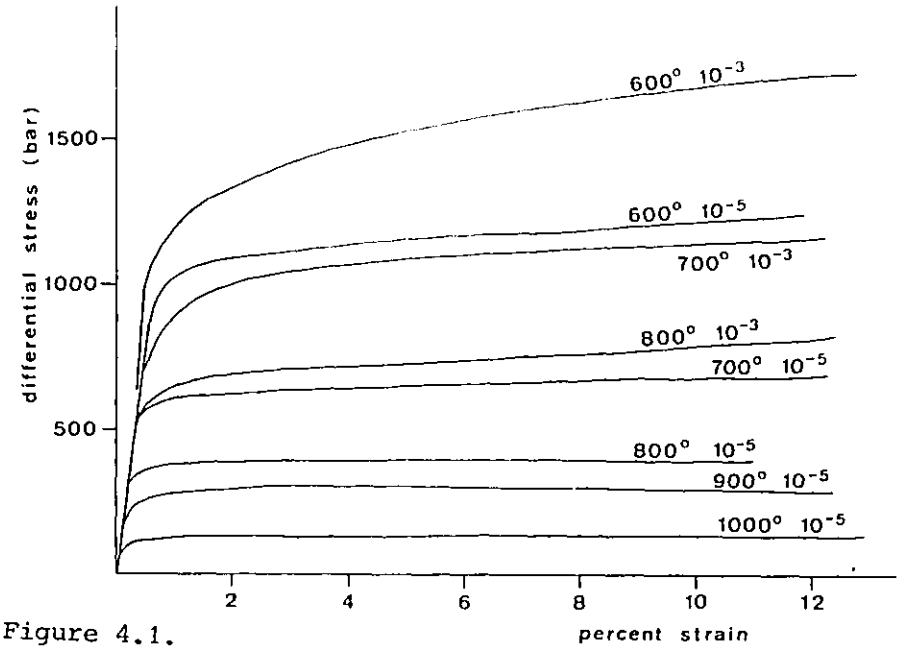

Figure 4.1.

Stress—strain curves for Carrara marble deformed under 3 kbar confirming pressure. After Schmit et al (1980)

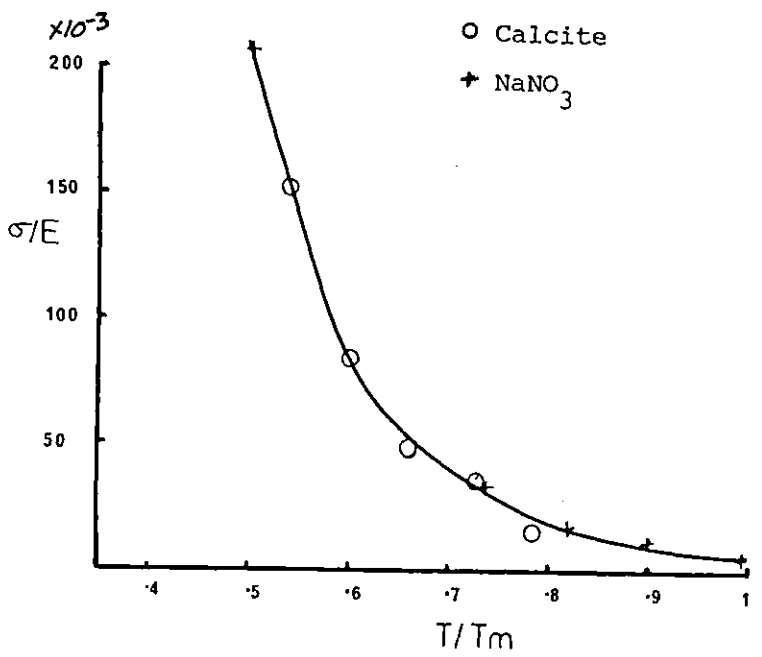

Figure 4.2.

Normalised stress/temperature graph for sodium nitrate and calcite

The foregoing descriptions indicate that the microstructural changes of sodium nitrate recorded in chapter 3, are very similar to those observed in calcite. Both exhibit twinning under high flow stress conditions, followed by a lower stress regime characterised by the formation of a substructure which can be highly misorientated, particularly at grain boundaries. Also the formation of very large dynamically recrystallised grains and grain boundary sliding are common to both materials at high temperatures. Although it was known that the two materials were isostructural, and had the same slip and twin planes, the microstructural developments of sodium nitrate under different deformation conditions were unknown. This study has clearly demonstrated that sodium nitrate undergoes very similar microstructural changes to those observed in calcite.

4.1.2 Stress-Strain Curves

The stress strain curves obtained for sodium nitrate during this study (figures 3.20 to 3.23) are very similar to those obtained for marble, figure 4.1. Although no peaks were observed in the curves for marble, the onset of an effectively steady state flow stress at relatively small strains is common to both materials. Figure 4.2 shows how the normalised flow stresses for sodium nitrate and calcite do in fact lie on the same curve. Changes in microstructure with flow stress for sodium nitrate have a direct correspondence with the microstructural regimes determined for marble.

4.1.3 Relation of Recrystallized Grain and Subgrain Size to Flow Stress

Schmid et. al. found that the dynamically recrystallized grain and the subgrain sizes were the same, and that the slope of the logarithmic plot against flow stress was $-1 \cdot 01 \pm 0.05$. Hence the

size of the equiaxed grains, and of the corresponding subgrains was determined to be almost exactly inversely proportional to the flow stress. This is in contrast to the values found for sodium nitrate during this study. A logarithmic plot of subgrain size and dynamically recrystallized grain size with stress (figure 3.28) resulted in gradient values of -0.85 for subgrains and -0.65 for recrystallized grains. These results for sodium nitrate will be discussed in more detail in section 4.4.

4.1.4 Stress Exponent n

Two values of the stress exponent n were determined for marble by Schmid et. al. In regime 2, n was found to be 7.6, and in regime 3, n = 4.2. These values are very similar to those determined during this study on sodium nitrate. The stress relaxation test at room temperature, gave rise to two n values, 7.5 at strain rates above $10^{-7}s^{-1}$ and 2.3 below $10^{-7}s^{-1}$. Microstructures from constant strain rate tests above $10^{-7}s^{-1}$ were similar to those described for marble at the border between regimes 1 and 2. Thus the value of n = 7.5 for sodium nitrate corresponds to the value of 7.6 found for marble. Microstructures of sodium nitrate between 200°C and 280°C are consistent with those described for marble in regime 3. Hence the average value of n , found over this range, of 4.4 for sodium nitrate corresponds with the value of 4.2 determined for marble.

So not only is there a correspondence of microstructural changes with flow stress between sodium nitrate and calcite, there is also a correspondence between the stress exponents associated with particular microstructures.

4.2 COMPARISON BETWEEN THE DEFORMATION BEHAVIOUR OF SODIUM NITRATE AND METALS

At room temperature, the twinning behaviour of sodium nitrate

is similar to the deformation behaviour of metals with a high Peierls-Nabarro force, e.g. iron at low temperatures. (Honeycombe 1968); but at higher temperatures the well developed subgrain structures are very similar to the microstructures of creep deformed aluminium (McLean 1951-52; 1952-53). Several features noted by McLean suggest that the behaviour of sodiumn nitrate above 150°C is very similar to the creep behaviour of pure aluminium.

In McLean's papers it was reported that the subgrains initially appeared at grain boundaries, but with further strain, they were observed throughout the grains. Similar observations have been made during this study, e.g. figure 3.39. Micrographs of aluminium show both the banded subgrain structure similar to figure 3.34a, and the progressive change in contrast towards a grain boundary, as shown in figure 3.36. McLean also reports that the misorientation across subgrain boundaries increased with stress, with some misorientation being as high as 40°. Again this compares with the behaviour of sodium nitrate. However, as discussed below, more recent work suggests that large misorientations between subgrains does not occur in aluminium.

The misorientations across subgrain boundaries were measured by McLean by viewing anodized sections with a polarised light microscope. At particular orientations a subgrain would go into extinction, the specimen was then rotated until a neighbouring subgrain went into extinction. The angle of rotation was noted, and used to calculate the misorientation across the boundary. Although the technique was not fully understood, it was assumed that the anodic layer was some form of epitaxial growth, reflecting the orientation of the crystal below it.

However, Wong, McQueen and Jonas (1967) have noted a discrepancy between the apparent misorientations of subgrains measured

using polarized light microscopy, and the misorientations determined by electron diffraction techniques, during studies on extruded aluminium. In their study, the apparent misorientations between subgrains using the polarized light technique were found to have values up to 45°. However, electron diffraction patterns from subgrains gave the misorientations to be less than 3 or 4°.

Although aluminium has been widely studied, there have been no other reports supporting McLean's results. Exell and Warrington (1972) measured subgrain misorientations with increasing strain after high temperature deformation of aluminium, but the average misorientations were found not to exceed 1°. More recent work using back scattered electron channelling patterns to measure misorientations between subgrains in deformed aluminium (Humphreys, 1982) found the average misorientation to be 3° with a maximum of 7°.

Thus it would seem that although the appearance of dynamically recovered substructures of sodium nitrate and aluminium are very similar, there is no conclusive evidence for the build up of high misorientations between subgrain in aluminium. In fact there is little evidence for the build up of large misorientations between subgrains in deformed metals. Several review papers (Takeuchi and Argon, 1976; Mukherjee, 1975) report that subgrain misorientations have been found to increase with strain during their early development, but the misorientations have been found not to exceed 2 or 3° in many metals.

An exception to this has recently been reported for magnesium (Ion, Humphreys and White, 1982). In this paper an electron micrograph, from a high temperature compression sample, clearly shows progressive lattice bending near an old grain boundary, with misorientations around 15° across sub-boundaries. The bending of the crystal lattice close to a grain boundary was thought to be caused by the geometry of slip in the hexagonal crystal system.

4.3 ANALYSIS OF CREEP PARAMETERS

It has been found that in general, many materials exhibit several common properties under creep conditions and conform to a common empirical creep equation (Mukherjee, 1975). After an initial transient period, the creep rate often decreases to a steady state value during secondary creep, and an empirical power law creep equation has been determined for this regime. A typical form of creep equation is

$$\dot{\varepsilon} = A\,\sigma^{n} \exp(Q_c/RT)$$

(Takeuchi and Argon, 1976)

where
- $\dot{\varepsilon}$ = strain rate
- A = constant
- σ = stress
- Q_c = Activation energy for creep
- R = gas constant
- T = temperature

4.3.1 Stress Exponent n

Values of the stress exponent n for various solid solution alloys and pure metals vary from about 3 to 7, and in general, are substantially constant over a wide range of stress and temperature (Mukherjee, 1975). A typical stress exponent for a pure metal is 5 (Takeuchi and Argon, 1976).

There are many proposed diffusion controlled creep mechanisms and each one has a value of n associated with it. The dislocation climb controlled creep mechanism has n values between 4 and 7 (Misro and Mukherjee, 1975). Hence the values of n found for

sodium nitrate (4.4 between 280°C and 200°C, 6 at 150°C and 7.5 at 25°C) are all consistent with a dislocation climb controlled creep mechanism.

Results from the stress relaxation test at room temperature indicate that the value of n changed at low stresses to 2.3. This could be indicative of a change in the creep mechanism at low stresses. However, after constant strain rate tests at room temperature, there was evidence of statically recrystallized grains (figure 3.32a). Hence the reduction of the value of n could be due to the stress relaxation sample recrystallizing. An important consideration in the determination of n , is that the microstructure should remain constant during the test.

The observed value of 2.3 for n at low stresses is consistent with n values associated with creep by grain boundary diffusion (Mukherjee, 1975). However, diffusion mechanisms during creep are usually observed at low stresses and at temperatures higher than 0.5 Tm . Thus the change in the value of n to a lower value at low stresses cannot be consistently explained by such a change in creep mechanisms .

It would be interesting to experimentally verify the cause of this result from the stress relaxation test. This could be done by performing a constant strain rate test at a very low strain rate (10^{-8} s^{-1}). By comparing the flow stress from this test with the stress relaxation test results (figure 3.24) it would be possible to confirm whether or not the change in gradient was caused by a change in the creep mechanism.

However, the length of time required to perform such a test, about a month, prevented its inclusion as part of this study, due to the availability of the apparatus.

A notable result from this study is the change in the value of the stress exponent with temperature. This at first may seem

to be at variance with observations made on metals. However, the changes in the exponent, for sodium nitrate, correspond to changes observed in the microstructures after deformation.

At 25°C, n = 7.5, the microstructure of deformed sodium nitrate contained twins at the edges of the samples, but most of the original grains exhibited no resolvable features when observed through the optical microscope.

150°C, n =6, the dominant microstructural feature was the alternating bands of subgrains (figure 3.34a).

Between 200°C and 300°C, n = 4.4, the samples had well recovered substructures, with a mosaic subgrain structure with high misorientations, but not banded as at 150°C.

Thus the changing characteristics of the microstructures are reflected by changes in the stress exponent n but the connection between the two is not clear.

4.3.2 Activation Energy Q

In general it has been found that above 0.5Tm the activation energy for creep in metals is equal to that of the activation energy for self diffusion (Weertman, 1968; Mukherjee, 1975), and appears to be insensitive to temperature (Sherby and Burke, 1967). However in the review by Sherby and Burke, two activation energies were reported for sodium chloride above 0.5Tm . Between 0.5 and 0.75Tm the activation energy observed for creep is about equal to that for chlorine ion diffusion in high dislocation density single crystals. Above 0.75Tm the activation energy for creep was found to be higher, but over the same temperature range, the activation energy for diffusion was also higher, and there was a good agreement between the two values. The higher activation energy for diffusion at higher temperatures is believed to represent intrinsic diffusion

behaviour, that is, diffusion not controlled by the presence of divalent cation impurities. Thus the two creep activation energies were due to there being two temperature dependent diffusion activation energies caused by the effects of impurities.

Sodium nitrate also exhibited an increase in creep activation energy at high temperatures (figure 3.25). Between 0.5Tm and 0.95Tm a single activation energy of 85 $KJmol^{-1}$ was determined, but figure 3.25 indicates a significant increase in the activation energy about 0.95Tm . Very little data has been reported in the diffusion literature about the activation energies for diffusion of solid sodium nitrate with which to compare these results. However, after a study on the electrical conductivity of sodium nitrate, Ramasatry and Murti (1968), determined the jump activation energy for the movement of positive ions to be $91KJmol^{-1}$. This value should be similar to the activation energy for diffusion, as diffusion occurs by the jumping of atoms from one site in the crysal lattice to another.

Although this value is within 10% of the creep activation energy determined in this study, it is the activation energy for the diffusion of the nitrate ion which should be compared. The nitrate ion complex is larger than the sodium ion, and thus one would expect it to be the slower diffusing species, and hence, be the rate controlling factor. In the absence of diffusion data, comparisons with the work on sodium chloride would suggest that the increase in activation energy about 0.95Tm could be due to a change in the activation energy for diffusion.

4.4 SUBGRAIN AND DYNAMICALLY RECRYSTALLIZED GRAIN SIZES

4.4.1 Subgrains

From a survey of creep reviews there is overwhelming evidence that well defined subgrains are formed during creep of metals and

and solid solution alloys, whenever the dislocation climb mechanism is rate controlling. The process ultimately responsible for subgrain formation is still unexplained, but polygonization of edge dislocations and climb recovery of dislocation tangles formed during the initial straining, are thought to be important factors (Mukherjee, 1975).

It has been found that the size of subgrains developed during steady state creep is a strong function of the creep stress, does not change during steady state creep, and is not an important function of temperature (Sherby and Burke, 1967). The subgrain size has been widely reported to obey a power relation of the form

$$\sigma = A\, d^{-n}$$

σ = stress
d = subgrain size
n = approx. 1

(Sherby and Burke, 1967; Takeuchi and Argon, 1976, Weertman, 1968).

This relationship is also valid under hot working conditions (McQueen and Jonas, 1975), and from the limited data available, is applicable to minerals, e.g. olivine (Nicholas, 1978), halite (Guillopé and Poirier, 1979) and calcite (Schmid, Paterson and Boland, 1980).

The value of n, determined for the relationship between the subgrain size and stress for sodium nitrate from figure 3.29 was 0.85. This is lower than the value of 1 expected from the literature. Another interesting observation are the three parallel lines of ligure 3.29, one for each strain rate. If the relationship between the stress and subgrain size is a simple one of the form $\sigma = A\, d^{-n}$, then a plot of $\ln\sigma$ vs $\ln d$ should be a single straight line for all conditions of deformation. Although changes in strain rate do not alter the value of n, the separation of a single line

into three parallel lines indicates that the value of A is not independent of the strain rate. A less general form of the equation is given by Takeuchi and Argon (1976) as

$$\sigma = \frac{K \mu b}{d}$$

where μ = shear modules

b = burgers vector

No indication is given in the literature that K is not a constant under all conditions of deformation.

Before continuing it is interesting to consider the relationship between subgrain size and stress in more detail. Although a simple relationship has been determined for the two variables in the past, how are they related? Is the subgrain size determined by the flow stress, or conversely, is the flow stress determined by the subgrain size, or are they related through a more fundamental mechanism? Schmid et. al. (1980), observed that an effectively steady state flow stress is attained at relatively small strains, while the optical microstructure continued to evolve with strain. This led the authors to the conclusion that the size of the subgrains that are correlated with the stress are consequential on, rather than determinative of, the basic flow mechanisms that itself determines the flow law. Redfern and Sellars (1970), found that second phase precipitates could change the subgrain size, and from observations of the changes in the flow stress, suggest that the subgrain size is only indirectly linked to the high temperature flow stress which is virtually independent of the particle spacing. They proposed that the flow stress and subgrain size were separately dependent upon the dislocation density within the subgrains.

4.4.2 Dynamically Recrystallized Grains

Most experiments on dynamic recrystallization of metals or minerals have produced evidence for a simple relationship between

the applied stress σ , and the dynamically recrystallized grain size D .

$$\sigma = K D^{-n}$$

Although the value of n from various studies is not a consistent value for all materials, it is less than one, as is the case for the analogous relation for the subgrain size. Poirier and Guillopé (1978) give a value of n to be close to 0.7 or 0.8 for minerals, and Sellars (1978) gives a range between 0.5 and 1 for metals. Sellars suggests that this range may be due to variations of purity of the metal. However, a value of about 0.75 is common to several metals e.g.:-

Nickel, $n = 0.75$ (Luton and Sellars, 1969)

Copper and Copper aluminium alloys, $n = 0.75$ (Bromley and Sellars, 1972)

Alpha iron, $n = 0.71$ (Glover and Sellars, 1973)

These values are consistent with those given for minerals by Poirier and Guillopé. However, an exception to these values is a second value determined for nickel of $n = 0.5$ (Sah, Richardson and Sellars, 1974).

Results from this study clearly demonstrate two separate dynamically recrystallized grain sizes for sodium nitrate. The two types of dynamically recrystallized grains were observed in both the in situ experiments (figure 3.9) and in thin sections prepared from bulk compression samples (figure 3.26). At high temperatures there were both small and large dynamically recrystallized grains, but below a critical temperature only small grains were observed. Both large and small recrystallized grains increased in size with temperature. Figure 3.27 shows the decrease in the dynamically

recrystallized grain size with stress, and that the smaller recrystallized grains are about the same size as the subgrains.

Although the small recrystallized grains were of a similar size to the subgrains, the relation of size with stress was found to be

$$\sigma \propto D^{-n} \qquad n = 0.65$$

This value of n = 0.65 was determined for both the large and small dynamically recrytallized grains. Again the value is lower than the value of 0.75 which seems to be common for many materials. Although the values of n for both the subgrains, and the dynamically recrystallized grains, for sodium nitrate are lower than results from other materials, the smaller of the two values is for the dynamically recrystallized grains, which is consistent with other observations.

However, separation of the logarithmic plot of stress against dynamically recrystallized grain size (figure 3.30) into three parallel lines, one for each strain rate (as observed for the subgrains), indicates that the constant of proportionality K is not a constant, but varies with strain rate. Again no such dependence has been reported in the literature. Also, there have been no reports in the metallurgical literature of two dynamically recrystallized grain sizes, but similar observations have been made during studies on high temperature deformation of calcite (Schmid, Paterson and Boland, 1980) and halite (Guillopé and Poirier, 1979). Guillopé and Poirier explained the two dynamically recrystallized grain sizes as being the result of two mechanisms of dynamic recrystallization. This proposal will be discussed in detail in section 4.5.

4.5 DYNAMIC RECRYSTALLIZATION

4.5.1 Nucleation Mechanisms

Two of the most frequently cited nucleation mechanisms proposed

for dynamic recrystallization are, by bulging out of pre-existing high angle boundaries into areas of higher stored strain energy, and by progressive misorientation of subgrains.

4.5.1.1 Grain Boundary Bulging

As reviewed in chapter 1, many authors refer to the mechanism of strain induced grain boundary migration as an integral part of dynamic recrystallization. However, this mechanism alone does not fully explain the presence of recrystallized grains along the grain boundaries. Although Bailey and Hirsch (1962) acknowledged the formation of grain boundary bulges, and carried out a detailed investigation into the kinetics of bulge nucleation and growth, they did not attempt to account for the nucleation of recrystallization, or to explain the formation of the boundary which must occur behind the bulge, before it becomes a recrystallized grain. The growth of a grain boundary bulge will recrystallize the area it grows into, but this mechanism by itself cannot form a grain with a new orientation.

At very high temperatures (0.99Tm) and at low strain rates (10^{-4} s^{-1}), grain boundary bulging was observed to play an important role in the nucleation of dynamically recrystallized grains in very pure sodium nitrate. This mechanism was not generally observed, but it did happen during experiments using 'Specpure' (99.999%) sodium nitrate. An in situ sequence of the bulging of an existing grain boundary is shown in figure 3.19 a-c. However the sequence of events which followed, deviate from the classical bulge model, and due to rapid microstructural developments not all of the events were recorded using the 35 mm film camera.

The grain boundary bulge at c (figure 3.19c) was growing slowly when a small region at its very tip started to change colour, the boundary of this region then swept backwards from the tip into the bulged region. Figure 3.19d shows the new grain formed by the migration of this boundary, which was moving in the direction indicated by the arrow. Once the migrating boundary

reached the position of the original grain boundary it stopped. Figures 3.19e and f show the subsequent growth of the recrystallized grain.

An explanation for these observations is that a subgrain formed at the tip of the bulge became highly misorientated due to this region becoming deformed as it grew into the adjacent grain. The misorientation built up until a high angle boundary was formed, which then migrated back into the bulge until the position of the original grain boundary was restored. Thus, grain boundary bulging was an important factor but the formation and migration of a high angle boundary completed the process of forming the new grain.

However, although grain boundaries of metals have been observed to bulge, and recrystallized grains have been observed in the grain boundary regions, there is little direct evidence for the occurrence of the mechanism discussed above.

4.5.1.2. Subgrain Rotation

A second nucleation mechanism proposed for dynamic recrystallization, is that of progressive subgrain rotation. Although there is little supporting evidence of this mechanism operating in metals there is evidence that dynamic recrystallization by subgrain rotation does occur in minerals (Hobbs, 1968; White 1973; Guillopé and Poirier, 1979).

Results from this investigation conclusively demonstrate that dynamic recrystallization of sodium nitrate is initiated by subgrain rotation. Analysis of progressive strain tests on bulk samples (figure 3.39) clearly shows that subgrain misorientations increase with strain, and that misorientations up to 40° can be achieved at high strains (0.6). The misorientations do not necessarily build

up progressively across a grain from its centre to the grain boundary, as shown in figure 3.36, but single subgrains at grain boundaries may increase their misorientation until they become recrystallized grains, figure 3.38a. This mechanism of dynamic recrystallization by subgrain rotation means that dynamic recovery and dynamic recrystallization are not entirely separate mechanisms, but that the recrystallization is a product of dynamic recovery. There is no change in mechanisms when a subgrain becomes sufficiently misorientated to be recognised as a recrystallized grain.

The formation of subgrains during the early stages of deformation by dynamic recovery is common to both minerals and metals. However, the continuing misorientation of the substructure with strain which occurs in some minerals has not been observed in metals. Increasing misorientation of subgrains with strain has been reported in metals (Takeuchi and Argon, 1976) up to a strain of 0.4, but the misorientations did not exceed a few degrees.

Continuing subgrain rotation with increasing strain has been explained by the subgrain boundaries accumulating excess dislocations of the same sign (Guillopé and Poirier, 1979). However, an explanation as to how or why this should happen is not given. It is not clear how dynamic recovery can progressively misorientate the substructure with strain in ionic crystals, or why this is a difference in behaviour between ionic crystals and metals.

4.5.2 GROWTH OF DYNAMICALLY RECRYSTALLIZED GRAINS

In situ observations on sodium nitrate have revealed that once a dynamically recrystallized grain has formed by subgrain rotation, it could then grow by the migration of its boundaries in one of two ways. Some grains grew very slowly, increasing their original size by only a factor of two or three, but at high

temperatures, extensive and rapid growth of the dynamically recrystallized grains can occur. Large areas of the sample were recrystallized by the migration of a high angle boundary, formed during deformation (figure 3.5). A critical temperature was found, below which, no rapid migration was observed (figure 3.6).

Similar observations of both small (subgrain size) and very much larger dynamically recrystallized grains, have been reported during creep studies on halite (Guillopé and Poirier, 1979). The two recrystallized grain sizes were interpreted, by Guillopé and Poirier, to be the result of two recrystallization mechanisms, rotation recrystallization, and recrystallization by rapid grain boundary migration, which were explained within the framework of the Lücke and Stüwe (1971) theory of impurity controlled grain boundary migration. The observation which led to consideration of this theory was that as the impurity content of the halite crystals increased, so did the critical temperature required for migration recrystallization.

This present study on sodium nitrate gives much more conclusive experimental evidence that grain boundaries formed during deformation, do in fact have two distinct velocity regimes (figure 3.8).

Further in situ experiments using sodium nitrate with small additions of $Ca(NO_3)_2$, showed a very strong dependence of rapid grain boundary migration on the impurity content of the sample. Again the results were similar to those obtained for halite, small amounts of trace additions increased the critical temperature for migration (figure 3.12), but at higher concentrations (1 wt % $Ca(NO_3)_2$) the rapid migration of boundaries was completely suppressed. However, the addition of impurities did not significantly affect the rates of migration (figure 3.13).

The results from this investigation can be consistently interpreted using the Lücke and Stüwe theory, including the discontinuous change in grain boundary velocity shown in figure 3.11. Figure 3.11 shows very clearly the two velocity regimes of a migrating grain boundary. Initially, the boundary has a high velocity, but as the grain is deformed, the driving force is reduced, and the velocity gradually decreases. Then the velocity drops dramatically to a much lower value, before the boundary eventually stops. An explanation of this within the framework of the Lücke and Stüwe theory is that at high velocities the grain boundary is free from the dragging force of impurities, and its velocity is that which it would be in a pure crystal. Its velocity (V) depending only on its mobility (M) and the driving force (F).

$$V = M F$$

However, when the velocity drops below a critical value the impurities 'see' the boundary as a region of lower potential energy, and try to diffuse with it. Lagging behind the boundary they exert a dragging force, diminishing the velocity by an order of magnitude. The dragging force exerted by the impurities is dependent on the velocity of the boundary. This gives a new equation for the velocity of the boundary: $V = M \left[F - f(v) \right]$ where f (v) is the dragging force which is a function of velocity.

From a more detailed mathematical analysis, Lücke and Stüwe developed the graph shown in figure 4.3. Below a critical driving force, the boundaries are very slow moving due to the drag of impurities, but above Fc, the boundaries can break away from its impurities, and move freely with a much higher velocity. The transition from the loaded to the free boundary condition leads to a discontinuous change in velocity, as shown in figure 3.11.

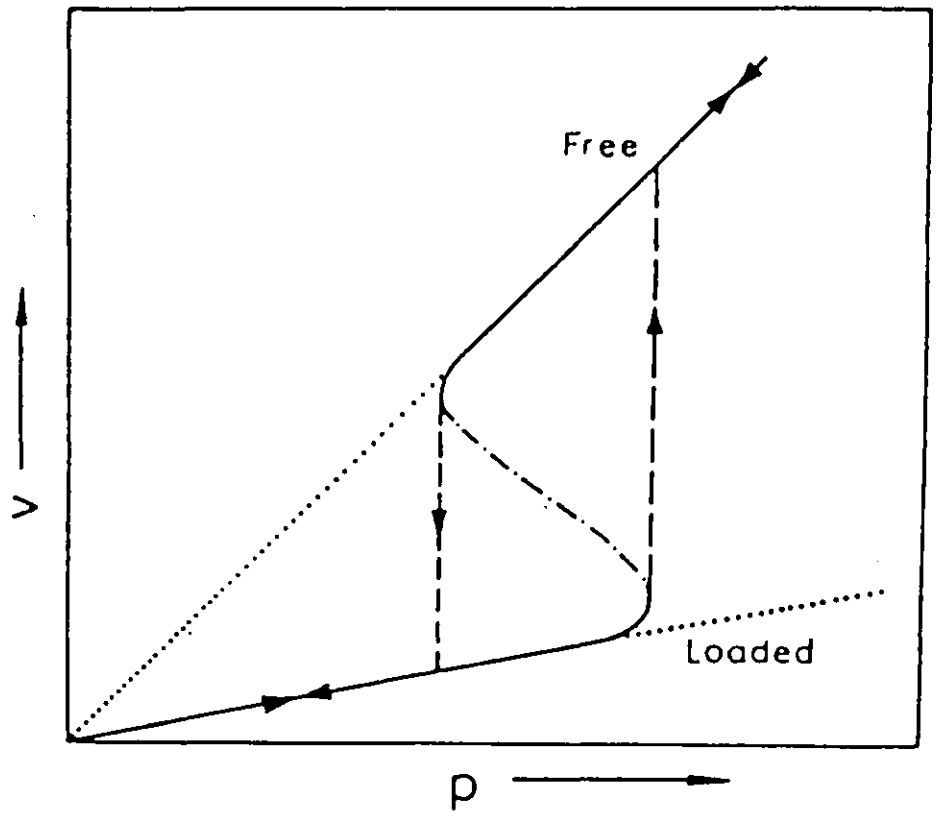

Figure 4.3.

Migration velocity as a function of the driving force (P) for a grain boundary in a crystal containing impurities. The dashed lines indicate the discontinuos changes of velocity (V); after Lücke and Stüwe (I97I).

4.6 EFFECTS OF PURITY ON MICROSTRUCTURAL DEVELOPMENT DURING DEFORMATION

Small changes in the impurity content of sodium nitrate markedly affected the microstructural changes during deformation. An addition of 1wt%$Ca(NO_3)_2$ completely suppressed the rapid migration of the recrystallized grain boundaries. However, it is interesting to note that, even without the rapid migrating boundary phenomenon, very large dynamically recrystallized grains could be formed by extensive slow migration of the grain boundaries (figure 3.14).

According to the Lücke and Stüwe theory, the free rapid migration rates of the impure material should be the same as the migration rates in the pure material. In order to verify this, further in situ experiments were performed on samples containing fewer impurities than laboratory grade sodium nitrate. However, as discussed below, reduction of the impurity levels also significantly changed the microstructural developments with strain.

4.6.1 'Specpure' Sodium Nitrate (99.999%)

This very pure form of sodium nitrate behaved in a very different way to laboratory grade sodium nitrate (98%). The most noticeable difference was the absence of a well developed substructure within the grains of the very pure material. Dynamic recrystallization by subgrain rotation did not happen the same way as observed during studies on laboratory grade sodium nitrate. For example, compare the substructure developed in laboratory grade sodium nitrate shown in figure 3.4 with figure 3.19.

This change in substructure would have affected the driving force for rapid migration. Hence it is not possible to make direct comparisons between the rate of rapid grain boundary

migration in laboratory grade sodium nitrate with the rate observed in the very pure material. However, figure 3.18 does show that the rates of migration are of the same order of magnitude in both materials.

Although the velocities of rapid migration were reduced at high temperatures in the pure sodium nitrate the mobility of the original grain boundaries was much more noticeable. Any slightly misorientated subgrains formed along a grain boundary were removed by the migration of the grain boundary (figure 3.17). Increased mobility of the grain boundaries also led to grain boundary bulging (figure 3.19), which was not observed in any of the less pure materials.

Small movements of grain boundaries during deformation have also been noted in aluminium (Humphreys, 1982) and grain boundary bulging has been associated with dynamic recrystallization of nickel (Luton and Sellars, 1969). Hence, very pure sodium nitrate, with its mobile boundaries and lack of highly misorientated substructure, would seem to behave in a more similar manner to metals than impure sodium nitrate.

4.6.2 'Analar' Sodium Nitrate (99.5%)

Substructure development of analar sodium nitrate (99.5%) was very similar to that observed for laboratory grade sodium nitrate. The main difference between the two materials, was that analar sodium nitrate displayed a much greater tendency for the alignment of the grain boundaries to 45° of the stress axis (figure 3.16). This in situ sequence shows the 45° alignment of the original grain boundaries, evidence of grain boundary sliding, and the same alignment of the dynamically recrystallized grain boundaries. A similar alignment of grain boundaries has been observed in many metals during high temperature fatigue, but has only been observed after monotomic

deformation in zinc and cadmium (Singh, Rao, Cocks and Taplin, 1977). The alignment leads to the formation of a diamond grain configuration. The mechanisms by which this configuration occurs in metals is not well understood, but grain boundary sliding and grain boundary mobility are thought to be important factors. Possible relationships between grain boundary sliding and grain boundary migration and the alignment of the boundaries along the directions of maximum shear stress have been discussed theoretically by Nix (1975).

Chapter 5

CONCLUSIONS
AND
SUGGESTIONS FOR FURTHER WORK

5. CONCLUSIONS AND SUGGESTIONS FOR FURTHER WORK

5.1 Conclusions

This investigation into the plastic deformation of polycrystalline sodium nitrate has demonstrated that both the mechanical properties and microstructural development of sodium nitrate are very similar to observations made on calcite.

Four deformation or microstructural mechanisms were identified for sodium nitrate:

(i) At low temperatures or high strain rates deformation twinning occurred.

(ii) Between 20°C and approximately 200°C inhomogeneous deformation together with dynamic recrystallization by subgrain rotation was observed.

(iii) Above a critical temperature rapid and extensive growth of the dynamically recrystallized grains could occur. However, the critical temperature was strongly dependent on impurities particularly divalent cations. An addition of one per cent calcium nitrate was sufficient to completely suppress the rapid migration phenomenon.

(iv) At higher temperatures grain boundary sliding was also observed.

Two growth rates were identified for the dynamically recrystallized grains, which resulted in two dynamically recrystallized grain sizes. These results were interpreted within the framework of an impurity controlled grain boundary migration theory proposed by Lücke and Stüwe (1971). Small changes in the impurity content of the samples were found to greatly influence dynamic recovery; the mechanisms of dynamic recrystallization; the growth of dynamically recrystallized grains and the occurrence of the diamond grain configuration.

Laboratory grade sodium nitrate underwent dynamic recrystallisation by the progressive misorientation of subgrains with strain. This mechanism seems to be common to several minerals, but there is no evidence for such a mechanism occuring in cubic metals. The mechanism of dynamic recrystallization in association with grain boundary bulging proposed for metals was not observed, except during in situ tests performed on very pure sodium nitrate.

Results of the bulk compression tests showed that after a strain of approximately 0.1, the flow stress for sodium nitrate remained essentially constant. Although at higher temperatures and lower strain rates there was a distinct peak in the stress strain curves.

Three values were determined for the stress exponent n 4.25 ± 0.25 between $200^{\circ}C$ and $300^{\circ}C$, 6.0 ± 0.5 at $150^{\circ}C$ and 7.5 ± 0.5 at $20^{\circ}C$. Although the correlation is not clear, each value of n could be associated with a particular type of microstructure.

The activation energy for plastic deformation was determined to be approximately $85 KJmol^{-1}$ between $20^{\circ}C$ and $280^{\circ}C$, with evidence of a significant increase at higher temperatures.

Recrystallized grain and subgrain sizes were found to obey the relationship $\sigma = Kd^{-n}$, with n having a value of 0.85 for subgrains and 0.65 for recrystallized grains. However, the value of K was not found to be a constant for all conditions of deformation, but increased with strain rate.

This investigation has demonstrated that sodium nitrate may be used as analogue material for deformation studies on calcite. However, due to the differences in mechanisms of dynamic recrystallization, its use as an analogue material for metals may be limited. Results obtained during this investigation have clearly shown the usefulness of the in situ technique as an aid

to understanding microstructural developments during high temperature plastic deformation.

5.2 Suggestions for Further Work

Following the differences in microstructural development of various sodium nitrate samples observed during the in situ experiments, it would be interesting to see if these differences were reflected in the mechanical properties as well. Hence further work on compression testing of bulk samples of specpure sodium nitrate, and various calcium nitrate alloys is suggested. Universal stage work on thin sections prepared from these bulk samples could also be compared with the results from this investigation. It would also be interesting to study the effects of other impurity additions, such as silver nitrate, in both in situ and bulk experiments.

As well as the effects of solid solution impurities, the in situ rig could also be used to study the effect of second phase particles on the evolution of the deformed microstructure and on the migration of grain boundaries. Other low melting point ionic crystals such as silver chloride could also be studied.

Modifications of the metal spacers inside the in situ cell could be made to alter the geometry of deformation, e.g. to simulate an extrusion press. For studying the geometry of plastic deformation it may prove worthwhile to study a group of organic crystals known as 'plastic crystals' in the in situ cell. A list of these crystals is given in a review by Timmermans (1961).

REFERENCES

BAILEY, J.E. and HIRSCH, P.B. (1962)
The recrystallization process in some polycrystalline metals.
Proc. Royal Soc. A 267, 11-30.

BARBER, D.J. and WENK, H.R. (1973)
The microstructure of experimentally deformed limestones.
J. Mat. Sci. 8, 500-508.

BROMLEY, R. and SELLARS, C.M. (1972)
High temperature deformation of copper and copper-aluminium alloys.
Proc. Third Int. Conf. Strength of Metals and Alloys, 380-385.

CAHN, R.W. (1956)
The kinetics of grain boundary nucleated reactions.
Acta Met. 4, 449-459.

CULLITY, B. D. (1956)

Elements of X-Ray Diffraction pp462

ETHERIDGE, M.A. and WILKIE, J.C. (1979)
Grain size reduction, grain boundary sliding and the flow strength of mylonites.
Tectonophysics 58, 159-178.

EXELL, S.F. and WARRINGTON, D.H. (1972)
Sub-grain boundary migration in aluminium.
Phil. Mag. 26, 1121-1136.

FELTHAM, P. (1953)
The plastic flow of iron and plain carbon steels above the A_3-point.
Proc. Phys. Soc. 66, 865-883.

FELTHAM, P. and MEAKIN, J.D. (1959)
Creep in face-centred cubic metals with special reference to copper.
Acta. Met. 7, 614-627.

GARDNER, K.J. and GRIMES, R. (1979)
Recrystallization during hot deformation of aluminium alloys.
Metal. Sci. 13, 216-222.

GAROFALO, F. (1965)
Fundamentals of creep and creep-rupture in metals.
Macmillan Series in Materials Science.

GIFKINS, R.C. (1958-59)
Recrystallization of lead during creep.
J. Inst. Met. 87, 255-261.

GITTINS, A. and SELLARS, C.M. (1972)
Application of theory of wedge-crack growth to rupture times in hot torsion.
Met. Sci. 6, 118-122.

GLOVER, G. and SELLARS, C.M. (1973)
Recovery and recrystallization during high temperature deformation of alpha iron.
Met. Trans. 4, 765-775.

GOTTSTEIN, G., ZABARDJADI, D. and MECKING, H. (1979)
Dynamic recrystallization in tension-deformed copper single crystals.
Met. Sci. March-April 1979, 223-227.

GREENWOOD, J.N. and WORNER, H.K. (1939)
Types of creep curve obtained with lead and its dilute alloys.
J. Inst. Metals, 64, 135-158.

GRIGGS, D.T., TURNER, F.J. and HEARD, H.C. (1960)
Deformation of rocks at 500° to 800°C.
Rock Deformation, Mem. Geo. Soc. Am. 79, 39-104.

GUILLOPE, M. and POIRIER, J.P. (1979)
Dynamic recrystallization during creep of single-crystalline halite: an experimental study.
J. Geophys. Res. 84, 5557-5567.

HARDWICK, D. and TEGART, W.J. McG. (1961-62)
Structural changes during the deformation of copper, aluminium and nickel at high temperatures and high strain rates.
J. Inst. Met. 90, 17-21.

HARDWICK, D., SELLARS, C.M. and TEGART, W.J. McG. (1961-62)
The occurrence of recrystallization during high temperature creep.
J. Inst. Met. 90, 21-22.

HEARD, H.C. (1963)
Effect of large changes in strain rate in the experimental deformation of Yule Marble.
J. Geol. 71, 162-195.

HEARD, H.C. and RALEIGH, C.B. (1972)
Steady-state flow in marble at 500°C to 800°C.
Bull. Geol. Soc. Am. 83 (1-4), 935-956.

HOBBS, B.E. (1968)
Recrystallization of single crystals of quartz.
Tectonophysics 6, 353-401.

HONEYCOMBE, R.W.K. (1968)
The plastic deformation of metals.
Edward Arnold (Publishers) Ltd.

HUMPHREYS, F.J. (1981)
Dynamic recrystallization - the influence of crystal structure.
Deformation of polycrystals: mechanisms and microstructures.
Proc. 2nd. Risø Int. Sym. Met. and Mat. Sci., 305-310.

HUMPHREYS, F.J. (1982)
Inhomogeneous deformation of some aluminium alloys at elevated temperature.
Int. Conf. Strength of Metals and Alloys No. 6., Melbourne, Australia.

HUNT, J.D. and JACKSON, K.A. (1966)
Binary eutectic solidification.
Trans. Met. Soc. AIME, 236, 843-852.

ION, S.E., HUMPHREYS, F.J. and WHITE, S.H. (1982)
Dynamic recrystallization and the development of microstructure during the high temperature deformation of magnesium.
Acta Met.

JONAS, J.J., SELLARS, C.M. and TEGART, W.J. McG. (1969)
Strength and structure under hot working conditions.
Met. Rev., 14, 1-23.

KELLY, A. and GROVES, G. W. (1970)

Crytallography and Crystal Defects pp 112

KRACEK, F.C. (1931)
Gradual transition in sodium nitrate. 1. Physico-chemical criteria of the transition.
J. Am. Chem. Soc. 53, 2609-2624.

KRACEK, F.C., POSNJAK, E. and HENDRICKS, S.B. (1931)
Gradual transition in sodium nitrate. II. The structure at various temperatures and its bearing on molecular rotation.
J. Am. Chem. Soc. 53, 3339-3348.

LÜCKE, K., and STÜWE, H.P. (1971)
On the theory of impurity controlled grain boundary motion.
Acta Met. 19, 1087-1099.

LUTON, M.J. and SELLARS, C.M. (1969)
Dynamic recrystallization in nickel and nickel-iron alloys during high temperature deformation.
Acta Met. 17, 1033-1043.

LUTON, M.J. and TEGART, W.J. McG. (1969)
Fracture behaviour of nickel and nickel-iron alloys under hot working conditions.
Metals Sci. J. 3, 142-146.

McLEAN, D. (1951-52)
Creep processes in coarse-grained aluminium.
J. Inst. Met. 80, 507-519.

McLEAN, D. (1952-53)
Crystal fragmentation in aluminium during creep.
J. Inst. Met. 81, 287-292.

McQUEEN, H.J. (1979)
Metallography and the mechanisms related to hot working of metals.
Microstructural Science, 7, 71-85.

McQUEEN, H.J. (1981)
The discovery of the dynamic restoration mechanisms in hot working.
Metals Forum, 4, 81-91, Aust. Inst. Met.

McQUEEN, H.J. and BERGERSON, S. (1972)
Dynamic recrystallization of copper during hot torsion.
Met. Sci. J. 6, 25-29.

McQUEEN, H.J. and JONAS: J.J. (1975)
Recovery and recrystallization during high temperature deformation.
Treatise of Materials Science and Technology, 6, 393-493.

MEANS, W.D. (1980)
High temperature shearing fabrics: a new experimental approach.
J. Struct. Geol., 2, 197-202.

MISRO, S.C. and MUKHERJEE, A.K. (1975)
The relative contribution of cobble creep, dislocation climb and superplasticity at elevated temperatures.
Rate Processes in Plastic Deformation of Materials.
A.S.M. 4, 434-458.

MUKHERJEE, A.K. (1975)
High temperature creep.
Treatise of Materials Science and Technology, 6, 163-224.

NICOLAS, A. (1978)
Stress estimates from structural studies on some mantle peridotites.
Phil. Trans. Roy. Soc. London, A 288, 49-58.

NIX, W.D. (1975)
On the possible relation between grain boundary migration and the kinetics of grain boundary sliding in polycrystals.
Rate Processes in Plastic Deformation of Materials.
A.S.M. 4, 384-406.

PALACHE, C., BERMAN, H. and FRONDEL, C. (1951)
Dana's System of Mineralogy.
7th Ed. New York, Wiley.

PHILLIPS, W.R. (1971)
Mineral Optics, Principles and Techniques.
Pub. W.H. Freeman and Company.

POIRIER, J.P. and GUILLOPE, M. (1979)
Deformation induced recrystallization of minerals.
Bull. Mineral, 102, 67-71.

POIRIER, J.P. and NICOLAS, A. (1975)
Deformation induced recrystallization due to progressive misorientation of subgrains, with special reference to mantle peridotites.
J. of Geol. 83, 707-720.

RAMASASTRY, C. and MURTI, Y.V.G.S. (1968)
Electrical conduction in sodium nitrate crystals.
Proc. Roy. Soc. A. 305, 441-455.

REDFERN, G.A. and SELLARS, C.M. (1970)
High temperature deformation of chromium steels.
J. Iron and Steel Inst. June 1970, 576-581.

RICHARDSON, G.J., SELLARS, C.M. and TEGART, W.J. McG. (1966)
Recrystallization during creep of nickel.
Acta Met. 14, 1225-1236.

ROBERTS, W. and AHLBLOM, B. (1978)
A nucleation criterion for dynamic recrystallization during hot working.
Acta Met. 26, 801-813.

ROBERTS, W., BODEN, H. and AHLBLOM, B. (1979)
Dynamic recrystallization kinetics.
Met. Sci. March-April 1979, 195-205.

ROSSARD, C. (1973)
Mechanical and structural behaviour under hot working conditions.
Proc. 3rd. Int. Conf. Strength of Metals and Alloys, 2, 175-203.

ROSSARD, C. and BLAIN, P. (1959)
Evolution de la structure de l'acier sous l'effet de la deformation plastique a chaud.
Mem. Sci. Rev. Met., 56, 285-299.

SAH, J.R., RICHARDSON, G.J. and SELLARS, C.J. (1974)
Grain size effects during dynamic recrystallization of nickel.
Met. Sci. 8, 325-331.

SANDSTRÖM,R. and LAGNEBORG, R. (1975)
A model for hot working occurring by recrystallization.
Acta Met. 23, 387-398.

SCHMID, S.M., BOLAND, J.N. and PATERSON, M.S. (1977)
Superplastic flow in fine grained limestones.
Tectonophysics, 43, 257-291.

SCHMID, S.M., PATERSON, M.S. and BOLAND, J.N. (1980)
High temperature flow and dynamic recrystallization in Carrara marble.
Tectonophysics 65, 245-280

SELLARS, C.M. (1978)
Recrystallization of metals during hot deformation.
Phil. Trans. R. Soc. Lond. A. 288, 147-158.

SELLARS, C.M. (1979)
The physical metallurgy of hot working.
Proc. Int. Conf. Hot Working and Forming Processes.
The Metals Soc. Lond.

SELLARS, C.M. (1979, b)
Dynamic recrystallization.
Metalurgia I Odlewnictwo 5, 377-404.

SHERBY, O.D. and BURKE, P.M. (1967)
Mechanical behaviour of crystalline solids at elevated temperature.
Progress in Materials Science, 13, 325-390.

SIMPSON, C.J., AUST, K.T. and WINEGARD, W.C. (1969)
On the mobility of non-coherent twin boundaries in an organic compound.
Scripta Met. 3, 171.

SINGH, V., RAO, P.R., COCKS, G.T. and TAPLIN, D.M.R. (1977)
On the formation of the diamond grain configuration during high temperature creep and fatigue.
J. Mat. Sci. 12, 373-383.

SPIERS, C.J. (1978)
Fabric development in calcite polycrystals experimentally deformed at moderate homologous temperatures.
C.N.R.S. Conf. Deformation Mechanisms in Rocks and Minerals, Perros Guirec, France.

STRØMME, K.O. (1969)
The crystal structure of sodium nitrate in the high temperature phase.
Acta. Chem. Scan. 23, 1616-1624.

STÜWE, H.P. and ORTNER, B. (1974)
Recrystallization in hot working and creep.
Met. Sci. 1974, 8, 161-167.

TAKEUCHI, S. and ARGON, A.S. (1976)
Steady-state creep of single-phase crystalline matter at high temperature.
J. Mat. Sci., 11, 1542-1566.

TIMMERMANS, J. (1961)
Plastic crystals: a historical review.
J. Phys. Chem. Solids, 18, 1-8.

TURNER, F.J., GRIGGS, D.T. and HEARD, H.C. (1954)
Experimental deformation of calcite crystals.
Bull. Geo. Soc. Am., 65, 883-934.

TWISS, R.J. (1977)
Theory and applicability of a recrystallized grain size paleopiezometer.
Pageoph, 115, 227-244.

WEERTMAN, J. (1968)
Dislocation climb theory of steady-state creep.
Trans. A.S.M. 61, 681-694.

WEERTMAN, J. (1975)
High temperature creep produced by dislocation motion.
Rate Processes in Plastic Deformation of Materials,
A.S.M. 4, 315-336.

WHITE, S.H. (1973)
Syntectonic recrystallization and texture development in quartz.
Nature, 244, 276-278.

WHITE, S.H. (1979)
Difficulties associated with paleo-stress estimates.
Bull. Mineral, 102, 210-215.

WHITE, S.H., BURROWS, S.E., CARRERAS, J., SHAW, N.D. and HUMPHREYS, F.J. (1979)
On mylonites in ductile shear zones.
J. Struct. Geol. 2, 175-187.

WHITE, F.E. and ROSSARD, C. (1966)
A mechanism for the fracture of steel in high temperature torsion and its relationship to structural changes.
Deformation Under Hot Working Condition.
I.S.I., 108, 14-20.

WILSON, C.J.L. (1979)
Boundary structures and grain shape in deformed multi-layered polycrystalline ice.
Tectonophysics, 57, 119-25

WONG, W.A., McQUEEN, H.J. and JONAS, J.J. (1967)
Recovery and recrystallization of aluminium during extrusion.
J. Inst. Met. 95, 129-137.

URAI, J.L., HUMPHREYS, F.J. and BURROWS, S.E. (1980)
In-situ studies on the deformation and dynamic recrystallization of rhombohedral camphor.
J. Mater. Sci., 15(5), 1231-1240.

ACKNOWLEDGEMENTS

I would like to express my gratitude to my supervisor Dr. F. J. Humphreys for all his help, guidance and encouragement throughout the course of this research project. I also wish to thank friends and colleagues of the Electron Microscopy and Structural Geology groups for their stimulating discussions and helpful suggestions, especially Mr. M. R. Drury. In particular I would like to thank Mr. G. W. Briers, Mr. D. Evans and Mr. K. Richter for their advice and technical assistance. I would also like to thank Dr. B. K. Atkinson for performing the bulk compression tests using the Heard type deformation apparatus.

I am also indebted to Professor D. W. Pashley for the provision of laboratory facilities and to the Science and Engineering Research Council for financial support.

Finally, I would like to thank Mrs. H. Arnold and Mrs. M. Poole of 'Words and Numbers' for typing the thesis and Mr. J. Rossdale for reproducing the micrographs.